UNIVERSIDAD NACIONAL AUTÓNOMA DE MÉXICO
PROGRAMA DE MAESTRÍA Y DOCTORADO EN INGENIERÍA
ENERGÍA - TERMOCIENCIAS

Aplicación de termodinámica irreversibe en la destilación de una mezcla multicomponente de hidrocarburos

T E S I S

QUE PARA OPTAR POR EL GRADO DE:
DOCTOR EN INGENIERÍA

PRESENTA:
M. I. PAULINA BURGOS MADRIGAL

TUTOR PRINCIPAL:
DR. MARIANO LÓPEZ DE HARO
INSTITUTO DE ENERGÍAS RENOVABLES, UNAM

TEMIXCO, MORELOS. Enero 2017

JURADO ASIGNADO:

Presidente: Dr. Jesús Antonio del Río Portilla

Secretario: Dr. Oscar Alfredo Salgado Jaramillo

Vocal: Dr. Mariano López de Haro

$1^{er.}$ Suplente: Dr. Federico Vázquez Hurtado Federico

$2^{do.}$ Suplente: Dr. Miguel Ánguel Olivares Robles

Lugar donde se realizó la tesis:

Instituto de Energías Renovables, UNAM
Temixco, Morelos

TUTOR DE TESIS

DR. MARIANO LÓPEZ DE HARO
INSTITUTO DE ENERGÍAS RENOVABLES, UNAM

FIRMA

Agradecimientos

El presente trabajo de tesis me brindó la valiosa oportunidad de entender que hay retos en la vida que tomarán más tiempo, esmero, dedicación y paciencia de lo que se tenía estimado. Lo cual no significa que debamos rendirnos en el transcurso del camino, sino saber descansar para retomar fuerzas. Esta experiencia me permitió conocer, convivir, apreciar y amar a muchas personas valiosas a las que agradezco a continuación:

En primer lugar, quiero agradecer a mi asesor, Dr. Mariano López de Haro, por su gran dedicación, entrega y por enseñarme a vencer los obstáculos que impone la ciencia y la vida. Su calidad de ser humano es admirable y me ha permeado de algo más que solo conocimiento. En un comienzo no lograba apreciar nuestras discusiones derivadas del presente trabajo y la exigencia de sus revisiones. Ahora entiendo que fueron necesarias para lograr un resultado con el que estoy satisfecha.

Al importante apoyo brindado por el Dr. Jesús Antonio del Río Portilla, director del honorable Instituto de Energías Renovables (IER). Su compañía, amistad y consejo fueron indispensables para culminar el presente trabajo. La oportunidad de ser alumna del Dr. Antonio en dos ocasiones, así como colaborar en uno de sus proyectos brindó el escenario que permitió que el Dr. Antonio me mostrara que siempre puedo dar mejores resultados de lo que yo esperaba. Ha sido una de las personas que ha logrado sacar siempre lo mejor de mí, poniéndome retos alcanzables. Lo considero un admirable líder.

Al Instituto de Energías Renovables. Una visita curiosa a la Institución con la finalidad de informarme del posgrado en energía me hizo sentir que debía ser parte del mismo. Esta Institución me ha brindado momentos muy gratos, me dio amigos muy valiosos, el espacio adecuado para aprender, descubrir mi gusto por compartir conocimiento y un cambio en mi panorama profesional. Ahora que concluye mi estadía en él, sé que definitivamente no soy la misma, soy mejor. ¡Gracias!

A mis queridos sinodales y profesores, Dr. Miguel Ángel Olivares, Dr. Oscar Jaramillo y Dr. Federico Vázquez, porque su conocimiento, comentarios y aportaciones han sido muy valiosas para mí y para este trabajo.

Al Dr. Diego Fernando Mendoza de la Universidad Autónoma del Caribe (Colombia). Su investigación fue un punto de partida importante en esta tesis. Colaborar con él fue una grata experiencia que deseo repetir.

A la Facultad de Química de la UNAM, que me brindó las herramientas, en particular el acceso al software de Aspen Plus V8.4, y el conocimiento necesario para poder lograr los resultados del presente trabajo. Al Instituto Mexicano del Petróleo por proporcionar la información necesaria para poder trabajar con un caso real de destilación de petróleo.

A el Consejo de Ciencia y Tecnología, CONACYT, por el apoyo económico brindado durante la realización de este proyecto.

A Nissan Mexicana y EVM Energía del Valle de México, empresas que me enseñaron a colaborar y trabajar con muchas personas de diferentes perfiles laborales. Adicionalmente, me permitieron obtener el recurso financiero necesario para regresar a terminar en aquel entonces, mi sueño inalcanzable: terminar el doctorado.

Al CeMIE Sol, un proyecto que permitió que retomara la ciencia con un punto de vista diferente, el de transferencia de conocimiento. Esta visión me acompañará de

ahora en adelante.
A la Dra. Beatriz de la Mora y al Dr. Jorge Alejandro Wong, por sus sabios consejos que me ayudaron a no rendirme con mi artículo a pesar de los numerosos rechazos que tuve que afrontar.
A Luis Mayer, más allá de su excelente trabajo como terapeuta, quien me ha ayudado a superar los episodios más difíciles, las confusiones más terribles, los días más tristes. Por brindarme las herramientas emocionales y el crecimiento personal que permitió que mi perseverancia no se agotara y que el futuro que me depara sea prometedor.
A mis ilustradores de confianza, Dr. Víctor Duarte Alaniz del Departamento de Física y Química del Instituto de Química de la UNAM y DGC. Hernán Abraham Pérez del Instituto Politécnico Nacional, porque hicieron arte donde yo solo veía esquemas.
Por supuesto, agradezco a todos mis valientes amigos. No los mencionaré uno por uno porque la lista es larga y el tiempo transcurrido ha sido extenso. Algunos me han acompañado todo el camino, otros solo por un periodo. De cualquier manera, sin su compañía este reto hubiera sido un escenario frío y desolado. La felicidad es verdadera solo cuando es compartida.
A mi hermosa familia, porque no importa lo complicado que puedan ponerse los días, su apoyo es incondicional. Nunca me ha faltado su compañía, amor y sus dosis de buen humor en mi vida. Les dedico este trabajo con todo mi corazón.
Finalmente, pero no menos importante, a ti amor mío, Rodrigo Olivares, por lograr hacerme reír y ver cada detalle de la vida como una oportunidad para alegrarse. Tu existencia en este mundo lo hace un lugar maravilloso por el que vale la pena luchar.
Gracias a todos por acompañarme en esta aventura y transformarme en el trayecto.

Abstract

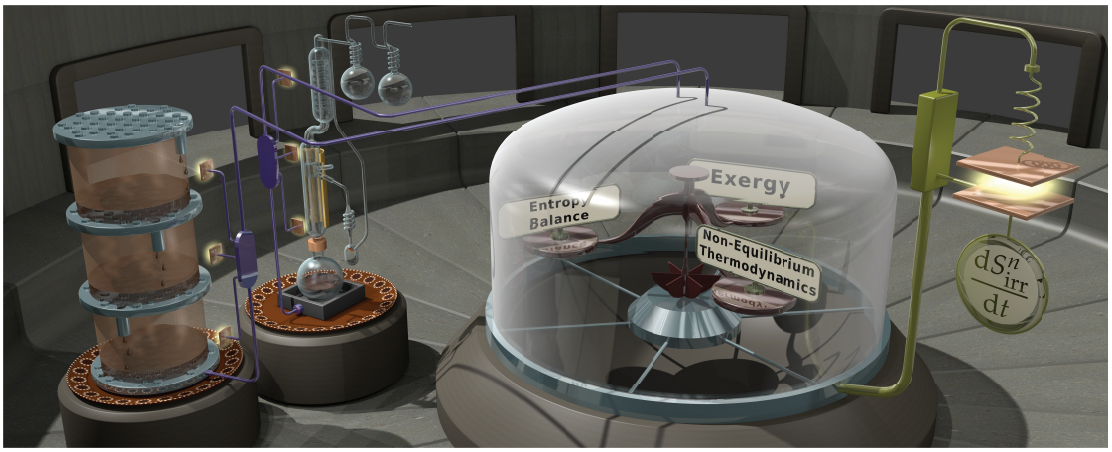

One of the main goals of this thesis is to extend the application of the nonequilibrium thermodynamics approach to a real process, namely that of the distillation of a multicomponent hydrocarbon mixture. To achieve this goal, we took the following strategy: we started by analyzing the Mendoza's case of study [1] and the experimental extractive distillation column considered by de Koeijer and Rivero [2]. Both equipments used the well known binary ethanol-water mixture. In order to correctly address a mixture of hydrocarbons we next reproduced the results of a prototype example, namely those of the depropanizer column described and previously considered by Taylor and Krishna [3] who used the Chemsep software. Finally, we moved to another (real) system with a hydrocarbon mixture consisting of a (laboratory scale) batch distillation column used in the Instituto Mexicano del Petróleo to study and characterize a weighed sample of Mexican crude oil.

In order to carry out the above mentioned extension, we performed computations in two steps. In the first one, the distillation process may be analyzed in the scale that embodies the whole column and allows us to obtain the operational profiles. That is, the temperature, the composition and the flow profiles. Also, in a intermediate scale associated to a column stage, in this first step we estimated the required transport coefficients. These computations were completed with the aid of the Aspen Plus V8.4 software using the rate-based model. Such model allows one to avoid the assumption of equilibrium at the vapor-liquid contact in a column stage. In the second step, the resulting distillation profiles and transport coefficients are incorporated into the corresponding nonequilibrium thermodynamics formulation.

Furthermore, we analyzed two different nonequilibrium approximations, namely the film model and the integrated interface model. The film model had been used earlier to analyze the Mendoza's case while the integrated interface model was considered in connection with the experimental extractive distillation column considered by de Koeijer and Rivero. In the cases of the two hydrocarbon distillation processes dealt with in this work we used a somewhat hybrid model by combining features of both the film model and the integrated interface model. This combination allowed us to incorporate the coupling between heat and mass transfer in the description of the process. To derive

the results, several simplifying assumptions were made: steady-state conditions, one dimensional flow of the vapor and liquid phases, that the vapor rising through the liquid within the tray is completely mixed and that there is no significant pressure gradient along the vapor and liquid flow directions. In order to evaluate the different formulations, we took as our benchmark the results of the popular exergy analysis and compared them with the values of the entropy production rates stemming out of such formulations.

The main outcome of our approach is the following: in the depropanizer column, the effect of the coupling between heat and mass transfer is found to be negligible, while for the fractionating column it does become appreciable.

Resumen

Uno de los objetivos principales en esta tesis es extender la aplicación del enfoque de la termodinámica de no equilibrio a un proceso real, en este caso, la destilación de una mezcla multicomponente de hidrocarburos. Para alcanzar dicho objetivo, se implementó la siguiente estrategia: comenzamos por analizar el caso de estudio de Mendoza [1] y la columna experimental de extracción considera por Koeijer y Rivero [2]. Ambos equipos usaron la conocida mezcla binaria de etanol-agua. Con la finalidad de tratar correctamente la mezcla de hidrocarburos reproducimos los resultados de un ejemplo prototipo conocido como la columna despropanizadora descrita previamente por Taylor and Krishna [3] quienes usaron el software de Chempsep. Finalmente, continuamos con otro sistema (real) con una mezcla de hidrocarburos que consiste en una columna de batch (escala labortatorio) utilizada por el Instituto Mexicano del Petróleo para caracterizar una cantidad definida de muestra de crudo mexicano.

Para llevar a cabo la modelación de las columnas mencionadas anteriormente, los cálculos se llevaron a cabo en dos pasos. En el primero, el proceso de destilación se analiza en una escala que considera la columna completa y nos permite obtener los perfiles de operación. Estos son, los de temperatura, los de composición y los perfiles de flujo. Adicionalmente, en una escala intermedia asociada a una bandeja de la columna, se estiman los coeficientes de transporte requeridos. Estos cálculos se realizaron con la ayuda del software Aspen Plus V8.4 utilizando el modelo de no equilibrio (rate-based model). Dicho modelo nos permite evitar la suposición de equilibrio en el contacto de vapor-liquido en la bandeja de la columna. En el segundo paso, los perfiles de la destilación y los coeficientes de transporte fueron incorporados en la correspondiente formulación de la termodinámica de no equilibrio.

Adicionalmente, analizamos dos formulaciones distintas de no equilibrio, conocidas como el modelo de película y el modelo de la interface integrada. El modelo de película ha sido utilizado para analizar el caso de Medoza mientras que el modelo de la interface integrada fue utilizado con el proceso experimental de la columna de destilación extractiva considerada por Koeijer y Rivero. Para el caso de los dos procesos de destilación de hidrocarburos abordados en este trabajo, utilizamos un modelo híbrido resultado de la combinación de las características de ambos modelos, tanto el de película como el modelo de la interface integrada. Esta combinación nos permitió incorporar el acoplamiento entre la transferencia de calor y masa en la descripción del proceso. Para obtener los resultados, se hicieron varias suposiciones simplificadoras: condiciones de estado estacionario, un flujo unidimensional de las fases de vapor y líquido, que el vapor que sube a través del líquido dentro de la bandeja se mezcla completamente y que no hay un gradiente de presión significativo a lo largo de la dirección del flujo del vapor y líquido. Para evaluar las diferentes formulaciones, tomamos como punto de referencia los resultados del conocido análisis de exergía y los comparamos con los valores del flujo de producción de entropía derivadas de dichas formulaciones.

El principal resultado de nuestro enfoque es el siguiente: en la columna despropanizadora, el efecto del acoplamiento entre la transferencia de calor y masa se considera despreciable, mientras que para la columna batch se vuelve apreciable.

Table of Contents

List of Figures **ix**

List of Tables **xiii**

Nomenclature **xv**

1 Introduction **1**
1.1 Motivation 1
1.2 Distillation 3
1.2.1 Hydrocarbon mixture 4
1.2.2 Distillation systems studied 7
1.2.3 Distillation column models 11
1.3 Simulation of a distillation column 16
1.3.1 The case of extractive distillation columns 20
1.3.2 The case of the depropanizer column 24
1.3.3 The case of the batch column 26
1.4 Thesis description 28

2 Nonequilibrium description **29**
2.1 Theoretical framework 29
2.1.1 Second law analysis 29
2.1.2 Exergy analysis 30
2.1.3 Theory of Nonequilibrium Thermodynamics 30
2.1.4 Calculating the entropy production 34
2.2 Thermodynamic description of the system 34
2.2.1 Film model 36
2.2.2 The integrated interface model 40
2.2.3 The present approach 44
2.2.4 Exergy Analysis and Global Entropy Balance 48

3 Results and discussion **49**

4 Concluding Remarks **55**

A Mexican oil mixture assay **57**
A.1 Detailed hydrocarbon analysis 57
A.2 API gravity 58
A.3 Properties of the pseudo components 58

B Standard Test Method for Distillation of Crude Petroleum. ASTM D2892 **61**
B.1 Test method 61
B.2 Apparatus 62

C TBP Distillation. Raw Results vs Time **65**

D Property Methods **67**
D.1 The NRTL Property Method 67
D.2 The Peng-Robinson Property Method 71

E Transport coefficients for the case of study Ext KR extractive column **75**

F Transport coefficient's results of the Mexican crude oil **77**

G Manuscript: On entropy generation and the effect of heat and mass transfer coupling in a distillation process **79**

Bibliography **99**

List of Figures

1.1 **Schematic diagram for a tray type distillation column.** This column has one feed (F), a total overhead condenser (q_c) and a partial reboiler (q_r). Here n is the stage number listed from top to bottom that takes into account the partial reboiler and the overhead condenser, $\mathcal{L}_n$ is the liquid flow, $\mathcal{V}_n$ is the vapor flow, D is the distillate and B the bottom product. 4

1.2 **Extracting distillation sequence.** Here $C1$ is the double feed extractive column and $C2$ the solvent recovery column. 8

1.3 **Flow scheme of a refinery saturated gas plant.** Here C_1 is the naphtha stabilizer, C_2 is a deethanizer column, C_3 is a depropanizer column. The process starts with a naphtha feed F_1 in C_1. The first distillate D goes to $C2$ and the bottom B is the feed $F2$ of the depropanizer column. We will analyze only $C3$ framed with a green dotted line. 9

1.4 **Diagram of a sieve tray column.** The sieve tray is the more common simulation stage due to the fact that is the simpler kind of tray. It consists of a flat perforated plate with one or two flow passes. 9

1.5 **Schematic of batch distillation column.** The column consists of a pot or reboiler q_r, a column with n trays and a condenser q_r with accompanying reflux drum. . . . 10

1.6 **Schematic diagram of an equilibrium and nonequilibrium stage.** (a) *General schematic representation of stage n.* F_n is the molar flow in the n-th tray, temperature T_{F_n} and with composition in mole fractions $z_{i,n}$. Also, entering stage n is interstage liquid from adjacent stage $n-1$ above at molal flow rate $\mathcal{L}_{n-1}$, temperature T_{n-1} and mole fraction $x_{i,n-1}$. Similarly, interstage vapor from adjacent stage $n+1$ below enters at molal flow rate $\mathcal{V}_{n+1}$, temperature T_{n+1} and mole fractions $y_{i,n+1}$. (b) *Schematic diagram of a nonequilibrium stage.* It is composed of three regions: the liquid bulk phase, the vapor bulk phase and the vapor-liquid region which includes the vapor and liquid films as well as the interface. The interface and the phases next to it are considered as a separate thermodynamic system. The labels are the same of those of (a). 13

1.7 ***Flowchart of the simulation procedure.*** 18

1.8 **Temperature and composition profiles of the ExtM column.** (a) Temperature profiles from Mendoza's thesis. Here T^L is the liquid temperature and T^V is the vapor temperature. (b) Temperature profiles by using Aspen Plus. The labels are the same as those of (a). (c) Liquid composition profile from Mendoza's thesis. Here x_{eth} is the ethanol mole fraction, x_{egl} is the ethyl glycol mole fraction, and x_w denotes the water mole fraction. (d) Liquid composition profile by using Aspen Plus. The labels are the same of (c). 22

1.9 **Temperature, composition and flow profiles of the Ex KR column**. (a) Experimental data of the liquid temperature profile. Here T^L is the liquid temperature and T^V. (b) Liquid composition profile. Where x_w is the water mole fraction and x_e is the ethanol mole fraction. (c) Experimental flow profile. Here $\mathcal{L}$ is the liquid flow and $\mathcal{V}$ is the vapor flow. (d) Computed flow profile. The labels are the same of (d). . 24

1.10 **Temperature, composition and flow profiles of the depropanizer column**. (a) Temperature profiles from Taylor and Krishna's simulations. T^L is the liquid temperature and T^V is the vapor temperature. (b) Temperature profiles by using Aspen Plus. The labels are the same as those of (a). (c) Liquid composition profile from Taylor and Krishna's simulations. Where x_{eth} is the ethane mole fraction, x_{prop} is the propane mole fraction, x_{bu} is the n-butane mole fraction and x_{pen} is the n-pentane mole fraction. (d) Liquid composition profile by using Aspen Plus. The labels are the same of (c). (e) Flow profile from Taylor and Krishna's simulations.The label $\mathcal{L}$ stands for the liquid flow, the label $\mathcal{V}$ is for the vapor flow. (d) Flow profile by using Aspen Plus. The labels are the same of (e). 26

1.11 **Temperature, composition and flow profiles of the batch column**. (a) Liquid and vapor temperature profiles. T^L is the liquid temperature and T^V is the vapor temperature. (b) Flow profile.The label $\mathcal{L}$ stands for the liquid flow, the label $\mathcal{V}$ is for the vapor flow. (c) Liquid composition profile. Where $x1$ is the pseudo component 1 mole fraction, $x2$ is the pseudo component 2 mole fraction, $x3$ is the pseudo component 3 mole fraction and $x4$ is the pseudo component 4 mole fraction. 28

2.1 **The system**. (a) This is a representative scheme of a tray (stage) in the distillation columns studied with a high concentration of vapor. (b) We show a representation of a nonequilibrium stage. 35

2.2 **Average coefficients of the vapor-liquid region**. (a) Coefficient of heat transfer $\bar{q}q$. (b) Heat and mass coupling coefficient. $\bar{r}_{1q}$ correspond to the ethanol-heat coefficient. (c) Coefficient of the transfer of ethanol. Here, $\bar{r}_{11}$ is the coefficient obtained by Kjelstrup and de Koiejer and $\bar{r}_{11}$ *Aspen* is our results derived of the operational profiles obtained with Aspen Plus. (d) Coefficient of transfer of water. Here, $\bar{r}_{22}$ is the coefficient obtained by Kjelstrup and de Koiejer and $\bar{r}_{22}$ *Aspen* is our results derived of the operational profiles obtained with Aspen Plus. 44

2.3 **Thermal diffusion coefficients in each stage**. (a) Hydrocarbon mixture of the depropanizer column. Here, D^T_{prop} is the thermal diffusion coefficient of propane, D^T_{but} refers to the thermal diffusion coefficient of butane and D^T_{pen} is the thermal diffusion coefficient of the pentane. (b) Mexican oil mixture. Here, D^T_{cut2} is the thermal diffusion coefficient of pseudo component 2, D^T_{cut3} refers to the thermal diffusion coefficient of pseudo component 3 and D^T_{cut4} is the thermal diffusion coefficient of pseudo component 4. 48

3.1 **Global entropy production rate of the extractive distillation columns for an ethanol-water mixture**. (a) Ext M column. Here, *Ex* is the exergy analysis, *Mend* correspond to the values obtained by Mendoza and *Film* are our results by using the film model. (b) Ext KR column. Here, *KR* correspond to the values obtained by Kjelstrup and de Koeijer and *Int* are our results by using the integrated interface model. 49

3.2 **Global entropy production rate of the hydrocarbon distillation columns.** Labels indicate the different theoretical approaches. *NET* corresponds to our nonequilibrium approach including the contribution of the two bulks; *Ex* refers to the exergy analysis and *EB* corresponds to the entropy balance analysis. (a) The depropanizer column. (b) The batch column with the Mexican oil mixture. 50

3.3 **Vapor heat of transfer.** (**a**) Vapor heat of transfer in the depropanizer column, where q^{*V}_{eth} is the ethane vapor heat of transfer, q^{*V}_{prop} is the propane vapor heat of transfer, q^{*V}_{bu} is the n-butane vapor heat of transfer and q^{*V}_{pe} is the n-pentane vapor heat of transfer. (**b**) Vapor heat of transfer in the batch column, where q^{*V}_1 is the pseudocomponent 1 vapor heat of transfer, q^{*V}_2 is the pseudocomponent 2 vapor heat of transfer, q^{*V}_3 is the pseudocomponent 3 vapor heat of transfer and q^{*V}_4 is the pseudocomponent 4 vapor heat of transfer. 51

3.4 **Thermal driving forces.** (**a**) Vapor thermal driving force of the depropanizer column, where X^V_q includes the coupling between heat and mass transfer while $*X^V_q$ does not (**b**) Vapor thermal driving force of the batch column. The labels are the same of those of (a) 52

3.5 **Mass driving forces.** (a) Vapor thermal driving force of the depropanizer column, where X^V_3 includes the coupling between heat and mass transfer and $*X^V_3$ does not (b) Vapor thermal driving force of the batch column. The labels are the same of those of (a). 52

3.6 **Contribution of the liquid and vapor heats of transfer in the films to the global entropy production rates.** (a) Depropanizer column, in the cases where the thermal and mass driving forces include the coupling between heat and mass transfer and where they do not (b) batch column. The labels are the same of those of (a). . . 53

B.1 **Batch column**. Typical distillation equipment with all components conforming to the requirements specified in ASTM D2892. ASTM distillation is carried out in a relatively simple apparatus consisting of a flask holding the sample connected to an inclined condenser, which condenses the rising vapors. 63

F.1 **Low mass transfer coefficients in each stage**. (a) Liquid low mass transfer coefficients. Here, k^L_{ij} is the conjugate low mass transfer coefficient of the pseudo component i with the pseudo component j. (b) Vapor low mass transfer coefficients coefficients. The labels are the same of (a). 78

F.2 **Maxwell Stefan diffusion coefficients in each stage**. (a) Liquid Maxwell Stefan diffusion coefficients. Here, D^L_{ij} is the conjugate low mass transfer coefficient of the pseudo component i with the pseudo component j. (b) Vapor Maxwell Stefan diffusion coefficients. The labels are the same of (a). 78

List of Tables

1.1 **Oil laboratory distillation standard test methods**. We present the main applicability of the principal laboratory distillation test. 11

1.2 **Operating and stream characteristics of the extractive distillation column Ext M**. Here $C1$ is the extractive column, $C2$ the solvent recovery column, $F1$ is the EGL, $F2$ is the EtOH-W and B is the solvent recovered from $C1$. 21

1.3 **Operating and stream characteristics of the pilotscale rectifyng column Ext KR.** Here $F1$ is the ethanol water mixture feed. 23

1.4 **Operating and stream characteristics of the depropanizer column**. Here F is the hydrocarbon mixture feed, D the distillate and B the bottom current. 25

1.5 **Operation, stream and batch column data**. 27

2.1 **Coefficients in the films for a binary mixture.** Here, $D_{i,j}$ are the Fick's diffusion coefficients and S^T is the Soret coefficient. The Soret coefficient in the vapor is neglected due to the fact that it is much smaller than the one of the liquid [4]. 43

A.1 **Gas chromatography analysis.** The results correspond to the first and second fractions of the Mexican oil mixture. Here $\%\ V$ is the volume percent in the mixture. 57

A.2 **% Volumen vs API gravity in distillate.** 58

A.3 **Properties of the Mexican oil pseudo components.** Here the satured, unsatured and aromatics are given in $\%V$ and the $Kfactor$ is dimensionless 58

A.4 **Characteristics of the Mexican Oil mixture**. Here, (l) refers to light, (m) to medium, and (h) to heavy. Also, $\%V$ indicates the vaporized volume percent of the mixture. 59

B.1 **Plates properties for the fractionating column.** Here, the height equivalent to one theoretical plate (HETP) is expressed as the percentage of one theoretical plate that is achieved on one real plate. 62

C.1 **Record of the experimental data at atmospheric pressure.** . . . 65

C.2 **Record of the experimental data at 13.3 kPa.** 66

C.3 **Record of the experimental data at 0.27 kPa.** 66

D.1 **NRTL Property Method.** 67
D.2 **Peng Robinson Property Method.** 71
D.3 **Method used for the computation of the transport and thermodynamic properties.** 73

E.1 Physical chemical properties 76

F.1 **Transport properties of the Mexican oil mixture.** 77

Nomenclature

A	interfacial area, m^2
a_p	Specific surface area of the packing, m^2/m^3
B	bottom product
B_{ij}	matrix containing Maxwell-Stefan diffusion coefficient
C_p	heat capacity, $J/molK$
c_t	total molar density, mol/m^3
c_i	molar density of component i, mol/m^3
d_p	nominal diameter of packing, m
dS^n_{irr}/dt	total entropy production, W/K
D	distillate, mol/s
$\mathcal{D}_{ij}$	Maxwell-Stefan diffusion coefficient, m^2/s
$\mathcal{D}_{av}$	average Maxwell-Stefan diffusion coefficient, m^2/s
$E_{i,n}$	energy balance equation, $W/m^2\,W$
E^I_n	energy balance equation around the vapor-liquid interface region, *dimensionless*
$\mathcal{E}_n$	net energy flow, W
Ex	Exergy, W
Ex^{loss}	Exergy Loss, W
$\mathbf{f}$	external body force
F	Feed material
F_n	Feed molar flow, mol/s
Fr	Froude number, *dimensionless*
g	Acceleration due to gravity, m/s^2
k_{av}	average low mass transfer coefficients, $mol\,m^2/s$
k_{ij}	low mass transfer coefficients, $mol\,m^2/s$
H	enthalpy, J/mol
$\mathcal{H}$	enthalpy balance equations, J/mol
$\bar{H}$	partial molar enthalpy, J/mol
h	heat transfer coeffiecient, W/m^2K
$\Delta_{vap}H_i$	heat of vaporization
J_e	flux of energy , W/m^2
J_α	conjugate Fluxes, mol/s or J/s
$\mathbf{J}_i$	diffusion flow
J'_i	local flux of component i, $mol/s\,m^2$
$\mathbf{J}_q$	heat flux
J'_q	local flux of measurable heat transfer, $W\,m^2$
J_s	entropy flux
$\mathbf{J}_u$	conductive flux
$K_{i,n}$	equilibrium ratio (K value), *dimensionless*
k_{ij}	binary mass transfer coefficient, $mol\,m^2/s$
$l_{\alpha\beta}$	phenomenological coefficient (conductance)
$\mathcal{L}$	liquid flow mol/s
M	molecular weight, kg/mol or g/mol
$\mathcal{M}^T_n$	total material balance equation, mol/s
$\mathcal{M}_{i,n}$	component material balance equation, mol/s
N_t	total molar flux, mol/s

N_i	component molar flux, mol/s
$\mathcal{N}_i$	mass transfer rate of i, mol/s
P	pressure, bar
P_c	critical pressure, bar
$P_i^{*,L}$	vapor pressure of the liquid
$\mathbf{P}$	pressure tensor
Q_n	duty, W
q_i^*	heat of transfer, J/mol
R	ideal gas constant, $J/mol\,K$
Re	Reynolds number, *dimensionless*
$r_{\alpha\beta}$	phenomenological coefficient (resistance)
$\mathfrak{r}$	surface tension
s	specific entropy
Sc	Schmidt number for the binary pair i and j
SG	specific gravity, *dimensionless*
S^{*ig}	ideal gas entropy, $J/mol\,K$
S_n	molar entropy of n- stage, $J/mol\,K$
S_i^T	Soret coefficient of component i, $1/K$
$\bar{s}_i$	partial entropy of the i- substance
$\mathcal{S}$	summation equation, *dimensionless*
T	temperature, K
T_b	boiling point temperature, K
T_c	critical temperature, K
T_r	reduced temperature, K
T_0	reference temperature, K
u	specific internal energy
$\mathfrak{U}$	viscosity, $Pa\ s$
$\mathcal{V}$	vapor flow, mol/s
$\mathbf{V}$	molar volume
V	symmetric part of the velocity gradiente tensor
$\%V$	volume percent
v	superficial mass velocity of liquid m/s
$V_i^{*,L}$	pure component liquid molar volume
$V_{i,A}^{\infty}$	partial molar volume of componet i at infinite dilution in a pure solvent A
V_m^L	liquid molar volume of the mixture
V_p^L	pseudo component liquid molar volume
V^{L_r}	real component liquid molar volume
$\mathbf{v}$	mass average velocity, m/s
$\mathbf{v}_i$	velocity of component i, m/s
We	Weber number, *dimentionless*
w	work, J
w_i	mass fraction of substance, *dimensionless*
x	liquid molar fraction, *dimensionless*
X	global force conjugate rate, $J/mol\,K$ or $1/K$
X_α	thermodynamic force
X''	local force, $J/mol\,K\,m$ or $1/K\,m$
y	vapor molar fraction, *dimensionless*
y^*	mole fraction in equilibrium with the liquid that leaving the stage, *dimensionless*
$z_{i,n}$	liquid and vapor molar fraction, *dimensionless*.

Greek letters

γ	activity coefficient, *dimensionless*
Γ	Thermodynamic factor, *dimensionless*
δ	film thickness, m
η^{MV}	Muphree vapor phase efficiency
$\eta_j^{*,\pi}$	pure component viscosity
Λ	production rate of component i by chemical reaction
λ	thermal conductivity, $W/m\,K$
μ	chemical potential, J/mol
μ	viscosity, $N\,s/m^2$
ρ	density, kg/m^3
σ	local entropy production rate, W/Km^3
ϕ	fugacity coefficiente, *dimensionless*

Subscripts and superscripts

i	component
ig	ideal gas
L	liquid
mix	mixture
q	heat
n	stage number
T	total
V	vapor
π	liquid or vapor
$*$	pure component

Chapter 1

Introduction

1.1 Motivation

One of the most fundamental processes in the petroleum refining and petrochemical industries is the distillation of crude oil. This process involves a high energy consumption and has an inherently low thermodynamic efficiency. In general, the reduction of energy consumption in distillation has been the subject of intensive research [3,5–8]. Quantifying the energy efficiency of the process, identifying regions with poor energy efficiency and possible improvements are therefore important issues. One may address these issues through the pinch analysis, the exergy analysis or the nonequilibrium thermodynamics analysis (NET) [2,9–11]. The pinch analysis is a methodology for minimizing energy consumption of a processes by calculating thermodynamically feasible energy targets and integrating an efficient heat exchanger network [12]. However, some of the modifications imposed by the pinch analysis may require substantial capital investment and changes in the internal stage design of ditillation columns [9]. On a different vein, exergy analysis was developed to identify parts of systems with excessive irreversibilities and to control the lost work. Nowadays exergy analysis has been increasingly applied to industries for the design and analysis of thermal systems and provides a systematic method within the scope of equilibrium thermodynamics to diagnose and to reduce the inefficiency.

On the other hand, NET offers a systematic way to derive the local entropy production rate, σ, of a given system or process globally out of equilibrium. This quantity, which has received a lot of attention in the literature [5,8,13] is a measure of the irreversibilities present in a system or process such as fluid friction, heat and mass transfer, chemical reaction and mixing [14,15]. Hence, it may provide information for its design or performance and also accounts for the presence of couplings among various transport phenomena such as the Soret effect or the Duffour effect [16–18]. Both effects are an important research topic in scientific and engineering applications including petroleum engineering, which involves not only temperature difference but also concentration difference.

Given these statements, it is then important to know that the NET equations may also describe non linear phenomena, by including internal variables in the thermodynamic description and the necessary information to estimate the transport coefficients

of the system and phenomena to be analyzed. As a result, one can extend the application of NET to real processes. Therefore, it is a powerful theoretical tool that may serve to complement the exergy analysis by revealing the exact location and the mechanisms of entropy generation thus permitting to quantify the associated exergy losses. Thus, NET appears as a versatile theory that applies to many practical conditions, the distillation columns being one of them [19].

To our knowledge, the use of the NET approach in the distillation of a truly multicomponent mixture is rather scarce. Notable exceptions in binary distillation are the works of Wesselingh [20] and Liang, Zhou, Wu, Geng and Zhang [14] which served as an inspiration for this thesis. Here we will consider two further examples, one theoretical (a depropanizer distillation column) and one of a real (pilot scale) laboratory fractionating distillation column, in which the application of this approach may provide valuable information and pave the way to the NET analysis application to industrial scale oil mixture. Previosly to these hydrocarbon distillation column, we start analyzing the Mendoza's case of study [1] and the experimental column of de Koeijer and Rivero [2]. Both equipment used the well known binary ethanol-water mixture.

The scarcity of work related to the NET approach mentioned before is due to the fact that modelling multicomponent distillation system, where simultaneous heat and mass transfer occurs, is a challenging task. The difficulty is not only related to the interaction effects among the different components in the mixture, but also because one has to decide whether to account explicitly for the direct coupling. It is common to neglect such coupling in distillation since the Soret and the Duffour effects are considered to have little significance in unit operations [21,22]. Nevertheless, several works [15,23–28] claim that the coupling between heat and mass transfer is needed to correctly describe the distillation process, as a non zero coupling coefficient between heat and mass fluxes, influences both mass fluxes and heat fluxes.

These latter authors have formulated the interface approach in order to introduce the complications of the Soret and Dufour effects. Kjelstrup and de Koeijer [23] have provided the associated set of transport equations for heat and mass transfer across the liquid and vapor interface in the distillation columns. These equations comprise overall transport coefficients that include contributions from the interface, the vapor and the liquid films. In the case of an ethanol-water mixture they computed the entropy production rate by using the experimental data from de Koeijer and Rivero [2] for the water and ethanol compositions, vapor and liquid flows, and temperatures in 10 trays of an adiabatic rectifying column. In a relatively recent paper, van der Ham, Bock and Kjelstrup [27] presented a model for coupled transfer of mass and thermal energy in the vapor-liquid region of a nitrogen-oxygen mixture and they also calculated the entropy production rate using irreversible thermodynamics and entropy balance. This model served as a basis to incorporate mass-heat transfer coupling to model a nonequilibrium distillation stage [28].

In this work, we will address the importance of including the coupling between heat and mass transfer in the themodynamic driving forces for the description of the two chosen multicomponent distillation columns. This will be done with the aid of the Aspen Plus V8.4 software to compute the temperature, composition and flow profiles using both the equilibrium stage model and the rate-based model. Also, we will use a set of transport equations for heat and mass transfer in our hydrocarbon mixture

that includes the necessary empirical correlations for the phenomenological transport coefficients. This allows us to evaluate the importance of thermal diffusion with the introduction of particular ratios of forces (specified later) as functions of the stage number.

Instead of considering the resistivities as in the paper by Kjelstrup and de Koeijer [23], we deal directly with the transport coefficients. In fact our development follows very closely a parallell one for a homogeneous one - phase - three - component mixture in the book by Kjelstrup and Bedeaux [26]. This is a local formulation that gives us the local entropy production. In order to asses the NET results, we compare the entropy production rate obtained for both cases with the exergy analysis and the EB, both useful benchmark.

Although the usefulness of NET in describing industrial problems is not a resolved issue due to the non linear character of those problems, here we will consider two further examples. Also because both columns are a common process in the oil refinery and we consider they as a first step before analyzing the more complex case and larger operation scale of a petroleum distillation column where more components are separated from the rest of the oil mixture. This will be the subject of future work.

1.2 Distillation

Due to the fact that distillation is an important part of the thesis an introduction is given here. The general objective of distillation is the physical separation of a mixture into two or more components that have different boiling points. Distillation is the most widely used separation technique in the chemical industry. Consequently exist extensive literature on the subject that one may consult [7, 9, 12, 29, 30].

In Fig. 1.1 we illustrate a typical tray type distillation column and the common nomenclature taken from Seader [29]. The separation operation utilizes vapor and liquid phases almost at the same temperature and pressure for the coexisting zones. To bring the two phases into intimate contact devices such as packing and plates or trays are used. The feed material F, which is to be separated into fractions, is introduced at one or more points along the column shell. Because of the difference in gravity between vapor and liquid phases, liquid $\mathcal{L}_n$ runs down the column, cascading from tray to tray, while vapor flows $\mathcal{V}_n$ up the column, contacting liquid at each tray. Liquid reaching the bottom of the column is partially vaporized in a heated reboiler to provide boil-up, which is sent back up the column. The remainder of the bottom liquid is withdrawn as bottoms, or bottom product B. Vapor reaching the top of the column is cooled and condensed to liquid in the overhead condenser. Part of this liquid is returned to the column as reflux to provide liquid overflow. The remainder of the overhead stream is withdrawn as distillate D, or overhead product.

The overall separation achieved between the distillate and the bottoms depends primarily on the relative volatilities of the components, the number of contacting trays and the ratio of the liquid phase flow rate to the vapor phase flow rate. There exists a large variety of types and configurations that may be possible for a specified task. The height of the column is determined by the feed composition, by the required product purities, by the reflux ratio, and by the type of column interior that is used. The most

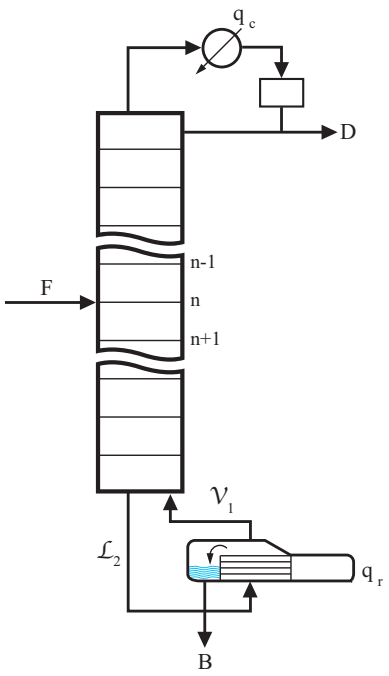

Figure 1.1: **Schematic diagram for a tray type distillation column.** This column has one feed (F), a total overhead condenser (q_c) and a partial reboiler (q_r). Here n is the stage number listed from top to bottom that takes into account the partial reboiler and the overhead condenser, $\mathcal{L}_n$ is the liquid flow, $\mathcal{V}_n$ is the vapor flow, D is the distillate and B the bottom product.

common column internals are physical trays and random packing.

The NET analysis requires to know the characteristics of the distillation column, the properties of the mixture and operation conditions. For this reason, in the following sections we will describe the hydrocarbon mixture and the different columns studied in this thesis.

1.2.1 Hydrocarbon mixture

The most accurate method for estimating properties of a mixture is through knowledge of the exact compositions of the mixture. But, due to the diversity of the composition of a hydrocarbon mixture and its resulting distillation products, the calculation methods developed for pure hydrocarbons and simpler mixtures are not always applicable. The acquisition of experimental data, to measure or calculate accurately the thermodynamic an physical properties, need special considerations. First, many different types of hydrocarbons and inorganic and organic compounds are present. This means that the number of carbon atoms in the different compounds may vary from 1 to more than 50. Further, some of the compounds exhibit only small differences in volatility [29].

For these reasons, the methods of characterization of hydrocarbon mixtures involve two main aspects. The first one is how to present the hydrocarbon mixture in terms of a number of pseudo components (petroleum fractions) and link them to the commercial resulting products. The second aspect is to represent all the pseudo components in

common terms. The resulting information is called crude assay and is therefore valuable since it determines the yields of the different pseudo components. For this thesis the corresponding crude assay of the Mexican oil mixture was provided by the Instituto Mexicano del Petróleo (IMP) and it is included in Appendix A. A brief description of the properties contained in a crude assay is as follows [29, 31, 32],

1. *True Boiling Point curve (TBP curve).* This curve can be avaible either by the direct laboratory measurements through ASTM D1160 and ASTM D2892 (see also Table 1.1) or through the conversion of the ASTM D86 distillation into the TBP distillation curve. TBP cut point ranges are used to define pseudo components with average temperature of the cut, also named Normal Boiling Point (NBP). All pseudo components from a distillation column have a known boiling range, except the residuum for which the upper boiling point is usually not known. If the petroleum fraction contains components lighter than pentanes, the composition of the lighter ends has to be available experimentally through chromatographic analysis of the vapors.

2. *Specific Gravity (SG).* It is defined as the ratio of density of a hydrocarbon liquid with respect to that of water at a defined temperature, commonly $15°C$. Namely

$$SG = \frac{density\, of\, liquid\, hydrocarbon\, at\, T}{density\, of\, water\, at\, T}. \tag{1.1}$$

   Therefore, it is a dimensionless quantity. The specific gravity is also presented in terms of *API gravity.* It is a useful parameter to characterize petroleum fluids, to determine composition and the quality of a fuel and to estimate other properties such as critical constants, density at various temperatures, viscosity and thermal conductivity.

3. *Molecular weight (M).* It is used to convert molar quantities into mass basis needed for practical applications. It is also used to characterize oils, to predict composition and quality of oils and also to compute physical properties such as viscosity. Most crude oils and petroleum fractions have average molecular weights from $100 g/mol$ to $500 g/mol$.

4. *Type composition.* The composition of crude oil presents three main classes of hydrocarbons based on the type of carbon-carbon bonds present. The first class corresponds to the *saturated hydrocarbons* that contain a carbon-carbon single bond. If they are acyclic then they are known as paraffins or alkanes. On the contrary, if they are cyclic then they are named naphthenes or cycloalkanes. The second class correspond to the *unsaturated hydrocarbons*, compounds with multiple carbon-carbon bonds. These are unsaturated because they contain fewer hydrogens per carbon than paraffins. They are commonly known as olefins. Finally, the *aromatic hydrocarbons*, they are special class of cyclic compounds related in structure to benzene.

   The composition of pseudo components in terms of paraffins, olefins, aromatics, and sulfur content is important to determine the quality of a pseudo component as well as to estimate physical properties through pseudo component methods.

5. *Watson characterization factor (K factor).* The purpose of this factor is to classify the type of hydrocarbons in the oil mixture. For example, the aromatics have low *K factor* while paraffins have high values. However, there is an overlap between values of the *K factor* from different hydrocarbon classes and for this reason it is recommended to complemente it with others parameters like de API gravity. This factor is defined as

$$K\,factor = \frac{(1.8T_b)^{1/3}}{SG}, \tag{1.2}$$

where T_b is the normal boiling point. Furthermore, the $K\,factor$ also helps to determine the quality and composition of the pseudo component.

Once these parameters are determined, the pseudo components can be treated as any defined component for the calculation of the thermophysical and thermodynamic properties. Process simulators are used to characterize crude oil and compute the thermophysical and thermodynamic properties of crude oil and fractions. As we point out in section 1.3.3 we used Aspen Plus software and we defined the pseudo components of a crude oil according to the crude assay provided by the IMP.

The number of pseudo components depends on the hydrocarbon mixture and the refinery process. The principal pseudo components are given here [29, 31, 32],

1. *Liquefied Petroleum Gas.* It is a group of hydrocarbon-based gases derived from crude oil refining of natural gas fractionation. They include ethane, ethylene, propane, propylene, normal butane, butylene, isobutane and isobutulene. Some of these pseudo components are present in the hydrocarbon mixture used in one of our cases of study, the depropanizer column.

2. *Gasoline.* It is the most important product in a refinery. Also it is called "distillate". It contains hydrocarbons from C_4 to C_{11} and molecular weight about 100 to 110. Its main characteristics are the volatility, stability and density.

3. *Naphtha.* It constitutes a category of petroleum solvents. It is an industrial intermediate with only commercial specifications.

4. *Kerosene and jet fuel.* It is a light petroleum distillate mainly used for lighting and jet engines, respectively. The main characteristics are sulfur content, density and ignition quality.

5. *Diesel fuel.* It is used for motor fuel and domestic purposes. Its quality can be expressed as cetane number or cetane index. Its principal characteristics are ignition, volatility, viscosity, density and sulfur content.

6. *Fuel oil.* The fuel oils are mainly used in space heating and thus the market is quite high specially in cold climates.

7. *Residual fuel oil.* It is used for industrial fuel, for thermal production of electricity and as motor fuel. It is mainly composed of vacuum residue. Critical specifications are viscosity and sulfur content.

The pseudo components are not the final products of a refinery. After the first crude distillation they go through further physicochemical and finishing processes to get the characterisitics set by the market and government regulations. Finally, the pseudo components are converted into petroleum products [31, 33].

1.2.2 Distillation systems studied

In our work, we have considered four distillation columns. Our starting point was the Mendoza's case of study [15] and secondly the experimental rectifying column of de Koeijer and Rivero [2]. Both equipments used the binary ethanol-water mixture. These two extractive distillation columns were useful for implementing the simulations and getting acquainted with the Aspen Plus V8.4 software. They were also of help in developing the calculation sequence in Mathematica for the NET approach, the Ex analysis and the entropy balance. The next column was the prototype example in hydrocarbon mixtures namely the depropanizer column described by Taylor and Krisnha [3]. Finally, we considered the batch laboratory column used in the Instituto Mexicano del Petroleo (IMP) to study and characterize a weighed sample of Mexican crude oil. In what follows we provide a brief description of these systems.

Extractive distillation columns

Extractive distillation is used throughout the petrochemical and chemical processing industries for the separation of the close-boiling or azeotropic systems for which simple single feed distillation is either too expensive or almost impossible. This distillation is a partial vaporization process in presence of a solvent which is added to an azeotropic feed mixture to alter the volatilities of the key components without the formation of any additional azeotropes. The classical implementation of an extractive distillation process for the separation of a binary system is shown in Fig. 1.2. The configuration consists of a double feed extractive column, $C1$, and a solvent recovery column $C2$. In this thesis, we are going to analyze only the extractive column, $C1$. As in the case of Mendoza [15] and Kjelstrup and de Koeijer [23] (see section 1.3.1), the azeotropic mixture is ethanol-water.

In the distillation process, the solvent is introduced into the extractive column at a high concentration a few stages below the condenser, but above the primary feed stage. Since the solvent is chosen to be nonvolatile, it remains at a relatively high concentration in the liquid phase throughout the sections of the column below the solvent feed stage.

The upper section of the column, above the entrainer feed location, is called the rectifying section. The purpose is to separate D and the entrainer. The middle section of the column, between the entrainer feed stage and the fresh feed stage, is called the extractive section. The purpose of this section is to suppress water from going to the column. The bottom section of the column, below the fresh feed location, is called the stripping section, and its purpose is to keep D its from going down the column.

Due to the fact that the solvent is nonvolatile, at most a few stages above the solvent feed stage are sufficient to rectify the solvent from the distillate. The bottoms product consisting of B and the solvent, is sent to the recovery column. The distillate from the recovery column is pure B, and the solvent-bottoms product is recycled back to the

extractive column [29].

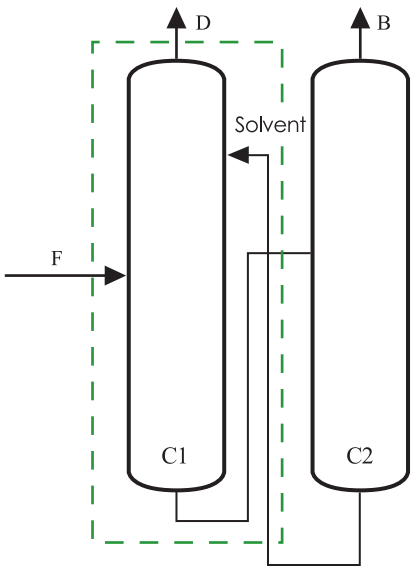

Figure 1.2: **Extracting distillation sequence.** Here $C1$ is the double feed extractive column and $C2$ the solvent recovery column.

Depropanizer column

The depropanizer column is a distillation column to separate specifically propane from other components in the *light ends* based on the volatility of the substance. The *light ends* in a hydrocarbon mixture means any component lighter than heptane which can be identified. This includes everything from hydrogen through hexane.

The Fig 1.3, taken from Watkins [33] shows the part of interest of a refinery saturated gas plant where the depropanizer column appears in the system.

The composition of distillate and bottom products also depends on the feed composition that is fed into the column. The feed tray divides the column into rectifying and stripping trays.

In a depropanizer column there are several trays, each one consisting of two channels on each side called *flow passes*, as we ilustrated in Fig. 1.4. Liquid falls through flow passes from one tray to another. The tray is designed to maximize the contact area between vapor and liquid and so it contains many holes through which the vapor passes. In turn, the vapor flows to the top of the column and forces the liquid to pass through the flow passes (the openings) on each tray.

The vapor at the top of the column is cooled by a condenser. Once the vapor is condensed, the majority of the resulting liquid is returned to the column and is called reflux. On the other hand the rest of the liquid is the distillate, D. The remaining liquid will exit from the reboiler and is known as bottom product, B.

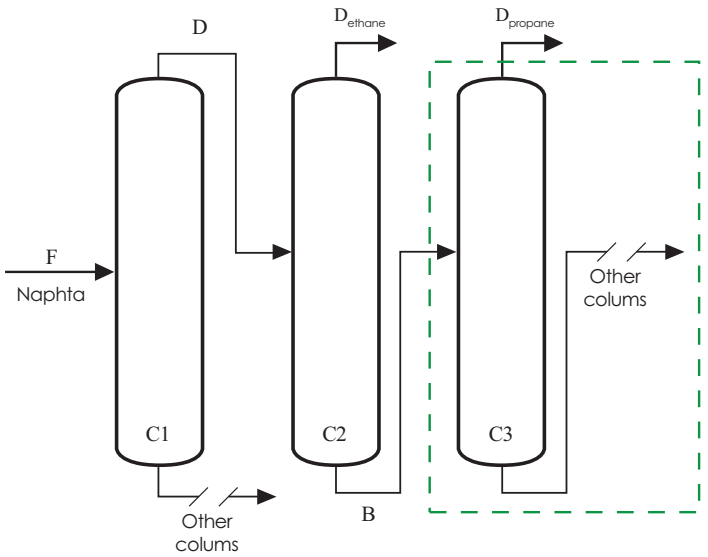

Figure 1.3: **Flow scheme of a refinery saturated gas plant.** Here C_1 is the naphtha stabilizer, C_2 is a deethanizer column, C_3 is a depropanizer column. The process starts with a naphtha feed F_1 in C_1. The first distillate D goes to $C2$ and the bottom B is the feed $F2$ of the depropanizer column. We will analyze only $C3$ framed with a green dotted line.

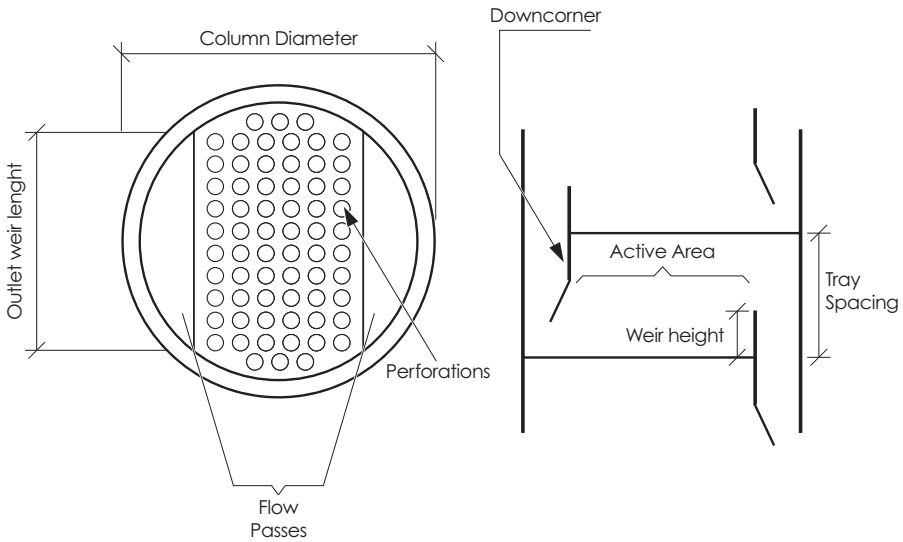

Figure 1.4: **Diagram of a sieve tray column.** The sieve tray is the more common simulation stage due to the fact that is the simpler kind of tray. It consists of a flat perforated plate with one or two flow passes.

The scale of the depropanizer column is generally large. This distillation operation is conducted in large pieces of equipment that consume a large amount of energy. Therefore, the simulation and thermodynamic analysis are important in the petroleum refinery. We will analyze only $C3$ shown in Fig. 1.3.

Batch laboratory column

Crude oil comes from different parts of the world and has different physical and chemical characteristics. Additionally, it is a complex liquid mixture made up of a vast number of hydrocarbon compounds that consist mainly of carbon and hydrogen in different proportions together with small amounts of organic compounds containing sulfur, oxygen, nitrogen and metals [31, 32]. For this reason, it is necessary determines the yield of the products that can be obtained from this crude oil when it is processed. For example, a light crude oil will produce higher amounts of gasoline that a heavier crude oil. The crude assay, allows to determine these yields and consequently, the refinery configuration.

In order to obtain the crude assay, the strategy is to distillate a small quantity in a laboratory, break down in pseudo componets and identify them. The pseudo components are also knows as cuts or petroleum fractions. To obtain this fractions a batch laboratory column like the one shown in Fig. 1.5 is used.

It consists of a pot or reboiler, a fractionating column, a condenser, a splitting off a portion of the condensed vapor (distillate) as reflux, and receivers. The temperature of the distillate is controlled in order to return the reflux at or near to the column temperature to permit a true indication of reflux quantity and to improve column operation. A subcooling heat exchager is then used for the remainder of the distillate, which is sent to the receiver. The column may also operate at elevated pressure or vacuum. Pot design is based on batch size and required vaporization rate [29].

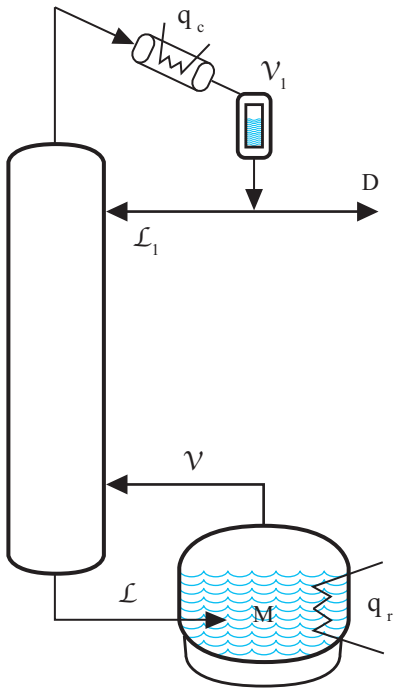

Figure 1.5: **Schematic of batch distillation column.** The column consists of a pot or reboiler q_r, a column with n trays and a condenser q_r with accompanying reflux drum.

In operation, a batch of liquid is charged to the pot and the system is first brought to steady state under total reflux. A portion of the overhead condensate is then continuously withdrawn in accordance with the estabished reflux specified in the American Standard Method (ASTM) selected. Cuts are made by switching to alternate receivers, at which time operating conditions may be altered. The entire column operates as an enriching section. As time proceeds, composition of the material being distilled becomes less rich in the more volatile components, and distillation of a cut is stopped when the accumulated distillate attains the desired average composition.

The volatility of crude oil and petroleum fractions is characterized in terms of one or more laboratory distillation tests that are summarized in Table 1.1. For light cuts (gasoline, kerosene, diesel and heating oil) the distillation is run at atmospheric pressure under ASTM D86 test. On the other hand, for heavier fractions an ASTM D1160 test at reduced pressure is employed [31]. In this thesis the batch column operated according to the ASTM D2892 shown in the Appendix B.

Table 1.1: **Oil laboratory distillation standard test methods**. We present the main applicability of the principal laboratory distillation test.

Test name	**Reference**	**Main applicability**
ASTM atmospheric	ASTM D86	Petroleum fractions or products that do not tend to decompose when vaporized at 101.3 kPa.
ASTM vacuum	ASTM D1160	Heavy petroleum fractions or products that tend to decompose in the ASTM D86 test but can be partially or completely vaporized at a maximum liquid temperature, 673.15 K, at pressures down to 0.13 kPa.
TBP atmospheric or TBP 1.3 kPa	Nelson, ASTM D2892	Crude oil and petroleum fractions.
Simulated TBP	ASTM D2887	Crude oil and petroleum fractions.

Once we have briefly described the distillation system studied we can now address the models for simulation column performances.

1.2.3 Distillation column models

The building and operation of industrial scale distillation columns involves substantial amounts of money. As a natural result, considerable efforts have been made to develop predictive and more realistic distillation column models that allow for an accurate simulation of column performances.

The models that are commonly used to simulate distillation columns can be considered to consist of two parts: a theoretical part and a empirical part. Two main types of theoretical models can be distinguished: the theoretical equilibrium stage and the nonequilibrium models. The latter one is commonly know as the rate-based model.

The theoretical equilibrium stage model is the simplest one and allows one to simulate many of the properties of real systems. For instance, the temperature and concentrations in the streams. To describe an equilibrium stage we only need phase equilibrium data and mass and energy balances. Its success not only lies in the fact that it is practical and consistent but also that it makes possible a first design attempt despite the complex heat and mass transfer phenomena that occur in the stage. However, for a practical process the equilibrium condition could hardly be achieved, so that the simulation results based on the ideal equilibrium stages are only a first attempt sometimes away from the real cases.

Instead, the rate-based model, that gives us a much more complete description of the equipment, naturally requires much more data due to the fact that it avoids the assumption of equilibrium and provides a more rigorous simulation. In addition to the information that the theoretical equilibrium stage model needs, it is important to have not only all the properties to describe the flow, the heat and mass transfer in the equipment, but also the phenomenological coefficients and all the data required to estimate them [3, 14, 20, 28]. For instance, viscosities, densities, thermodynamic factor, activity coefficients, diffusion coefficients, thermal diffusion coefficients and heat and mass transfer coefficients.

Before describing the two different methods of simulation of distillation mentioned above, it is necessary to introduce the concept of *stages*, namely those parts of the column that have well defined boundaries. For a tray column, we can regard a single tray as a stage and for a packed column we consider a packed section as a stage. The entire column is taken to consist of a sequence of such stages that are numbered starting at the top with the condenser as the stage 1.

A distillation stage for both theoretical models is represented in Fig. 1.6. The crucial difference between the theoretical model is the way in which the balance equations, knows as MESH equations, are used. In the equilibrium one, Fig. 1.6 (a), the balance equations are written around the stage as a whole. The composition of the leaving streams is related through an assumption that they are in equilibrium and by using an efficiency equation. This implies that the chemical potential of the components and the temperature of the vapor and the liquid have the same value. For the rate-based model, separate balance equations are written for each phase in the stage, one for the vapor phase and one for the liquid phase. The vapor and liquid bulks next to the interface are considered as a separate thermodynamic system. The stage has an interface region positioned between the liquid bulk and the vapor bulk, as shown in Fig. 1.6 (b).

There exits two different tendencies of modeling the vapor-liquid region: The film approach [3], where equilibrium between the two phases is assumed at the interface. This model is more commonly used. Taylor, Kooijiman and Hung [34] extended the initial development by adding the effects of tray pressure drop, entreinment, occlusion, and interlinks with other columns. The second one, is the integrated-interface approach [23, 24, 27, 28], where the interface is out of equilibrium. Until now, it has only been applied to simple mixtures like the ethanol-water and nitrogen-oxygen mixtures and has not been completely explored.

The main assumptions and equations of these models are discussed below. More elaborate descriptions of the models, including calculation routines and practical examples can be found in the book by Taylor and Krishhna [3], by Seader et. al. [29] and by

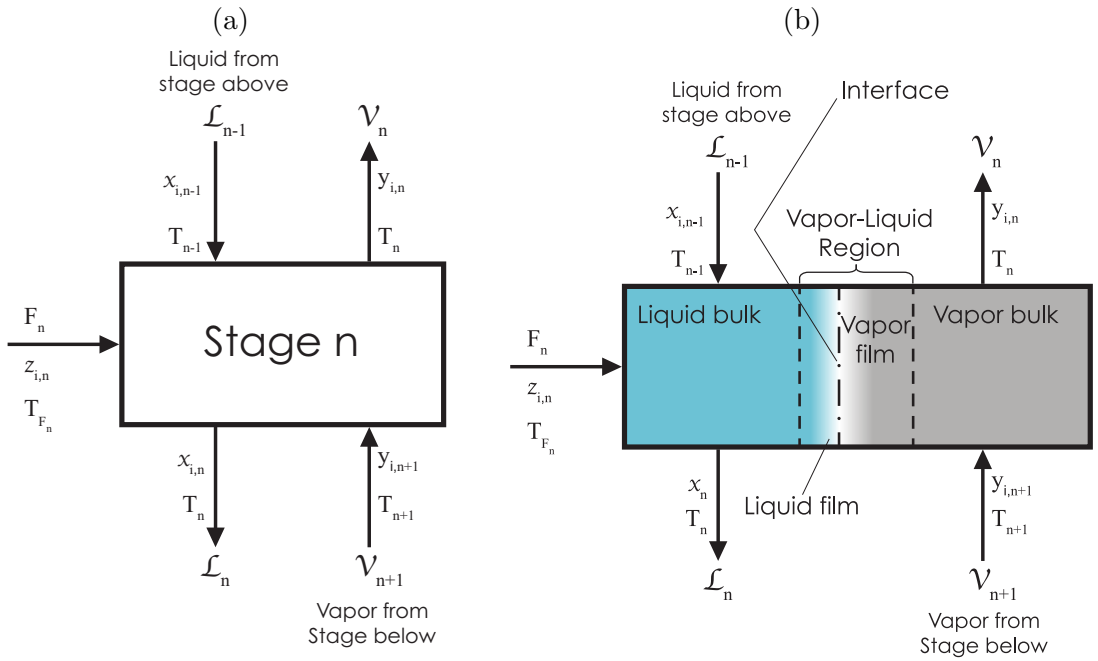

Figure 1.6: **Schematic diagram of an equilibrium and nonequilibrium stage.** (a) *General schematic representation of stage n.* F_n is the molar flow in the n-th tray, temperature T_{F_n} and with composition in mole fractions $z_{i,n}$. Also, entering stage n is interstage liquid from adjacent stage $n-1$ above at molal flow rate $\mathcal{L}_{n-1}$, temperature T_{n-1} and mole fraction $x_{i,n-1}$. Similarly, interstage vapor from adjacent stage $n+1$ below enters at molal flow rate $\mathcal{V}_{n+1}$, temperature T_{n+1} and mole fractions $y_{i,n+1}$. (b) *Schematic diagram of a nonequilibrium stage.* It is composed of three regions: the liquid bulk phase, the vapor bulk phase and the vapor-liquid region which includes the vapor and liquid films as well as the interface. The interface and the phases next to it are considered as a separate thermodynamic system. The labels are the same of those of (a).

Kjelstrup and Bedeaux [26]

Theoretical equilibrium stage model

The definition of efficiency is crucial in this model due to the fact that the trays in a real distillation column are not equilibrium stages. Efficiency is defined as a measure of how close the values of the compositions in the equilibrium separation approximate the ones that the real column or tray reach. Overall column or section inefficiencies are complicated functions of tray design, fluid properties, and operating conditions. There are many definitions of efficiency [3, 12, 29, 30, 35], but the most widely used in separations process calculations is the Murphree tray efficiency defined as:

$$\eta^{MV} = \frac{y_n - y_{n-1}}{y_n^* - y_{n-1}} \tag{1.3}$$

where the composition of vapor below the tray is y_{n-1}, the average composition of vapor above the froth is y_n and the mole fraction of component i in vapor in equilibrium with the liquid that is leaving the tray is y_n^*, determined from a bubble-point calculation for the liquid composition x_n. Note that such definition of efficiency assumes that vapor

streams are completely mixed and uniform in composition. An analogous efficiency may be defined for the liquid phase [29].

The set of equations that model a complete distillations column have been known as the MESH equations. MESH is the acronym commonly used when referring to the different types of equations that form the mathematical model. The initial $\mathcal{M}$ is related to *material balance equations*, which may appear in two forms. The total material balance for stage n and the component material balances

$$\mathcal{M}_n^T = \mathcal{V}_n + \mathcal{L}_n - \mathcal{V}_{n+1} - \mathcal{L}_{n-1} - F_n = 0 \tag{1.4}$$

$$\mathcal{M}_{i,n} = \mathcal{V}_n y_{i,n} + \mathcal{L}_n x_{i,n} - \mathcal{V}_{n+1} y_{i,n+1} - \mathcal{L}_{n-1} x_{i,n-1} - F_n z_{i,n} = 0 \tag{1.5}$$

where the subscripts $n-1$ and $n+1$ identify the upper and lower segments, respectively.

The E is related to the *equilibrium relations*, here modified to include the Muphree efficiencies defined by

$$E_{i,n} = \eta_{i,n}^{MV} K_{i,n} x_{i,n} - y_{i,n} - (1 - \eta_{i,n}^{MV}) y_{i,n+1} = 0 \tag{1.6}$$

where $K_{i,n}$ is the vapor-liquid equilibrium ratio.

The $\mathcal{S}$ is related to equations that serve to verify that *sum of the molar fractions* adds up to one, namely

$$\mathcal{S}_n^V = \sum_{i=1}^{n} y_{i,n} - 1 = 0 \tag{1.7}$$

$$\mathcal{S}_n^L = \sum_{i=1}^{n} x_{i,n} - 1 = 0. \tag{1.8}$$

The $\mathcal{H}$ is related to the *enthalpy balance equations* that read

$$\mathcal{H}_n = \mathcal{V}_n H_n^V + \mathcal{L}_n H_n^L - \mathcal{V}_{n+1} H_{n+1}^V - \mathcal{L}_{n-1} H_{n+1}^L - F_n H_n^F + Q_n \tag{1.9}$$

where $H_n^{L,V}$ are the enthalpies of the vapor and liquid streams leaving the nth stage, H_n^F is the enthalpy of the feed stream and Q_n is the duty.

In addition to the MESH equations, the reboiler and the condenser for the column must be considered. These stages differ from the other stages in the column by the heat source.

Rate-Based model

The film and the integrated-interface approaches, differ not only in the equilibrium assumption in the interface, but also in their definitions for the thickness of the interface region, the structure of their transfer equations and how to compute the rates of heat and mass transfer, as we will show below.

Film model. In the present approach two films are distinguishable, one of either side of the interface, through which the components diffuse across the interface. One also considers a heat flux through the films. The transfer rates through the interface regions are functions of transfer coefficients and of the differences in temperature or

composition between the bulk phases. The coupling of mass and heat flux is usually neglected.

The principal balance equations are as follow. We will use the superindex "π" to refer to liquid and vapor bulk or film. The mass balance for a component j in the liquid and vapor, $\mathcal{M}^{\pi}_{j,n}$, phases for an n-th column tray can be written as

$$\begin{aligned} \mathcal{M}^{L}_{j,n} : x_{j,F_n} F^{L}_{n} + x_{j,n-1}\mathcal{L}_{n-1} - x_{j,n}\mathcal{L}_{n} - \mathcal{N}^{L}_{j,n} &= 0 \\ \mathcal{M}^{V}_{j,n} : y_{j,F_n} F^{V}_{n} + y_{j,n+1}\mathcal{V}_{n+1} - y_{j,n}\mathcal{V}_{n} - \mathcal{N}^{V}_{j,n} &= 0. \end{aligned} \tag{1.10}$$

The last term in Eq. (1.10) represents the net gain or loss of component j in the phase due to vapor-liquid mass transfer. It is calculated as the integral of the local mass transfer rates J_j over the stage interface area A_n.

$$\mathcal{N}^{\pi}_{j,n} = \int_0^{A_n} J^{\pi}_{j,n} dA \tag{1.11}$$

The flux is positive when directed from the vapor to the liquid phase. In a steady-state operation there is no accumulation of mass in any part of the system, which means that mass transfer flows are equal on each side of the vapor-liquid transfer region

$$\mathcal{N}^{V}_{j,n} - \mathcal{N}^{L}_{j,n} = 0. \tag{1.12}$$

The total mass balances for the liquid and vapor phases, $\mathcal{M}^{L}_{n}$ and $\mathcal{M}^{V}_{n}$ are. respectively,

$$\begin{aligned} \mathcal{M}^{L}_{n} : F^{L}_{n} + \mathcal{L}_{n-1} - \mathcal{L}_{n} - \mathcal{N}_{t,n} &= 0 \\ \mathcal{M}^{V}_{n} : F^{V}_{n} + \mathcal{V}_{n+1} - \mathcal{V}_{n} - \mathcal{N}_{t,n} &= 0 \end{aligned} \tag{1.13}$$

The last term in Eq. (1.13) is the total mass flow, of the components in the mixture, $\mathcal{N}_{t,n} = \sum_{j=1}^{n} \mathcal{N}_{j,n}$.

The energy balance for the vapor and liquid phases, E^{V}_{n} and E^{V}_{n}, reads, respectively,

$$\begin{aligned} E^{L}_{n} : Q^{L}_{n} + F^{L}_{n} H^{L}_{F_n} + \mathcal{L}_{n-1} H^{L}_{n-1} - \mathcal{L}_{n} H^{L}_{n} - \mathcal{E}^{L}_{n} &= 0 \\ E^{V}_{n} : Q^{V}_{n} + F^{V}_{n} H^{V}_{F_n} + \mathcal{V}_{n+1} H^{V}_{n+1} - \mathcal{V}_{n} H^{V}_{n} - \mathcal{E}^{V}_{n} &= 0 \end{aligned} \tag{1.14}$$

where Q^{V}_{n} and Q^{L}_{n} represent the external heat transfer for the vapor and liquid phases, if it is the case, and H^{π} is the enthalpy of the stream. The last terms in Eq. (1.14) are the net energy flows across the liquid and vapor phases, respectively

$$\mathcal{E}^{\pi}_{n} = \int_0^{A} J^{\pi}_{e,n} dA \tag{1.15}$$

where J_e is the flux of energy in the phase:

$$J^{\pi}_{e} = J'^{\pi}_{q} + \sum_{k=1}^{c} J^{\pi}_{i} \bar{H}^{\pi}_{i} \tag{1.16}$$

The first term on the right hand side, J'_q, is the measurable heat flux, the second term is the energy transported by component k associated with the partial molar enthalpy, $\bar{H}_k$.

The energy balance around the vapor-liquid transfer region, E_n^I, in the steady state, shows that the net energy change in the two phases is zero, namely

$$E_n^I = \mathcal{E}_n^L - \mathcal{E}_n^V = 0 \tag{1.17}$$

Eqs. (1.10)–(1.17) are general for all steady-state distillation models.

Once we have described the film model we can now address the integrated interface approach.

Integrated interface model. In this approach, the films on the two sides of the interface plus the interface will then appear as three sequenced interfaces called *one integrated interface approach* defined by a single thickness. As a result of this assumption, the average coefficients can be defined for the effective interface without any assumption of phase equilibrium at the interface.

Due to the fact that the integrated interface approach is based on the NET approach, exits a direct coupling between the mass and thermal energy transfer rates exits. Another property of the present approach, is the addition of the interface transfer resistance. In the film approach, this resistance is assumed negligible resulting in a constant temperature on both sides of the interface. On the other hand, in the integrated interface approach, the resistance of the vapor liquid interface creates a temperature jump over the interface.

For convenience, once we have described the Theory of Nonequilibrium Thermodynamics in section 2.1.3, we will give the equations for this approach in Chapter 2, where we give the nonequilibrium description of the cases of study.

1.3 Simulation of a distillation column

The simulation of distillation column is a subject of intensive research [9,12,20,34,36–38]. The reasons are several. First, it is necessary to have a tool that allows one to model and predict properly the operation of the distillation column by using mass and energy balances, equilibrium relationships, rate correlations and physical and thermodynamic properties. The second reason rests on having a tool that helps in the design process, where many column configurations have to be tested. For example, stream flow rates, operating conditions and equipment size.

Another reason is to achieve the optimization of the distillation process, particularly for crude oil separations, increasingly important because of the high energy cost, the ecological requirements and the quality of the petroleum products [7, 35, 39–44]. Computer simulations and commercial softwares are the instruments for successfully completing such task.

The commercial softwares such as UniSim, Chempsep, HYSYS and Aspen Plus, to name a few, are useful for analyzing distillation column systems. These softwares allow one to improve recovery and separation capacity, and to decrease the rate of entropy production. Chempsep is a nonequilibrium modelling program written by Taylor et.

al. [34] only available for educational institutions. On the other hand, UniSim, licensed by Honeywell Process Solutions, enables one to create detailed high fidelity plant simulations for analyzing and optimizing its operation [31]. However, UniSim's database is focused especially on oil mixtures and crude operations. On the other hand, HYSYS and Aspen Plus present advantages which positioned them as the softwares most used in industrial and academic process simulations and designs. They have the infrastructure for continuous development and also updated data from the US National Institute of Standards and Technology (NIST), which provides the access to the best available experimental property data.

To date, the simulation of hydrocarbon distillation has been carried out with different strategies. For example, by using the thermodynamic analysis and the exergy approach [39, 40, 45, 46]. The latter one has become popular in distillation simulation because it is an effective tool for achieving efficient energy utilization and for providing optimum designs and operations. In 1996, Hinderink et. al. [47] integrated the subroutines of exergy calculations with the simulator Aspen Plus.

As we mentioned in section 2.2, in an effort to get better simulations, the NET approach was used in binary distillation systems [14–16, 23, 27, 28]. This approach not only gives a detailed mathematical formulation of the lost work from the entropy production rate at local equilibrium (see section 2.1.3), but also takes into account the coupling between heat and mass transfer in distillation.

In order to obtain results by using the NET approach, the computations are carried out in two stages. In the first one, it is necessary to simulate the performance of the distillation column with a commercial software or a computer simulator. In the second stage, the resulting distillation profiles are incorporated into the NET formulation. Until now, NET and the consideration of the coupling between heat and mass transfer are two issues not contemplated in hydrocarbon distillation not only due to the complexity of the mixture composition and the multitude of products derived from the mixture, but also because of the requirements of detailed data of the equipment and the operation.

In this thesis, we will address the importance of including the coupling between heat and mass transfer in the themodynamic driving forces for the description of the two chosen hydrocarbon distillation columns. The simulation of the performance of the distillation column will be with the Aspen Plus V8.4 software by using the rate-based model. In the second stage of our calculations, we will compute the entropy production rate from the global entropy balance EB, the exergy analysis Ex, and the NET approach.

It is worth pointing out that the simulation of the distillation column is a fundamental part of this thesis. Hence, the selection of a simulation software became a strategic decision. We chose the Aspen Technology due to the fact that it is an integrated system that includes specialized packages like the physical property methods and a complete data base for a wide variety of mixtures and equipment.

Our simulations will focus in existing columns with specific operation conditions. For this reason, we are interested in obtaining reliable results of the distillation units behavior by using the software effectively. To achieve this main objective, the steps shown in Fig. 1.7 must be followed. A general description based on three manuals of Aspen [48–50] is presented below.

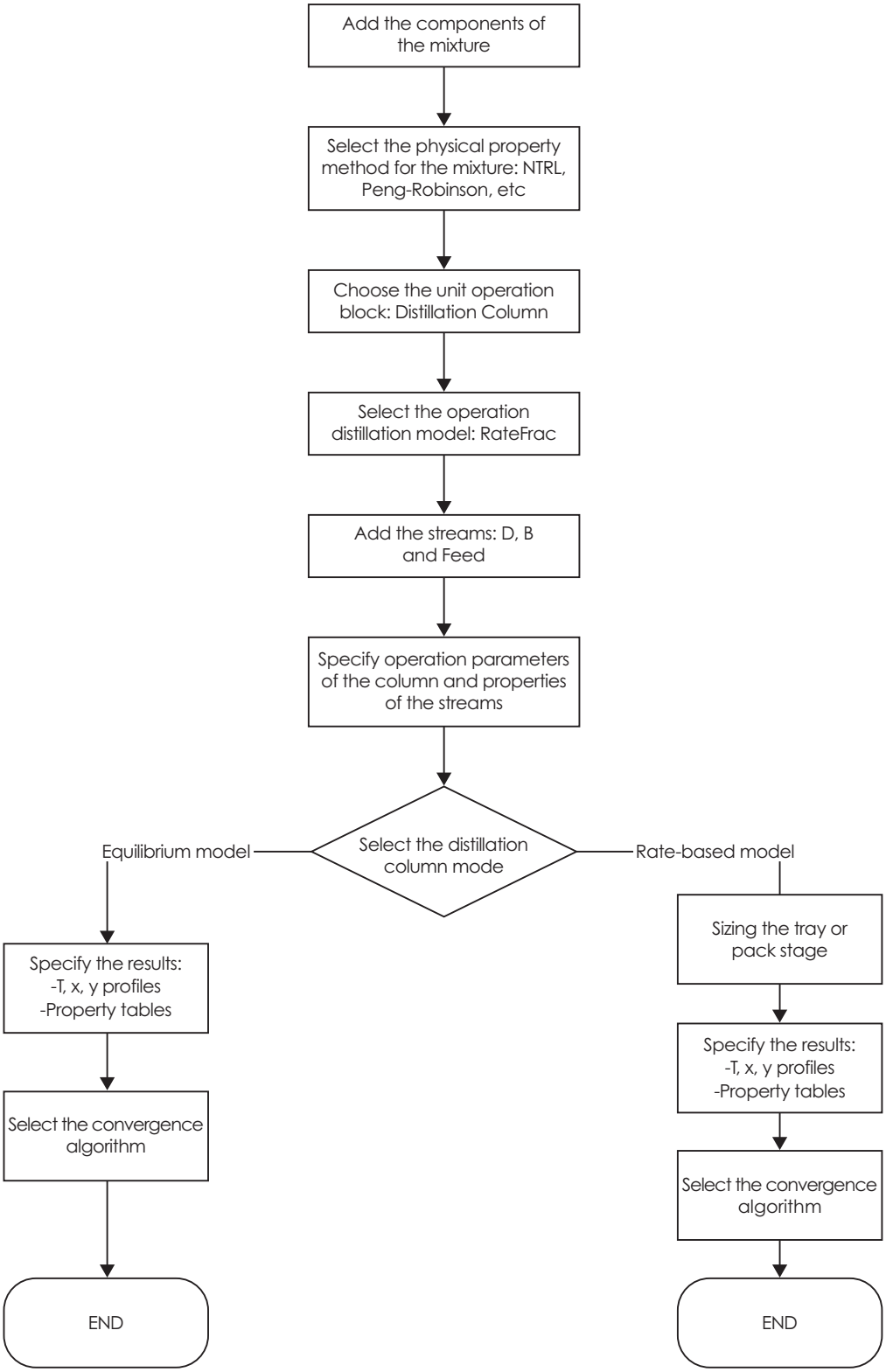

Figure 1.7: ***Flowchart of the simulation procedure.***

1. The first step is to define the mixture by adding the components in the flowsheet.

2. It is necessary to choose the appropriate set of physical properties according to the chemical characteristics of the the mixture involved in the distillation. A physical property method is a collection of methods and models that Aspen Plus uses to compute thermodynamic and transport properties. The most often requested thermodynamic properties are fugacities and enthalpy coefficients. Also, the necessary transport properties are viscosity, thermal conductivity, diffusion coefficient and surface tension.

   Each pure component property is calculated either from an empirical equation or from a semi-empirical correlation. The mixture properties are calculated by using appropriate mixing rules. In particular, selecting an adequate physical property method is crucial for obtaining reliable simulation results of the distillation process.

3. The third step is to choose the unit operation block. Here, one selects of the several types of columns the equipment of interest and also specifies all the parameters. For example, the number of stages in the column, the diameter and the sections of the column, the feed location, the flow rate of the distillate-bottoms product stream and the heat duty to the condenser or reboiler.

4. In the next step one can choose the unit operation model. In the presente work, for all the distillations column the RateFrac model was used since it allows us to simulate the distillation with the rate-based model. RateFrac is a rigorous model for simulating all types of multistage vapor-liquid fraction operation as an extractive distillation, a depropanizer column and a batch column. An important advantage of this model its extensive capability for sizing and rating trays and packings. It is possible to choose from several common tray types and random and structured packings. Also, Aspen Plus allows to specify different flow models to determine the bulk properties used to evaluate the mass and energy fluxes. Motions of vapor and liquid on the scale of a tray or packing, have a large effect on equipment performance. The usual flow pattern in separation equipment is contercurrent plug flow. These models are based on the stage model presented in Fig. 1.5 (b). The underlying assumptions are as follows: one dimensional flow of the vapor and liquid phases, that the vapor rising through the liquid within the stage is completely mixed and that there is no significant pressure gradient along the vapor and liquid flow directions. Further, the bulk properties for each phase are an average of the inlet and outlet properties. This method gives accurate results for packing columns, but is computationally intensive.

5. In the fifth step one adds the corresponding streams and identifies them with labels. Additionally, one has to specify the properties of the streams. For example, flow rate, composition, temperature and pressure.

6. At this stage of the simulation one has to decide the distillation column model, the theoretical equilibrium stage model or the rate-based model. In the first model, one only needs to give the number of stages and the location of the different

feeds. In contrast, the nonequilibrium model needs to contain a complete sizing of the tray or the packing of the column. For example, the number of trays in the different sections, the diameters of the sections, the tray height, the downcomer configurations, the hole diameters, the free areas and the weir heights. When the column is simulated in design mode, it is possible to let the software itself to determine these parameters. However, in a simulation of a real column, one must provide all these data.

7. Before finalizing the simulation, it is necessary to indicate what properties one wants to display in the report for the resulting stream (the distillate). For this thesis, where the main objective is to compute the entropy production with three approaches (EB, Ex and NET), we chose the report to include the transport coefficients, the molar entropy, the heat and mass transfer coefficients and other properties like densities and interfacial area.

8. In the last step, based on the mixture and the unit operation, one chooses the appropriate convergence algorithms. Aspen plus includes convergence algorithms as the inside-out algorithm that increase the robustness in distillation column computations [36]. Such algorithm consists of two nested iteration loops.

With this general description in mind, now we turn to explain the detailed information for each case of study.

1.3.1 The case of extractive distillation columns

As we mentioned previously in 1.2.2, we have analyzed two extractive distillation columns. The first one, was the Mendoza's case of study in his thesis [1]. Secondly, we will deal with the experimental rectifying column analyzed by Kjelstrup and de Koeijer [23]. For the purposes of this work, we will refer to the first column as "Ext M" and to the latter one as"Ext KR".

Ext M

The case analyzed by Mendoza, consists of a pilot size, extractive distillation column of the Chemistry Laboratory in the Universidad Nacional de Colombia. It processes 50 l/h of an ethanol-water mixture (EtOH-W), the entrainer (or solvent) used is ethylene glycol (EGL). The characteristics of the columns, the extractive and the solvent recovery column, $C1$ and $C2$ respectively, are specified in Table 1.2 [1] and the column configuration is illustrated in Fig. 1.2.

The purpose of the solvent entrainer in this extractive distillation column is to alter the relative volatility between ethanol and water, making ethanol to go to the top of the column and water go to the bottom of the column. The bottoms product, B, of the column is the mixture of water and the entrainer, and it is fed to another downstream solvent recovery column to separate these two components, so the entrainer can be recycled back to the extractive distillation column.

[1] In the rest of the thesis, the units of pressure will be Pa. However, since the thesis by Mendoza uses atm we decided to take the same units here to allow easy comparison.

Table 1.2: **Operating and stream characteristics of the extractive distillation column Ext M**. Here $C1$ is the extractive column, $C2$ the solvent recovery column, $F1$ is the EGL, $F2$ is the EtOH-W and B is the solvent recovered from $C1$.

Streams:	*C1* F1	*C1* F2	*C2 B*
Stage	3	16	
Pressure (atm)	0.734	0.734	
Vapor fraction	0	0	0
Temperature (K)	338.15	351.4	406.0
Flow (mol/s)	2.49	2.49	15
Molar fraction			
Ethylene glycol	0.999	0.0	0.77
Water	0.001	0.13	0.23
Ethanol	0.0	0.87	0
Column:	C1		C2
Condenser	Total		
Boiler	Partial (Kettle)		
Type of packing	Pall		
Size of packing (mm)	15.875		
Column diameter(m)	0.127		0.89
Number of segments	30		
Reflux ratio ($molar$)	0.5		1
Distillate rate ($kmol/h$)	0.786		3.457
Pressure (atm)	0.734		0.734

The extractive column has a double feed, $F1$, the entrainer in the 3-th stage and $F2$, the ethanol-water mixture in the 16-th stage. A total condenser (stage 1) and a partial reboiler (stage 30) were also used.

The property method utilized was the Non-Random Two Liquid (NRTL), which is appropriate for computing a highly non ideal liquid mixture. This method is described in detail in Appendix D.1. The operational model used was the RateFrac model.

For azeotropic distillation applications the convergence algorithm is the Newton algorithm together with the azeotropic initialization method. The Newton algorithm uses the classical Napthali-Sandholm approach [29]. This approach reduces the number of variables and solves column-describing equations simultaneously. The flow model that was employed for the column was the countercurrent plug flow.

The composition and temperature profiles obtained from both Mendoza's thesis and from the simulation by using the rate-based model, are shown in Fig. 1.8. As far as the temperature profiles are concerned, Mendoza found that the liquid and vapor temperatures were almost coincident while we find slight differences. In both liquid composition profiles, Mendoza's values and our computed values, the highest concentration of ethanol (x_{eth}) occurs at the top of the column and decreases abruptly in the 29th stage where the distillate is retired. Contrarily, the etrainer (x_{egl}) displays opposite behavior and after the feed stage its concentration decreases. So the qualitative behavior of ethanol and entrainer found by Mendoza is reasonably reproduced by our calculations. Note

that in the case of water the composition (x_w) also exhibits similar qualitative behavior in both calculations but in our case the water concentration increases more than Mendoza's values, reaching almost 0.4 molar concentration, which seems to be closer to the real operation of the column.

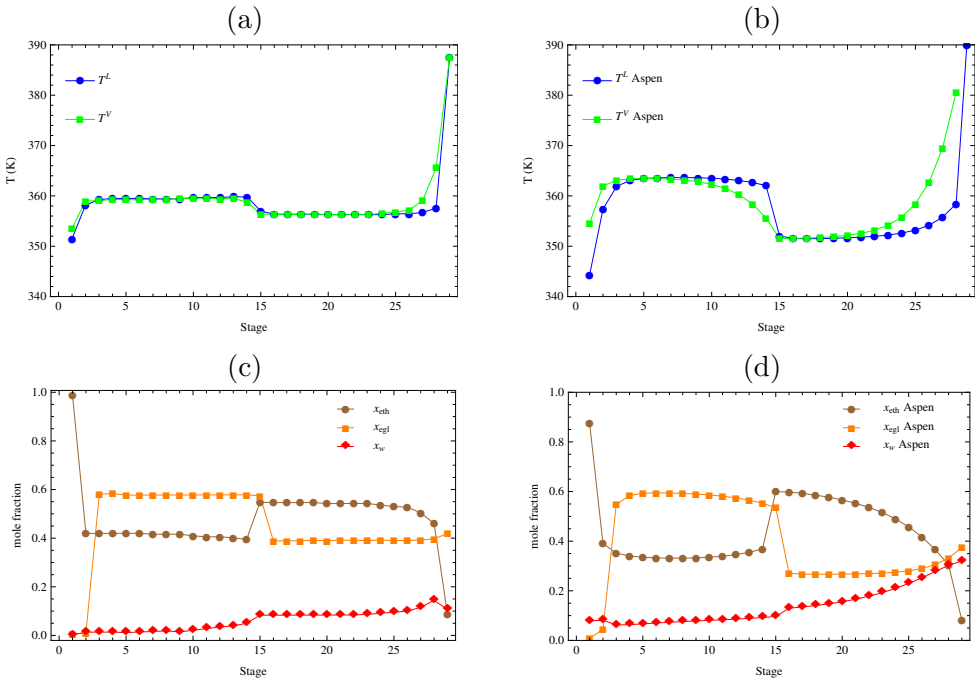

Figure 1.8: **Temperature and composition profiles of the ExtM column.** (a) Temperature profiles from Mendoza's thesis. Here T^L is the liquid temperature and T^V is the vapor temperature. (b) Temperature profiles by using Aspen Plus. The labels are the same as those of (a). (c) Liquid composition profile from Mendoza's thesis. Here x_{eth} is the ethanol mole fraction, x_{egl} is the ethyl glycol mole fraction, and x_w denotes the water mole fraction. (d) Liquid composition profile by using Aspen Plus. The labels are the same of (c).

Ext KR

In this case, we will use the experimental data of the pilot scale rectifying column of the Instituto Mexicano del Petroleo (IMP) studied earlier by Rivero in his PhD thesis [51]. The column consist of 12 trays and the feed stream is localized in the first stage. The feed flow is 0.331 mol/s of an ethanol water mixture. The column separated a water-ethanol feed of 0.331 mol/s with an ethanol mole fraction of 0.0710. The distillate had an ethanol mole fraction of 0.7073 and the bottom 0.0074.

Rivero measured in each tray the liquid temperature, the ethanol liquid and vapor mole fractions, x_e and y_{eth} respectively, and both the liquid and vapor flows. In his analysis, an important assumption is that the vapor temperature was deemed to be the same as the temperature of the liquid, $T_n^V = T_n^L$. A total condenser (tray 1) and a partial reboiler (tray 10) were also used. The characteristics of the column are given in Table 1.3. The experimental results so obtained allowed Kjelstrup and de Koeijer [23]

to avoid the assumption of equilibrium on all the trays and utilize the NET approach for describing the distillation column.

Table 1.3: **Operating and stream characteristics of the pilotscale rectifyng column Ext KR.** Here $F1$ is the ethanol water mixture feed.

Stream	F1
Feed stage	1
Vapor fraction	0
Feed	$0.331\,mol/s$
Temperature	$358.4\,K$
Feed mole fraction ethanol	0.0710
Column	
Condenser	Total
Boiler	Partial
Boiler duty (W)	13,489
Type of tray	Sieve
Tray's diameter (m)	0.15
Tray spacing (m)	0.127
Tray weir height (cm)	2.0
Number of flow passes	1
Number of segments	12
Distance between trays (m)	0.275
Total height (m)	2.90
Pressure (Pa)	0.994×10^5
Distillate (mol/s)	0.030
Bottom (mol/s)	0.301
Bottom pressure (Pa)	0.995×10^5
Distillate mole fraction	0.7073
Bottom mole fraction	0.0074

As in the previous case of Ext M, in our simulation with Aspen Plus we also utilized the NRTL Property Method (see Appendix D.1). The operational model used was the RateFrac model. The convergence algorithm was Newton algorithm together with the azeotropic initialization method. Finally, the flow model we took was the countercurrent plug flow.

In Fig. 1.9 we show the operational profiles as functions of the tray number. In the case of the temperature and liquid composition profiles, *(a)* and *(b)* respectively, we graph both experimental and the results obtained with the Aspen Plus software. The color code is as follows: brown and orange for the values obtained with the software, blue and green for the experimental data measured by Rivero. x_{eth} has an initial value of 0.707 that decrease during the distillation process to 0.007.

For the liquid and vapor flow profiles, *(c)* corresponds to Rivero's measurements and *(d)* to the computed values. Here, the color code is the following: we magenta for the vapor flow and blue for the liquid flow.

Note that once more the agreement between the experimental data and the results of simulation is very satisfactory.

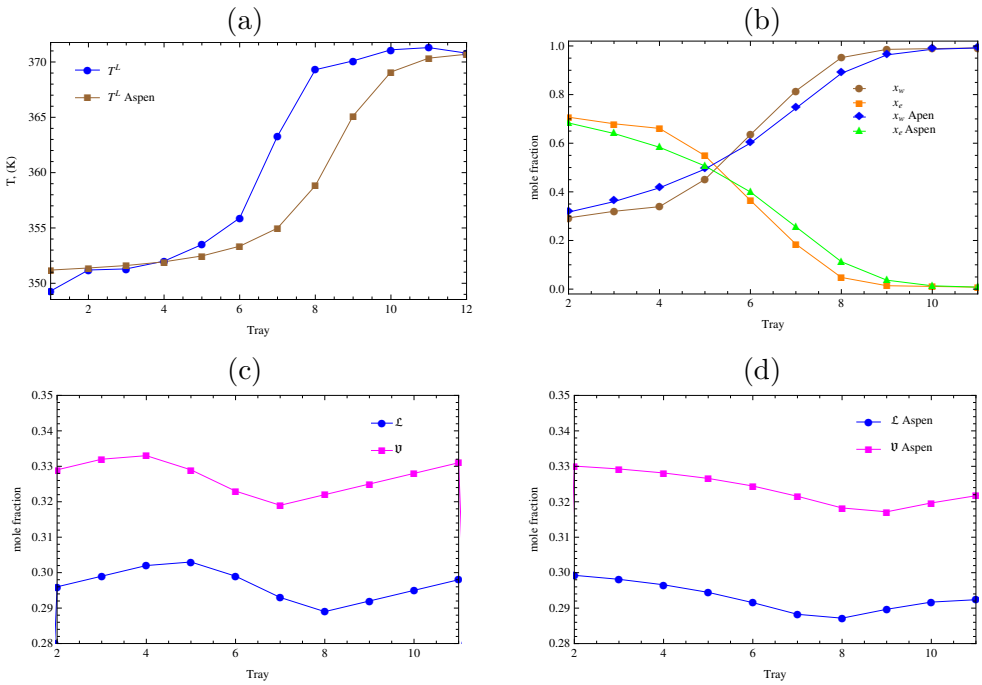

Figure 1.9: **Temperature, composition and flow profiles of the Ex KR column**. (a) Experimental data of the liquid temperature profile. Here T^L is the liquid temperature and T^V. (b) Liquid composition profile. Where x_w is the water mole fraction and x_e is the ethanol mole fraction. (c) Experimental flow profile. Here $\mathcal{L}$ is the liquid flow and $\mathcal{V}$ is the vapor flow. (d) Computed flow profile. The labels are the same of (d).

1.3.2 The case of the depropanizer column

As a strategy to correctly simulate a mixture of hydrocarbons, we first considered a prototype example, namely the depropanizer column described and previously simulated (with Chemsep) by Taylor and Krishna [3]. The characteristics of the column are given in Table 1.4. In this column, the main objective is to isolate propane from a mixture containing butane and other components. The column consists of 35 theoretical stages (trays) and has been designed to separate 1000 mol/s of a four component mixture containing ethane, propane, n-butane and n-pentane. Furthermore, the system is such that it contains 300 mol/s n-propane and 500 mol/s n-butane so that there is no more than 3.5 mol/s of n-propane present at the bottom product and no more than 3.5 mol/s of n-butane is present in the distillate. The bottom product flow rate is 600 mol/s and the reflux ratio is 2.5. Stage 16 is the feed stage. The operation takes place at a pressure of 1500 kPa, a temperature of 298 K and a 2.5 reflux ratio. For simplicity we will neglect heat and pressure losses in the column.

The property method utilized is the Peng-Robinson method, which is recommended for refinery and petrochemical applications due to its capacity for treating hydrocarbons and light mixtures. This method is explained in Appendix D.2. The operational model used was the RateFrac model. The convergence algorithm was the Gibbs algorithm and finally the flow model was the countecurrent plug flow.

Table 1.4: **Operating and stream characteristics of the depropanizer column**. Here F is the hydrocarbon mixture feed, D the distillate and B the bottom current.

Streams:	F	D	B
Stage	16	1	35
Pressure (kPa)	1500	1500	1500
Vapor fraction	0	1	0
Temp. (K)	298.15	308.15	378.15
Flow (mol/s)			
Ethane	100	100	1.5×10^{-3}
Propane	300	296.7	3.329
n-Butane	500	3.328	496.7
n-Pentane	100	9.2×10^{-3}	100
Total flow	1000	400	600
Sections:	1	2	
First stage	2	16	
Last stage	15	34	
Column diameter(m)	4.820	6.170	
Type tray	Sieve	Sieve	
Number of flow passes	5	5	
Tray spacing (m)	0.5	0.5	
Hole pinch (m)	0.01807	0.01685	

The operational profiles of the depropanizer column appear in Fig. 1.10. Clearly, our computed values obtained with Aspen Plus follow the trends given by Taylor and Krishna [34] and yield reasonable quantitative agreement.

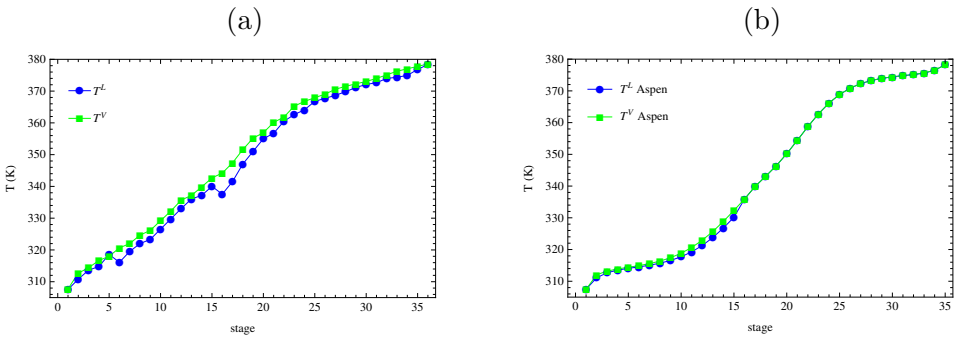

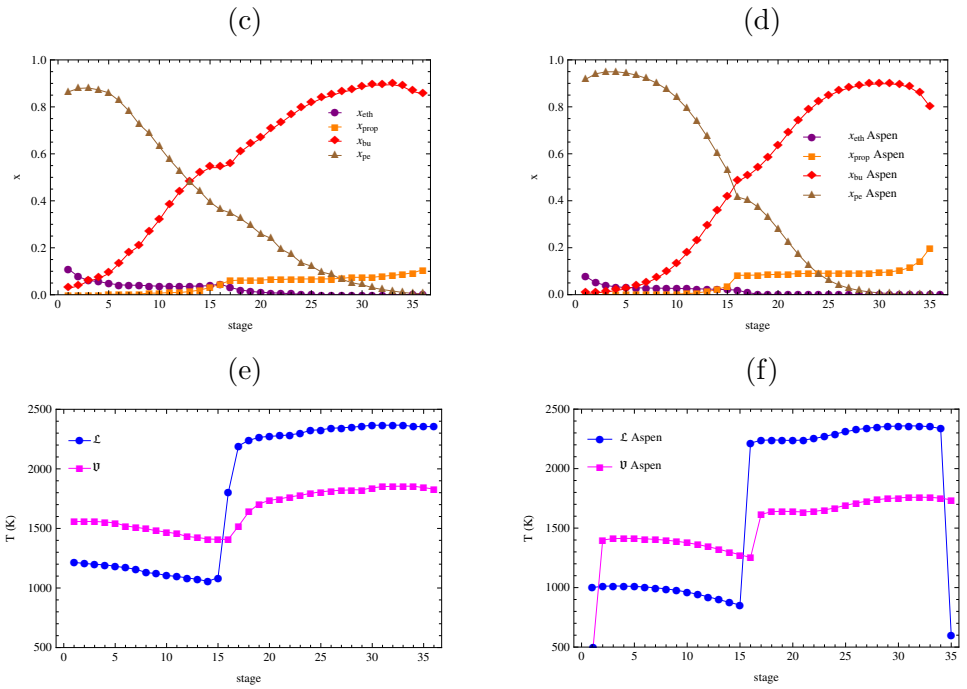

Figure 1.10: **Temperature, composition and flow profiles of the depropanizer column**. (a) Temperature profiles from Taylor and Krishna's simulations. T^L is the liquid temperature and T^V is the vapor temperature. (b) Temperature profiles by using Aspen Plus. The labels are the same as those of (a). (c) Liquid composition profile from Taylor and Krishna's simulations. Where x_{eth} is the ethane mole fraction, x_{prop} is the propane mole fraction, x_{bu} is the n-butane mole fraction and x_{pen} is the n-pentane mole fraction. (d) Liquid composition profile by using Aspen Plus. The labels are the same of (c). (e) Flow profile from Taylor and Krishna's simulations.The label $\mathcal{L}$ stands for the liquid flow, the label $\mathcal{V}$ is for the vapor flow. (d) Flow profile by using Aspen Plus. The labels are the same of (e).

1.3.3 The case of the batch column

The second system with a hydrocarbon mixture consists of a (laboratory scale) batch distillation column used in the Instituto Mexicano del Petroleo (IMP) to study and characterize a weighed sample of Mexican crude oil. This column, shown in Figs B.1, employs 18 trays and the distillate may be collected at a constant rate. The typical equipment consist of a heated or Engler flask containing a calibrated thermometer of suitable range to measure the temperature of the vapor at the inlet to the condensing tube, an inclined brass condenser in a cooling bath using a suitable coolant, and a graduated cylinder for collecting the distillate.

The method used to characterize this oil and its derivatives (petroleum fractions or cuts) obtained in the distillation process is the Test Method for Distillation of Crude Petroleum D2892-10 [52] explained in Appendix B. The test method involves operating at three different pressures, namely an atmospheric pressure (101.3 kPa) for the light boiling fractions and two other pressures (13.33 kPa and 2.66 kPa) for the high boiling fractions. Each of these three operations may be taken as a separate distillation process. Here, for the sake of having access to all the necessary data, we will restrict to the distillation taking place at 13.33 kPa, a reflux ratio of 2:1 and a maximum temperature

of 453 K. The necessary data for the simulation is presentend in Table 1.5 and A.4.

Table 1.5: **Operation, stream and batch column data**.

Stream characteristics:	
Stage	16
Pressure (kPa)	13.33
Vapor fraction	0
Temperature (K)	303.15
Flow (L/min)	0.085
Charge (g)	31,770

Fractionating column:	
Reboiler	Kettle
Condenser	Total
Number of stages	18
First stage	2
Last stage	17
Feed to stage	18
Column internals	Sieve tray
Column diameter (m)	0.80
Number of flow passes	4
Tray spacing (m)	0.09
Hole pinch (m)	0.0127

A key point in this case of study, not feasible in the theoretical case of the depropanizer column, is that we will be able to combine real operation data of the column with the Aspen simulation to obtain the corresponding composition, temperature and flow profiles. This real data are the TBP curve provided by the IMP after its performed the characterization of the mixture. We show the laboratory distillation data in Appendix C.

Due to the fact that in this mixture there are very many components, its simulation is much more complex than in the previous cases. Here, the complete characteristics of the Mexican oil mixture are given through the crude assay presented in Appendix A. The first step in the simulation consists in defining the lighter ends including their molar fractions in the mixture. This information has to be fed into the *components specifications* flowsheet of the software. For our system, the IMP has identified all the components of the first and second fractions of the oil mixture by gas chromatography. For the first fraction there are 34 different components and for the second one there are 112. We took the components with the highest concentration, namely n- pentane, 2 - metilpentane, 3 - metilpentane, and n-hexane.

The next step is to specify the distillation curve. We selected the TBP and entered the data shown in Table A.4. Additionally, we added also the API gravity data. As required by the software we had to specify that for the present system we are simulating only one blend (Maya oil alone).

With the above information one may now generate the pseudo components. This may be chosen in the software either by default or by setting them manually. Based on the IMP information we chose the 8 pseudo components identified experimentally in

the Mexican oil mixture. However, since four of the heaviest pseudo components are present in very low concentration, we finally worked only with the 4 cuts that volatilize in the operation up to a pressure of 13.33 kPa, corresponding to 28 % of the mixture.

In Fig. 1.11 displays the temperatures, flows and composition profiles of the batch column. We stress that in this case we have no other data or calculations to compare with. However, the successful comparisons of the previous cases suggest that we may use such profiles with confidence in our latter developments.

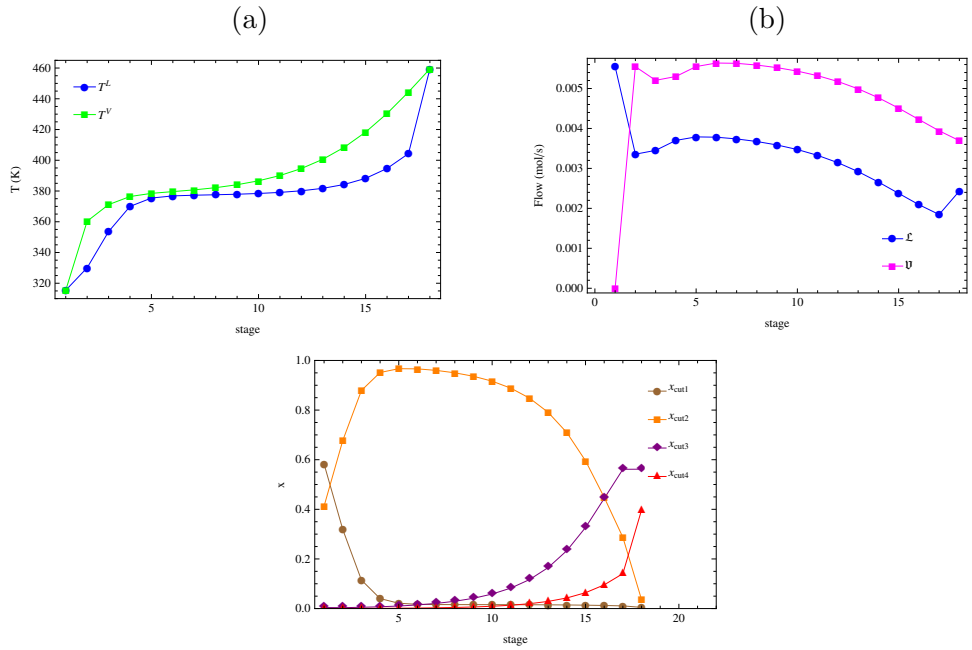

Figure 1.11: **Temperature, composition and flow profiles of the batch column**. (a) Liquid and vapor temperature profiles. T^L is the liquid temperature and T^V is the vapor temperature. (b) Flow profile.The label $\mathcal{L}$ stands for the liquid flow, the label $\mathcal{V}$ is for the vapor flow. (c) Liquid composition profile. Where $x1$ is the pseudo component 1 mole fraction, $x2$ is the pseudo component 2 mole fraction, $x3$ is the pseudo component 3 mole fraction and $x4$ is the pseudo component 4 mole fraction.

1.4 Thesis description

The thesis is organized as follows. The next Chapter we will explain the nonequilibrium description. We begin by providing the theoretical framework, the thermodynamic description of the system and finally the exergy analysis and the global entropy balance approach. In Chapter 3, we will present a comparison of the results for the global entropy production rate as given by the film and integrated interface models, the present approach, the exergy and the global entropy balance analysis. Furthermore, we will display the explicit inclusion of the coupling between heat and mass transfer in the vapor thermodynamic force and the entropy production rate. The thesis ends with Chapter 4 in which some discussion and concluding remarks are presented.

Chapter 2

Nonequilibrium description

This chapter is devoted to the theoretical determination of both the local entropy production rate and the global entropy production rate in the four cases of study. We begin by providing the theoretical framework behind our later calculations. In particular, we discuss its connection with both nonequilibrium models, namely the film approach and the integrated interface approach, utilized in the extractive distillation columns to describe the transport across the system. Secondly, we will describe the approach that we employed in the case of the hydrocarbon distillation columns.

2.1 Theoretical framework

The conventional thermodynamic theory is dedicated to the macroscopic description of the equilibrium states of a system, with experimentally determined properties and a relationship between various intensive and extensive equilibrium state variables. It is a theoretically well founded framework and in practice a very successful method, but restricted to equilibrium situations. Nevertheless, almost all the processes taking place in nature are irreversible and occur in systems that are not in equilibrium states. Thus, classical thermodynamics has been extended to include nonequilibrium systems with basic postulates that provide the NET. But, before entering fully to the theory, it is important to understand the connection of the second law efficiency with the *exergy loss* and the *entropy production*.

2.1.1 Second law analysis

It is common that the energy conversion processes are evaluated based on amounts of energy. A common way of assesing process performances is to divide the amount of useful energy that is leaving the process by the amount of useful energy that is added to it. The resulting quantity is called the energy efficiency or the First law efficiency. This efficiency is based only on quantities of energy alone.

The First law establishes the equivalence between heat and work but is silent about the restrictions on the transformation of one into the other. The role of the Second law of the thermodynamics is to place such limitations and to reflect the property that natural processes evolve spontaneously in one direction only.

Nowadays, it is increasingly argued that processes should be evaluated using criteria that also take the quality of energy into account, such as the exergy efficiency and the Second law efficiency. In addition, they can be used to locate process inefficiencies and thus indicate where in the process possible improvements can have largest impact. A process analysis based on this approach is known as Second law analysis.

Numerous examples applied in distillation processes exists that demonstrate the potential of the Second law analysis, see for example [38, 40, 53].

2.1.2 Exergy analysis

It is an important supplement to the NET approach and a useful benchmark. The exergy of a process is defined as its potential to perform work. Also, exergy is a broadly useful concept both in engineering and in proper resource management for reducing environmental destruction. Exergy expresses simultaneously the quantity and quality of energy; in this instance, quality is the ability to produce work under the conditions determined by the natural environment [54].

For each work consuming process, there exists a least amount of energy that must be supplied, defined by the Second law of thermodynamics, which is called the ideal work, w_{ideal}. This also is the minimum amount of net exergy input. But in practice, the amount of consumed work w is always larger that w_{ideal}. The difference between these two amounts is called lost work, $w_{loss} = w - w_{ideal}$ or exergy loss, Ex_{loss}. Exergy calculates the w_{ideal} and the w_{loss} from values at the system boundaries. In contrast to energy, exergy is not conserved and decreases in irreversible processes.

In all real processes, exergy loss always accompanies exergy transfer. The exergy loss in a continuous process is the difference in the exergy before and after the process. So, the exergy loss relative to the surroundings is [55],

$$Ex_{loss} = w - w_{ideal} = T_0 \left(\frac{dS_{irr}}{dt} \right), \tag{2.1}$$

where T_0 is the reference temperature and $dSirr/dt$ stands for the total entropy production. The exergy loss occurs due to the deviation of thermal parameters and the chemical composition between the product and the components of the environment. The thermal state and chemical composition of the natural environment represent a reference level (dead state) for the calculation of exergy. Note that exergy is a function of both the physical properties of a resource and its environment [54].

Eq. 2.1 is the Gouy-Stodola theorem. According to the second law, $Ex^{loss} \geq 0$. If the exergy loss increases, the net heat duty has to increase for the process to occur. Consequently, smaller exergy loss means less waste heat or thermodynamic imperfections. Exergy is a unifying concept of many forms of energy, such as heat, mechanical work, and chemical energy. We can derive the exergy relation from the energy and entropy balances for the composite system. In this thesis we will focus on computing the entropy balance.

2.1.3 Theory of Nonequilibrium Thermodynamics

Not only Nonequilibrium thermodynamics describes transport processes in systems that are out of global equilibrium, but also is constantly being applied in new contexts. In

particular, it is a necessary theory for a precise description of systems that exchange heat and mass. The principal aims of this theory are threefold. First to provide a thermodynamic support to the classical transport equations of heat, mass and momentum, as the Fourier's law and Fick's relation. A second objective is to propose a systematic description of the coupling between thermal and mass effects, as present in the Soret and Dufour effects. A third objective is the study of stationary nonequilibrium states, whose properties do not depend on time, but which are characterized by a non homogeneous distribution of the variables and non vanishing values of fluxes [56]. As a result, the distillation operation is an excellent candidate to be described by Nonequilibrium thermodynamics.

The theory is based on the hypothesis of *local equilibrium*: a volume element in a nonequilibrium system, which is small enough for a continuum development but big enough to neglect microscopic effects, is considered to obey locally the laws of equilibrium thermodynamics.

This important hypothesis states that at a given instant of time, equilibrium is achieved in each individual volume element but the state of equilibrium is different from one volume element to the other. Additionally, the local and instantaneous relations between thermodynamic quantities in a system out of equilibrium are the same as for a uniform system in equilibrium. [57].

The consequences of this assumption are that all the variables defined in equilibrium are defined outside equilibrium and are allowed to vary with time and space. Also, the local state variables are related by the same equations of state as in equilibrium. This means, in particular, that the Gibbs' relation between entropy and the state variables remains locally valid for each value of the time and the position. For example, in the case of an N-component fluid of total mass m (which will serve to illustrate the formulation), the local Gibbs' equation will be written as

$$T\,ds = du + p\,dv + \sum_{i=1}^{N} \mu_i dw_i \tag{2.2}$$

where s is the specific entropy, u is the specific internal energy, p the pressure of the system, v is the specific volume related to the mass density ρ by $v = 1/\rho$, μ_i is the chemical potential and w_i is the mass fraction of substance i.

The second law of the thermodynamic does not give a rate for the time variation of the entropy. At this stage it is convenient to introduce the entropy production rate, σ, and write the following balance relation

$$\rho\frac{ds}{dt} = -\frac{\partial}{\partial x}J_s + \sigma \tag{2.3}$$

where J_s is the entropy flux, that is the entropy crossing the boundary surface per unit area and unit time.

We shall now find an explicit expression for σ by combining balance equations, the first law of thermodynamics and the local form of the Gibbs equation. To this end we now quote the balance equations for mass, momentum and energy of the mixture. The following bibliography [57, 58] is recommended to review the full derivation of those equations.

The mass conservation equations reads

$$\rho \frac{dv}{dt} = \nabla \cdot \mathbf{v}, \tag{2.4}$$

where $\mathbf{v}$ is the mass average velocity defined by $\mathbf{v} = 1/\rho \sum_{i=1}^{N} \rho_i w_i \mathbf{v}_i$. Here, $\mathbf{v}_i$ is the velocity of substance i and ρ_i is the mass density of component i.

The balance equation for the amount of substance i in terms of the mass fraction, w_i, is

$$\rho \frac{dw_i}{dt} = -\nabla \cdot \mathbf{J}_i + \Lambda_i, \tag{2.5}$$

where $\mathbf{J}_i$ is the diffusion flow, relative to $\mathbf{v}$ and Λ_i the rate of production of substance i by chemical reactions. The sum of diffusion flows of all the substance is zero $\sum_{i=1}^{N} \mathbf{J}_i = 0$.

The momentum balance equation is given by

$$\rho \frac{d\mathbf{v}}{dt} = -\nabla \cdot \mathbf{P} - \sum_{i=1}^{N} \rho_i \mathbf{f}_i, \tag{2.6}$$

where $\mathbf{P}$ is the pressure tensor and $\mathbf{f}_i$ is the external body force on component i.

The internal energy balance reads

$$\rho \frac{du}{dt} = -\nabla \cdot \mathbf{J}_q - \mathbf{P} : \mathbf{V} + \sum_{i=1}^{N} \mathbf{J}_i \cdot \mathbf{f}_i, \tag{2.7}$$

where $\mathbf{J}_q$ is the heat flux and $\mathbf{V}$ is the symmetric part of the velocity gradient tensor.

The set of equations (2.4)–(2.7) describes the time evolution of the system. In other words, how the basic properties change with time at every point in space. The balance equations are next combined with the Gibbs equation, Eq. (2.2). This leads us to an explicit equation for the entropy evolution. Differentiation of Eq. (2.2) with respect to time yields

$$\rho \frac{ds}{dt} = \frac{\rho}{T} \frac{du}{dt} + \rho \frac{p}{T} \frac{dv}{dt} - \frac{\rho}{T} \sum_{i=1}^{n} \mu_i \frac{dw_i}{dt}. \tag{2.8}$$

After substituting Eqs. (2.4)–(2.7) into Eq. (2.8), we have

$$\rho \frac{ds}{dt} = -\frac{1}{T}(\nabla \cdot \mathbf{J}_q) - \frac{1}{T}(\mathbf{P} : \mathbf{V}) + \frac{1}{T} \sum_{i=1}^{N} \mathbf{J}_i \cdot \mathbf{f}_i + \sum_{i=1}^{N} \frac{\mu_i}{T}(\nabla \cdot \mathbf{J}_i) - \frac{1}{T} \sum_{i=1}^{N} \mu_i \Lambda_i \tag{2.9}$$

By comparing the above equation with Eq. (2.3) we can identify the entropy flux in the system, namely

$$J_s = \frac{1}{T} \mathbf{J}_q + \sum_{i=1}^{N} \bar{s}_i \mathbf{J}_i, \tag{2.10}$$

where $\bar{s}_i$ is the partial entropy of substance i. Hence, the entropy production rate, σ, turns out to be given by

$$\sigma = \nabla \frac{1}{T} \cdot \mathbf{J}_q - \frac{1}{T} \mathbf{P} : \mathbf{V} - \sum_{i=1}^{N} \left(\nabla \frac{\mu_i}{T} - \mathbf{f}_i \right) \cdot \mathbf{J}_i - \frac{1}{T} \sum_{i=1}^{N} \mu_i \Lambda_i. \tag{2.11}$$

In the above equation, the entropy production rate is the sum of four separate contributions due to heat transfer, mass transfer, momentum transfer, and chemical reactions. Although not explicitly shown in the case of the chemical reactions contribution, σ is found to consist of a sum of products of thermodynamic fluxes which we will generically refer to as J_α and thermodynamic forces referred to as X_α [16, 26, 54, 56, 58–61]. Note that the thermodynamic forces are not forces in the mechanical sense, but they are quantities generally related to the gradients of the intensive variables. In this formulation the second law may be expressed as

$$\sigma = \sum_\alpha J_\alpha X_\alpha \geq 0. \tag{2.12}$$

The choice of thermodynamic forces must be made so that in the equilibrium state when the thermodynamic forces vanish, the entropy production must also vanish. From the phenomenology, it is known that each of the thermodynamic fluxes is given by a linear combination of all thermodynamic driving forces of the same tensorial character, namely

$$J_\alpha = \sum_\beta l_{\alpha\beta} X_\beta. \tag{2.13}$$

Here $l_{\alpha\beta}$ is the coupling (phenomenological) coefficient that couples flux α with the driving force β.

Equation (2.13) expresses the relation between causes (forces) and effects (the fluxes) in terms of conductances $l_{\alpha\beta}$. It may also be written in terms of resistances $r_{\alpha\beta}$ as

$$X_\alpha = \sum_\beta r_{\alpha\beta} J_\beta. \tag{2.14}$$

The coefficients $l_{\alpha\beta}$ and $r_{\alpha\beta}$ are also referred to as Onsager coefficients. They are related to a transport coefficient such as thermal conductivity or mass diffusivity, and may be functions of local state parameters such as temperature T and pressure P, as well as the nature of the system [57].

The coefficients with the same indices $l_{\alpha\alpha}$, known as direct coefficients, relate the conjugate force X_α and its corresponding flux J_α, as in Navier-Newton's law in which the stress tensor is coupled to the velocity gradient through the shear viscosity. On the other hand, the cross coefficients $l_{\alpha\beta}$ with $\alpha \neq \beta$ link different transport processes, for instance in thermal diffusion in which a mass flow occurs due to a temperature gradient [16] and both are linked through the Duffour coefficient.

Onsager's fundamental theorem states that with a proper choice of fluxes and forces, the matrix of phenomenological coefficients is symmetric, so that the corresponding cross coefficients are equal. It is based on microscopic reversibility, which implies that the probability of a microscopic process proceeding in one direction is the same as in the reverse direction [58]. Another feature of the Onsager reciprocal relations is that they are independent of the state of a system or of any other macroscopic assumptions. The explicit equations for the Onsager relations depend on the nature of the system, and various kinds of couplings between fluxes and forces are possible. Nevertheless, all the phenomenological coefficients with similar and dissimilar indices must satisfy the conditions

$$l_{\beta\alpha} = l_{\alpha\beta}; \quad l_{\alpha\alpha} \geq 0; \quad l_{\alpha\alpha} l_{\beta\beta} \geq l_{\alpha\beta}^2 \qquad (\beta \neq \alpha) \tag{2.15}$$

These symmetry properties have been widely applied in the treatment of coupled irreversible processes taking place at the macroscopic scale even very far from equilibrium.

For the purposes of this thesis, we will be concerned only with heat and mass transfer and their coupling. Hence momentum transfer and chemical reactions transfer will be omitted in what follows. Also, the presence of external forces will be disregarded. With such simplifications, the entropy production σ for an N-component mixture of Eq. (2.11) reduces to

$$\sigma = \nabla \frac{1}{T} \cdot \mathbf{J}_q - \sum_{i=1}^{N} \nabla \frac{\mu_i}{T} \cdot \mathbf{J}_i. \tag{2.16}$$

2.1.4 Calculating the entropy production

Two different methods for explicitly calculating the entropy production can be distinguished: the first one considers process units as black boxes while the second one is based on the NET approach.

The black box approach, which is the simplest one, is based purely on a balance of the ingoing and outgoing process streams. That is,

$$\frac{dS_{irr}}{dt} = \sum_i F_{i,out} s_i - \sum_i F_{i,in} s_i - \sum_i S_{i,add}. \tag{2.17}$$

Here, $F_{i,out}$ labels the outgoing material streams, $F_{i,in}$ labels the incoming material streams, and $S_{i,add}$ are the directly added or removed amounts of entropy. The last term contains contributions of thermal energy fluxes and radiation. This approach can be applied both to single process units as well as to entire processes.

Contrary to the black box analysis, the NET approach focuses on the phenomena that are occurring inside a process unit. What one does is to calculate the lost work from the total entropy production and this latter is found by integrating the local entropy production rate σ over the volume of the system, namely

$$\frac{dS_{irr}}{dt} = \int \sigma \, dV. \tag{2.18}$$

The local resolution of dS_{irr}/dt is beyond the scope of exergy analysis, where only a balance around the outside of the process is conducted. On the other hand, the explicit expression of σ derived in the NET approach can be used to understand the origin of the entropy production in a volume element or the lost work in such volume. In comparison with the exergy analysis, the NET approach requires a more detailed description of the transport processes in the system being analyzed.

2.2 Thermodynamic description of the system

The distillation process may be analyzed in three different scales. The first one embodies the whole column as we showed in Figure 1.1. The analysis in this scale allowed us to obtain the operational profiles in Chapter 1. The intermediate scale is the one associated

to a stage as illustrated in Fig. 2.1 *(a)*. Finally, the smallest scale is the region around the liquid-vapor interface, depicted in Fig. 2.1 *(b)*.

The separation of the N-component mixture occurs when the liquid and vapor phases are in contact and exchange heat and mass. This includes such contact within the stage, bubbles and droplets. In a distillation column stage, one may distinguish three regions, namely, the liquid bulk, the vapor bulk and the vapor-liquid region which include the vapor film, the liquid film and the interface.

The mass transfer rates across the liquid-vapor interface vary as a bubble rises on one stage, but due to the fact that the operation of the column reaches a stationary state, we will consider the average mass and heat transfer rates for each stage. The mass transfer rates are constant through the films, while the heat transfer rate has a discontinuity due to the enthalpy differences between liquid and vapor. The transfer rates through the interface regions are functions of transfer coefficients and of the differences in temperature or composition between the bulk phases. We also have adopted the sign convention shown in Fig. 2.1 *(b)*, that the positive direction of transport is from vapor to liquid.

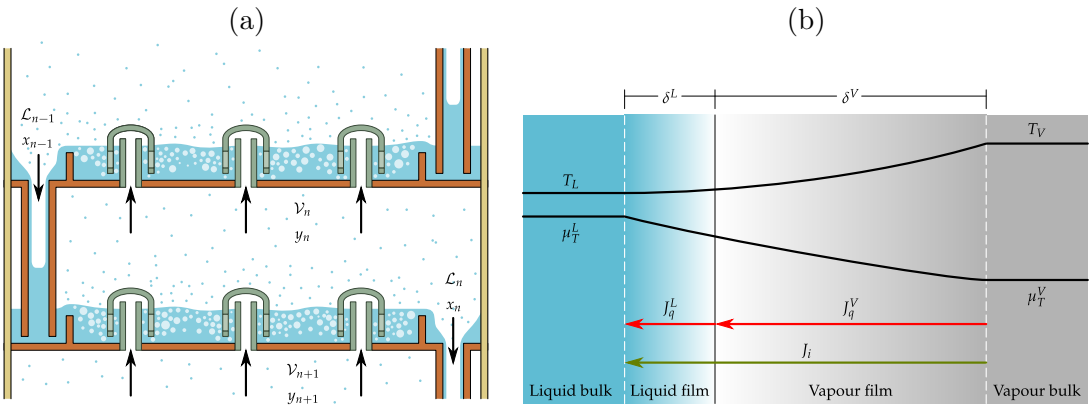

Figure 2.1: **The system**. (a) This is a representative scheme of a tray (stage) in the distillation columns studied with a high concentration of vapor. (b) We show a representation of a nonequilibrium stage.

According to the literature [20, 23, 24], mass transport accounts for the largest part of the entropy production rate on a stage. Hence, the contributions from turbulence, pressure drop, and mixing will be neglected.

Once we have the thermodynamic description of the system we can now address the entropy production rate in a stage. This quantity, besides being the sum of the contributions of the vapor-liquid region also includes the liquid an vapor bulks, namely

$$\frac{dS_{irr}^{n}}{dt} = \sum_{\pi=L}^{\pi=V} \left(\frac{dS_{irr}^{\pi,bulk}}{dt} + \frac{dS_{irr}^{\pi,film}}{dt} \right). \tag{2.19}$$

The global entropy production rate in the films is obtained by integrating the local entropy production, σ^{π} over the volume of the system, namely

$$\frac{dS_{irr}^{\pi}}{dt} = \int_{V^{\pi}} \sigma^{\pi} dV = \int_{0}^{A} \int_{0}^{\delta^{\pi}} \sigma^{\pi} dz dA, \tag{2.20}$$

where δ^π is the film thickness and A is the interface area.

Then, our first task is to determine σ^π. This quantity is computed as the sum of the products of the (local) conjugate fluxes, J_α, and thermodynamic driving forces, X_α, in the system. From the one dimensional version of Eq. (2.16), taking the z coordinate as the independent variable, we have

$$\sigma^\pi = J_q \frac{d}{dz}\frac{1}{T} - \sum_{i=1}^{N} \frac{J_i}{T}\frac{d}{dz}\mu_{i,T} = J_q X_q' + \sum_{i=1}^{N} J_i X_i', \tag{2.21}$$

where $\frac{d}{dz}\mu_{i,T}$ is the gradient of the chemical potential of component i at constant temperature.

With the above we are now ready to examine the three different approaches dealt with in this thesis.

2.2.1 Film model

For the extractive column Ext M we will consider the film theory together with the Maxwell-Stefan equations developed by Taylor and Krishna [3] (for details apart from the previous reference, see also the book by Seader and Henley [62]). In this approach, the mass transfer rates is conform of two contributions. The fist one is the molar flux defined by

$$\begin{aligned} N_i^V &= J_i^V + y_i N_t^V \\ N_i^L &= J_i^L + x_i N_t^L, \end{aligned} \tag{2.22}$$

Here $N_t^\pi = \sum_{i=1}^{N} N_i$ is the total molar flux, and J_i^π is the diffusion flux which is the flux of species i relative to the flux of the mixture as a whole. The J_i^π are computed as

$$\begin{aligned} J_i^V &= c_t^V k_{ij}^V (y_i^V - y_i^I) \\ J_i^L &= c_t^L k_{ij}^L (x_i^I - x_i^L), \end{aligned} \tag{2.23}$$

where c^π is the molar density of the mixture and k_{ij}^π are the matrices of multicomponent low-flux mass transfer coefficients.

The total mass transfer rates are obtained by combining Eq. (2.22) and Eq. (2.23) and multiplying by the interfacial area available for mass transfer. For the distillation of a multicomponent mixture the mass transfer rates in the vapor and liquid phases in the nth stage are, respectively

$$\begin{aligned} \mathcal{N}_i^V &= k_{ij}^V A_n (y_i^V - y_i^I) + \mathcal{N}_t^V (y_i^V) \\ \mathcal{N}_i^L &= k_{ij}^L A_n (x_i^I - x_i^L) + \mathcal{N}_t^L (x^L), \end{aligned} \tag{2.24}$$

where k_{ij}^π are calculated from

$$k_{ij}^\pi = \frac{[B_{ij}^\pi]^{-1}\Gamma_{ij}^\pi}{\delta^\pi}, \tag{2.25}$$

where Γ_{ij}^π is a matrix thermodynamic factors for the corresponding phase and B_{ij}^π is a matrix containing the Maxwell-Stefan diffusion coefficients for phase π. Γ_{ij}^π appears

because the fundamental driving force for mass transfer is the chemical potential gradient and not the mole fraction or concentration gradient. This matrix represents fluid mixture nonideality and is calculated from an appropriate thermodynamic model (see Appendices D.1 D.2). The elements of B_{ij}^{π} are calculated according to the following equations

$$B_{ii}^{\pi} = \frac{z_i}{\mathcal{D}_{iN}} + \sum_{k=1,k\neq 1}^{N} \frac{z_k}{\mathcal{D}_{ik}} \ (i = 1, ..., N-1) \tag{2.26}$$

$$B_{ij}^{\pi} = -z_i \left(\frac{1}{\mathcal{D}_{ij}} - \frac{1}{\mathcal{D}_{iN}} \right) \ (i = 1, ..., N-1; i \neq j) \tag{2.27}$$

where $\mathcal{D}_{iN}$ are the Maxwell-Stefan diffusion coefficients for each $i-j$ binary pair in the mixture and z stands for either x or y depending on what π is. Note that the Maxwell-Stefan that $\mathcal{D}_{ij} = \mathcal{D}_{ji}$.

In this manner, the transfer area, A_n, and the film thicknesses, δ_n^{π}, are incorporated into the calculations indirectly.

Similarly, heat transfer rates in the liquid and vapor phases may be written as

$$\begin{aligned} J_q^L &= h^L(T^L - T^I) \\ J_q^V &= h^V(T^I - T^L), \end{aligned} \tag{2.28}$$

where h^{π} are the heat transfer coefficients for the liquid and vapor phases, respectively. These quantities may be obtained from the relationship

$$\lambda^{\pi} = \delta^{\pi} h^{\pi}, \tag{2.29}$$

where λ^{π} is the thermal conductivity.

To complete the film model of interphase transport at a point, we assume that equilibrium prevails at the interface and relate the interface composition through the equilibrium relations, namely

$$y_j^I - K_j x_j^I = 0, \tag{2.30}$$

where K_j is the equilibrium ratio for component j in the multicomponent system evaluated at a given temperature, pressure and composition. The mole fractions at the liquid and vapor sides of the interface must add to unity, namely

$$\begin{aligned} \sum_{j=1}^{c} y_j^I - 1 &= 0 \\ \sum_{j=1}^{c} x_j^I - 1 &= 0. \end{aligned} \tag{2.31}$$

Now we return to the heat and mass transfer coefficients, h^{π} and k_{ij}^{π}. They are obtained by using correlations that apply to the type of physical stage. For example, sieve trays, bubble cap trays or packed stages. Due to the fact that the case of study Ext M is a packed column and also that we have done the column simulation with the

RateFrac model, it is natural to use the correlations developed by Onda et. al. [63] for the k_{ij}^{π} which are used in this model, namely

$$k_{ij}^{L} = 0.0051 \left(\frac{\rho_L \, v_L}{A_n \, \mathfrak{U}_L} \right)^{\frac{2}{3}} (Sc_{ij}^{L})^{-\frac{1}{2}} (a_p d_p)^{0.4} \left(\frac{\rho^L}{\mathfrak{U}_L g} \right)^{-\frac{1}{3}}, \tag{2.32}$$

where ρ_L is the liquid density, v_L is the liquid velocity, Sc_{ij}^{L} is the Schmidt number, a_p is the specific surface area of the packing, d_p is the nominal diameter of the packing or packing size, $\mathfrak{U}_L$ is the liquid viscosity and g is the acceleration due to gravity. The interfacial area available for mass transfer A_n is computed by using also the correlation developed by Onda et. al, namely

$$A_n = a_p \left\{ 1 - exp \left[-1.45 (Re^L)^{0.1} (Fr^L)^{-0.05} (We^L)^{0.2} \left(\frac{\mathfrak{r}}{\mathfrak{r}_c} \right)^{-0.75} \right] \right\}, \tag{2.33}$$

where $\mathfrak{r}$ and $\mathfrak{r}_c$ are the surface tension of the liquid and the critical surface tension of the packing, respectively. Regarding the dimensionless numbers in Eq. (2.33), Re^L is the Reynolds number based on the specific surface, Fr^L is the liquid phase Froude number and We^L is the Weber number. These are given by

$$Re^L = \frac{\rho^L v_L}{\mathfrak{U}_L a_p} \tag{2.34}$$

$$Fr^L = \frac{a_p v_L^2}{g} \tag{2.35}$$

$$We^L = \frac{\rho^L v_L^2}{a_p \sigma} \tag{2.36}$$

Finally, the liquid phase Schmidt number is given by

$$Sc_{ij}^{L} = \frac{\mathfrak{U}_L}{\rho^L \mathcal{D}_{ij}^{L}}, \tag{2.37}$$

where $\mathcal{D}_{ij}^{L}$ is the liquid binary Maxwell-Stefan diffusion coefficient.

On the other hand, the correlation for the vapor phase binary mass transfer coefficient reads

$$k_{ij}^{V} = 5.23 \left(\frac{\rho_V v_V}{a_p \mathfrak{U}_V} \right)^{0.7} (Sc_{ij}^{V})^{\frac{1}{3}} (a_p d_p)^{-2} \left(\frac{RT^V}{a_p \mathcal{D}_{ij}^{V}} \right)^{-1}, \tag{2.38}$$

where ρ_V is the vapor density, v_V is the vapor velocity, $\mathfrak{U}_V$ is the vapor viscosity, and $\mathcal{D}_{ij}^{V}$ is the binary vapor Maxwell-Stefan diffusion coefficient. The vapor phase Schmidt number is given by

$$Sc_{ij}^{V} = \frac{\mathfrak{U}_V}{\rho^V \mathcal{D}_{ij}^{V}}. \tag{2.39}$$

Due to the difficulty of evaluating the heat transfer coefficients for each phase, to estimate them it is usual to find the average mass transfer coefficients, and then to calculate h^{π} by using the Chilton-Colburn analogy [3, 50, 64], namely

$$h^{\pi} = k_{av}^{\pi} C_{p,mix}^{\pi} \left(\frac{\mathfrak{U}_{\pi}}{\rho^{\pi} \mathcal{D}_{av}^{\pi}} \right)^{\frac{2}{3}}, \tag{2.40}$$

where $C_{p,mix}$ is the molar heat capacity, k^{π}_{av} and $\mathcal{D}^{\pi}_{av}$ are the average mass transfer coefficients and the average diffusion coefficients, respectively. These average coefficients were proposed by Taylor and Krishna [3] and are given by

$$k^{\pi}_{av} = \sum_{i}^{N}\sum_{j}^{N}\frac{k_{ij}}{N^2} \tag{2.41}$$

$$D^{\pi}_{av} = \sum_{i}^{N}\sum_{j}^{N}\frac{\mathcal{D}_{ij}}{N^2} \tag{2.42}$$

It is known that film thicknesses can vary between 0.01 and $0.1mm$ in a liquid film and between 0.1 and 1.0 mm in a vapor film [3]. Note that Eqs. (2.25) and (2.29) may lead to a range of values for the film thicknesses. We will later on select the ones that lead to entropy production rates closer to the results of the EB approach which we took as our benchmark.

Once we have computed the mass and heat transfer rates, we now turn to obtain the average driving forces. The total thermodynamic forces in the corresponding films are calculated by integrating through the film thickness, as follows

$$\int_0^{\delta^{\pi}} J^{\pi}_i A X_i^{'\pi} dz = -\mathcal{N}^{\pi}_i X^{\pi}_i \tag{2.43}$$

$$\int_0^{\delta^{\pi}} J^{\pi}_q A X_q^{'\pi} dz = J^{\pi}_q A X^{\pi}_q. \tag{2.44}$$

Furthermore, the total thermodynamic forces of the liquid and vapor films involve the temperatures of the liquid and vapor films, T^L and T^V, respectively, and the chemical potentials of the components, μ_i. Hence, the entropy production rates due to heat and mass transfer of a segment of the column in each film are given by

$$\begin{aligned}
\frac{dS^L_{irr}}{dt} &= J^L_q A\left(\frac{1}{T^L}-\frac{1}{T^I}\right) - \sum_{i=1}^{N}\mathcal{N}^L_i\left(\frac{\mu^I_{i,T}-\mu^L_i}{T^L}\right),\\
\frac{dS^V_{irr}}{dt} &= J^V_q A\left(\frac{1}{T^I}-\frac{1}{T^V}\right) - \sum_{i=1}^{N}\mathcal{N}^V_i\left(\frac{\mu^L_{i,T}-\mu^I_i}{T^V}\right).
\end{aligned} \tag{2.45}$$

The chemical potentials follow from the fugacities, ϕ_i, and activity coefficients, γ_i, at the film average temperature, namely

$$\begin{aligned}
\frac{\mu^L_{i,T}-\mu^I_{i,T}}{T^L} &= R\ln\left(\frac{\gamma^L_i x^L_i}{\gamma^I_i x^I_i}\right)\\
\frac{\mu^I_{i,T}-\mu^V_{i,T}}{T^V} &= R\ln\left(\frac{\phi^I_i y^I_i}{\phi^V_i y^V_i}\right).
\end{aligned} \tag{2.46}$$

This completes the description of the film model. In the next subsection we will briefly describe the integrated interface model.

2.2.2 The integrated interface model

This approach was derived and applied by Kjestrup and de Koeijer [23], and Bedeaux and Kjelstrup [24]. It introduces the Soret effect and assumes that there is no equilibrium over the interface. Furthermore, the interface is the frame of reference for the transport equations. The extractive column Ext KR was analyzed with this model.

The mass transfer rate of component i across the interface is given by

$$J_{i,n} = \mathcal{V}_n y_{i,n} - \mathcal{V}_{n+1} y_{i,n+1} \tag{2.47}$$

The heat transfer rates in the vapor film were derived from the energy balance over the vapor phase, namely

$$J^V_{q,n} = (T^V_{n+1} - T^V_n)\frac{1}{2}\left(V_n\left[y_{1,n}C^V_{p,1} + y_{2,n}C^V_{p,2}\right] + V_{n+1}\left[y_{1,n+1}C^V_{p,1} + y_{2,n+1}C^V_{p,2}\right]\right) \tag{2.48}$$

A crucial part of the formulation of the transport equations is the determination of the resistivities of the vapor and liquid films and the interface, r^V, r^L and r^I, respectively. Such resisistivities in each film are derived from the knowledge of the phenomenological coefficients (see Appendix CC), namely, the diffusion coefficients, the thermal conductivities and the Soret coefficients. The aim is to provide a description of the three contributions using the same variables. The following sections follow very closely the Kjestrup and de Koeijer paper [23]. We start with the interface equations.

For an interface with a binary mixture, in a steady state for evaporation or condensation, there are three independent fluxes. Further, the local entropy production rate in the interface, σ^I, is a sum of products of fluxes and forces and also each driving force is a sum of products of resistivities r and fluxes.

$$\begin{aligned}
\sigma^i &= J^V_q X'^I_q + J_1 X'^I_1 + J_2 X'^I_2 \\
X'^I_q &= r^I_{q,q} J^V_q + r^I_{q,1} J_1 + r^I_{q,2} J_2 \\
X'^I_1 &= r^I_{1,q} J^V_q + r^I_{1,1} J_1 + r^I_{1,2} J_2 \\
X'^I_2 &= r^I_{2,q} J^V_q + r^I_{2,1} J_1 + r^I_{1,2} J_2.
\end{aligned} \tag{2.49}$$

Here, the chemical forces are the differences in chemical potential at the temperature of the interface on the liquid side divided by the temperature. On the other hand, the thermal force in the interface X^I_q is defined as the difference of the inverse of the temperature on each side of the interface. Thus, both driving forces are given by

$$\begin{aligned}
X'^I_i &= -\frac{1}{T^{I,L}}\Delta_I\left(\mu_{i,T^{I,L}}\right) \\
X'^I_q &= \Delta_I\left(\frac{1}{T}\right)
\end{aligned} \tag{2.50}$$

The global entropy production rate in the interface, σ^I, is obtained by integrating over the interface area. as follows,

$$\frac{dS^I_{irr}}{dt} = \int_A \sigma^I dA = \sum_\alpha J_\alpha X'^I_i. \tag{2.51}$$

As a result, the total entropy production rate and the corresponding force-rate relations for the interface are given by

$$\begin{aligned}
\frac{dS^I_{irr}}{dt} &= J^V_q X^I_q + J_1 X^I_1 + J_2 X^I_2 \\
X^I_q &= \bar{r}^I_{q,q} J^V_q + \bar{r}^I_{q,1} J_1 + \bar{r}^I_{q,2} J_2 \\
X^I_1 &= \bar{r}^I_{1,q} J^V_q + \bar{r}^I_{1,1} J_1 + \bar{r}^I_{1,2} J_2 \\
X^I_2 &= \bar{r}^I_{2,q} J^V_q + \bar{r}^I_{2,1} J_1 + \bar{r}^I_{1,2} J_2.
\end{aligned} \tag{2.52}$$

The principal reason to express forces in terms of rates and resistivities is that the rates of transfer can be determined with higher precision from experimental data than the forces. When the rates of transfer have been introduced, in order to preserve congruent units, the resisitivities have to be divided by the transfer area, $\bar{r}^I = r^I/A$. These coefficients are resistances for the interface alone. Each coefficient is a function of the average temperature and vapor mole fraction.

The next step consists of writing the entropy production rate in the vapor and liquid films with the same variables in the interface frame of reference. In a similar way as for the interface, the integration for the films is over the film thickness as well as over the transfer area, as we had shown in Eq. (2.20). The local entropy production rate in a film, σ^π gives the local driving forces as linear combinations of all fluxes, respectively

$$\begin{aligned}
\sigma^\pi &= J^\pi_q X^{'\pi}_q + J^\pi_1 X^{'\pi}_1 + J^\pi_2 X^{'\pi}_2 \\
X^{'\pi}_q &= r^\pi_{q,q} J^\pi_q + r^\pi_{q,1} J_1 + r^\pi_{q,2} J^2 \\
X^{'\pi}_1 &= r^\pi_{1,q} J^\pi_q + r^\pi_{1,1} J_1 + r^\pi_{1,2} J_2 \\
X^{'\pi}_2 &= r^\pi_{2,q} J^\pi_q + r^\pi_{2,1} J_1 + r^\pi_{1,2} J_2,
\end{aligned} \tag{2.53}$$

where the local chemical force and the local thermal force are

$$\begin{aligned}
X^{'L,V}_i &= -\frac{1}{T}\frac{d\mu_{i,T}}{dz} \\
X^{'L,V}_q &= \frac{d}{dz}\frac{1}{T}.
\end{aligned} \tag{2.54}$$

We will use the average driving force. The driving forces in distillation have their maximum value, when the vapor bubble enters to the tray and have their minimum value when the bubble leaves the tray. The average force is located between these points. It is considered that such representative average forces exist for a constant area.

The integrals of the fluxes over the area of transfer give the corresponding transfer rates. Hence, we have for the liquid and vapor film the following

$$\begin{aligned}
\frac{dS^\pi_{irr}}{dt} &= J^\pi_q X^\pi_q + J^\pi_1 X^{L,V}_1 + J^\pi_2 X^\pi_2 \\
X^\pi_q &= \bar{r}^\pi_{q,q} J^\pi_q + \bar{r}^\pi_{q,1} J_1 + \bar{r}^\pi_{q,2} J_2 \\
X^\pi_1 &= \bar{r}^\pi_{1,q} J^\pi_q + \bar{r}^\pi_{1,1} J_1 + \bar{r}^\pi_{1,2} J_2 \\
X^\pi_2 &= \bar{r}^\pi_{2,q} J^\pi_q + \bar{r}^\pi_{2,1} J_1 + \bar{r}^\pi_{1,2} J_2.
\end{aligned} \tag{2.55}$$

The coefficients, $\bar{r}$, in these equations are average coefficients of the film in question. Each resistance coefficient is equal to the corresponding resisistivity r multiplied by the film thickness, divided by the area of transfer, $\bar{r}^{\pi} = \delta^{\pi} r^{\pi}/A$.

The total entropy production shown in Eq. (2.19) only considers in the sum the contributions of the vapor-liquid region, that is, the liquid film, the interface, and the vapor phase. Furthermore, it uses the energy balance at the interface $J_q^L = J_q^V + J_1\Delta H_1 + J_2\Delta H_2$. As a result, from Eq. (2.19) we obtain,

$$\frac{dS_{irr}^n}{dt} = J_q^V(X_q^L + X_q^I + X_q^L) + J_1(X_1^L + X_1^I + X_1^V + \Delta H_1 X_q^L) + J_2(X_2^L + X_2^I + X_2^V \Delta H_2 X_q^L) \tag{2.56}$$

Note, in the latter equation that each rate of transfer is multiplied by the average force for the transport region. The conjugate driving forces of the three rates are, respectively

$$\begin{aligned} X_q &= X_q^L + X_q^I + X_q^L \\ X_1 &= X_1^L + X_1^I + X_1^V + \Delta H_1 X_q^L \\ X_2 &= X_2^L + X_2^I + X_2^V \Delta H_2 X_q^L. \end{aligned} \tag{2.57}$$

In view of equation Eq. (2.57) it is convenient to define overall coefficients. When Eqs. (2.52) and (2.55) are introduced into Eqs (2.57) we obtain all overall coefficients as combinations of the average coefficients of the two films and the interface as follows,

$$\begin{aligned} \bar{r}_{qq} &= \bar{r}_{qq}^I + \bar{r}_{qq}^V + \bar{r}_{qq}^L \\ \bar{r}_{1q} &= \bar{r}_{1q}^I + \bar{r}_{1q}^V + \bar{r}_{1q}^L + + \bar{r}_{qq}^L \Delta_{vap} H_1 \\ \bar{r}_{2q} &= \bar{r}_{2q}^I + \bar{r}_{2q}^V + \bar{r}_{2q}^L + + \bar{r}_{qq}^L \Delta_{vap} H_2 \\ \bar{r}_{11} &= \bar{r}_{11}^I + \bar{r}_{11}^V + \bar{r}_{11}^L + + \bar{r}_{qq}^L (\Delta_{vap} H_1)^2 + 2\bar{r}_{1q}^L \Delta_{vap} H_1 \\ \bar{r}_{22} &= \bar{r}_{22}^I + \bar{r}_{22}^V + \bar{r}_{22}^L + + \bar{r}_{qq}^L (\Delta_{vap} H_2)^2 + 2\bar{r}_{2q}^L \Delta_{vap} H_2 \\ \bar{r}_{12} &= \bar{r}_{12}^I + \bar{r}_{12}^V + \bar{r}_{12}^L + + \bar{r}_{qq}^L \Delta_{vap} H_1 \Delta_{vap} H_2 + \bar{r}_{1q}^L \Delta_{vap} H_1 + \bar{r}_{2q}^L \Delta_{vap} H_2 \end{aligned} \tag{2.58}$$

This set of resistances is equivalent to the one from the Maxwell-Stefan equations and Fourier's law, which are normally the way to describe the interface transport. Kinetic theory was used for the interface resistivities [24] while for the films resistivities we obtained from the expressions given by Taylor and Krishna [3], Krishna and Wesselingh [65], given in Table 2.1 (see also Appendix E).

The interface resistivities are given by the following expressions

$$
\begin{aligned}
r^I_{q,q} &= \frac{\sqrt{\pi}}{4c^V R(T^V)^2}\left[1+\frac{104}{25\pi}\left[\left(\frac{y_1\lambda^V}{\lambda^V_1}\right)^2\left(1+\frac{c^V_2}{c^V_1}\sqrt[4]{\frac{M_1}{M_2}}\right)+\left(\frac{y_2\lambda^V}{\lambda^V_2}\right)^2\left(1+\frac{c^V_1}{c^V_2}\sqrt[4]{\frac{M_2}{M_1}}\right)\right]\right]\\
r^I_{q,1} &= \frac{\sqrt{\pi}}{8c^V T^V v_{mp}}\left[1+\frac{16y_1\lambda^V_1}{5\pi\lambda^V}\left(1+\frac{c^V_2}{c^V_1}\sqrt[4]{\frac{M_1}{M_2}}\right)\right]\\
r^I_{q,2} &= \frac{\sqrt{\pi}}{8c^V T^V v_{mp}}\left[1+\frac{16y_2\lambda^V_2}{5\pi\lambda^V}\left(1+\frac{c^V_1}{c^V_2}\sqrt[4]{\frac{M_2}{M_1}}\right)\right]\\
r^I_{1,1} &= \frac{R\sqrt{\pi}}{16c^V v_{mp}}\left[33\left(\frac{1}{\varphi_1}+\frac{1}{\pi}-\frac{3}{4}\right)\left(1+\frac{c^V_2}{c^V_1}\sqrt[4]{\frac{M_1}{M_2}}\right)\right]\\
r^I_{2,2} &= \frac{R\sqrt{\pi}}{16c^V v_{mp}}\left[33\left(\frac{1}{\varphi_2}+\frac{1}{\pi}-\frac{3}{4}\right)\left(1+\frac{c^V_1}{c^V_2}\sqrt[4]{\frac{M_2}{M_1}}\right)\right]\\
r^I_{1,2} &= \frac{R\sqrt{\pi}}{16c^V v_{mp}}
\end{aligned}
\tag{2.59}
$$

where v_{mp} is the average of the most probable of the two components and φ_i is the condensation coefficient. All such resistivities are positive.

Table 2.1: **Coefficients in the films for a binary mixture.** Here, $D_{i,j}$ are the Fick's diffusion coefficients and S^T is the Soret coefficient. The Soret coefficient in the vapor is neglected due to the fact that it is much smaller than the one of the liquid [4].

Coefficient	**Liquid**	**Vapour**	**Units**
$r_{q,q}$	$\frac{1}{\lambda^L T^2}$	$\frac{1}{\lambda^V T^2}$	$\frac{K\,J}{s\,m}$
$r_{1,q}$	$-x_2 r^L_{qq} \mathrm{S}^T R T^2$	0	$\frac{K\,mol}{s\,m}$
$r_{2,q}$	$-\frac{x_1}{x_2} r_{eq^L}$	0	$\frac{K\,mol}{s\,m}$
$r_{1,1}$	$\frac{Rx_2}{x_1 c^L D^L_{1,2}} + \frac{(r^L_{q,1})^2}{r_{q,q}}$	$\frac{Ry_2}{y_1 c^v D^V_{1,2}}$	$\frac{mol^2\,K}{s\,J\,m}$
$r_{1,2}$	$-\frac{x_1}{x_2} r^L_{1,1}$	$-\frac{y_1}{y_2} r^v_{1,1}$	$\frac{mol^2\,K}{s\,J\,m}$
$r_{2,2}$	$\frac{x_1}{x_2} r^L_{1,2}$	$\frac{y_1}{y_2} r^V_{1,2}$	$\frac{mol^2\,K}{s\,J\,m}$

In Fig. 2.2 we show the average coefficients of the two films and the interface. The color code is as follows: blue for the results derived of the operation profiles computed with the Aspen Plus software and magenta for the values obtained by Kjelstrup and de Koeijer. Note that the agreement between both set of data are fairly good.

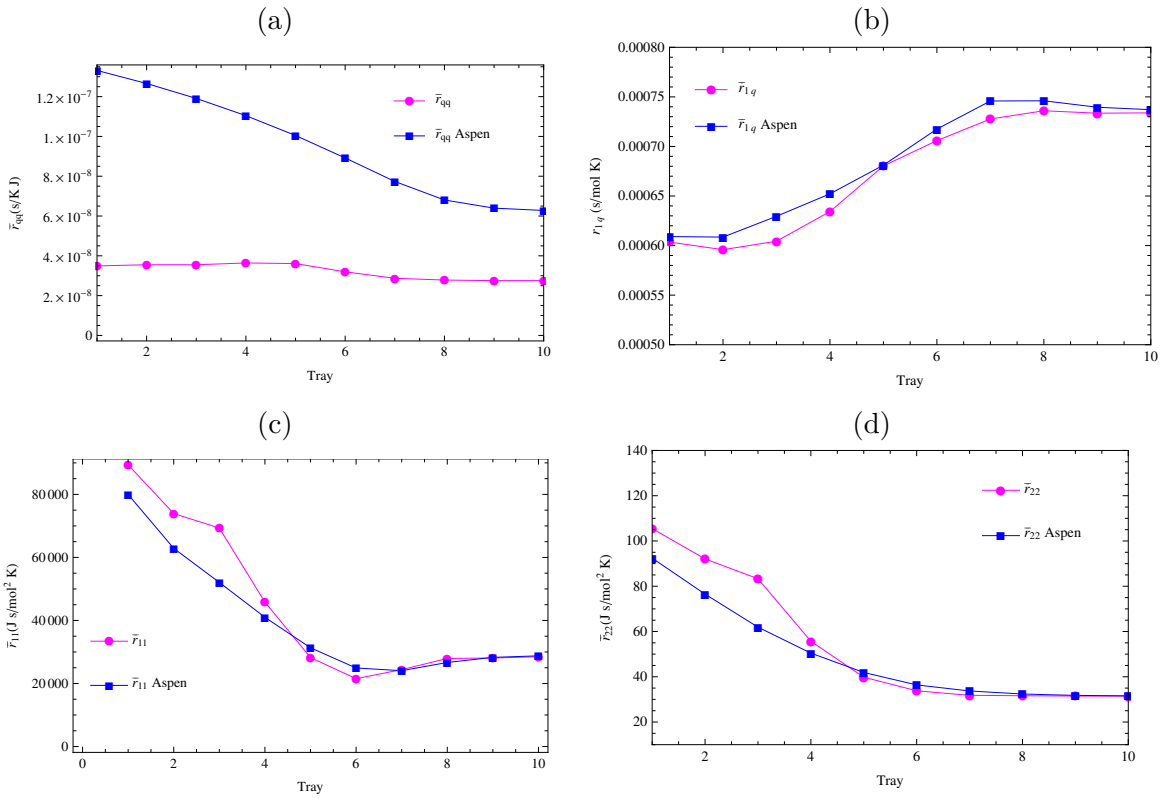

Figure 2.2: **Average coefficients of the vapor-liquid region**. (a) Coefficient of heat transfer $\bar{q}\bar{q}$. (b) Heat and mass coupling coefficient. $\bar{r}_{1q}$ correspond to the ethanol-heat coefficient. (c) Coefficient of the transfer of ethanol. Here, $\bar{r}_{11}$ is the coefficient obtained by Kjelstrup and de Koiejer and $\bar{r}_{11}$ *Aspen* is our results derived of the operational profiles obtained with Aspen Plus. (d) Coefficient of transfer of water. Here, $\bar{r}_{22}$ is the coefficient obtained by Kjelstrup and de Koiejer and $\bar{r}_{22}$ *Aspen* is our results derived of the operational profiles obtained with Aspen Plus.

2.2.3 The present approach

In this thesis we take into account both the film model and the integrated interface model. Due to the fact that in the case of a hydrocarbon mixture we are dealing with pseudo components and those are also multicomponent mixtures, we propose a formulation that deals directly with the phenomenological coefficients in the calculations. Furthermore, the proposed approach allows us to explicit include thermal diffusion in the hydrocarbon distillation columns.

In our case, the entropy production rate in a stage shown in Eq. (2.19), not only is the sum of the contributions of the vapor-liquid region, but also includes the liquid and vapor bulks. Furthermore, in the same fashion that in the film model [3], we consider that the entropy production rate at the interface is zero.

The global entropy production rate in the films, as we had shown in Eq. (2.20), is obtained by integrating the local entropy production rate σ^{π} over the film thickness δ^{π}. We rewrite Eq. (2.16), so the local entropy production rate, σ^{π}, in the case of a

multicomponent mixture it reads

$$\sigma = J_q \cdot X'_q + \sum_{i=1}^{N} v_i \cdot X'_i, \tag{2.60}$$

where we have introduced the velocity of component i with respect to the interface defined as $v_i = J_i/c_i$ where c_i is the molar density of component i. Further, $X'_q \equiv -\frac{1}{T^2}\nabla T$ and $X'_i \equiv -\frac{c_i}{T}\nabla \mu_{i,T}$ are the local forces conjugate to the corresponding heat and mass fluxes. Note that, to treat all the forces on an equal ground, in Eq. (2.60) we have included all the component driving forces, not only the independent ones. In fact, the component forces are related by the Gibbs-Duhem equation [66], namely

$$\sum_{i=1}^{N} X'_i = 0, \tag{2.61}$$

so that only $N-1$ of these forces are independent. Following the idea of the integrated interface model, X'_q and X'_i may be expressed in terms of the fluxes and the resistivities r_{qq}, r_{qi}, r_{ki} and r_{iq} as follows

$$\begin{aligned} X'_q &= r_{qq} J'_q + \sum_{k=1}^{N} r_{qk} v_k \\ X'_i &= r_{iq} J'_q + \sum_{k=1}^{N} r_{ik} v_k, \qquad (i = 1, 2, 3, \cdots N) \end{aligned} \tag{2.62}$$

These resistivities obey the Onsager reciprocity relations, that is $r_{qi} = r_{iq}$ and $r_{ik} = r_{ki}$ and so from Eq. (2.61) it follows that $\sum_{i=1}^{N} r_{ki} = \sum_{i=1}^{N} r_{ik} = 0$ and $\sum_{i=1}^{N} r_{qi} = \sum_{i=1}^{N} r_{iq} = 0$. It is convenient to rewrite Eq. (2.62) in the form

$$\begin{aligned} X'_q &= r_{qq} \left[J'_q - \sum_{k=1}^{N} c_k q_k^* v_k \right] \\ X'_i &= -c_i q_i^* X'_q + \sum_{k=1, k\neq 1}^{N} R_{ki}(v_k - v_i), \qquad (i = 1, 2, 3, \cdots N), \end{aligned} \tag{2.63}$$

where $q_i^* = -1/c_i\,(r_{qi}/r_{qq})$ is the heat of transfer and $R_{ik} = r_{ik} - (r_{iq} r_{qk}/r_{qq})$. In view of the symmetry relationships between the resistivities, one has that $R_{ik} = R_{ki}$, that $\sum_{i=1}^{N} c_i q_i^* = 0$ and that $\sum_{i=1}^{N} R_{ki} = \sum_{i=1}^{N} R_{ik} = 0$. We now follow Krishna and Wesselingh [67] and Kjelstrup and Bedeaux [26] in order to relate the resistivities R_{ik} and the heats of transfer q_i^* to the Maxwell-Stefan diffusion coefficients and the thermal diffusion coefficients. The result is

$$R_{ik} = -\frac{R c_i c_k}{c_t \mathcal{D}_{ik}} \qquad (i \neq k). \tag{2.64}$$

Here $c_t = \sum_{i=1}^{N} c_i$ is the total molar density. The diagonal elements R_{ii} are obtained from the relationship $\sum_{i=1}^{N} R_{ik} = 0$. Further, the heat of transfer is given by

$$q_j^* = \sum_{k=1}^{N} \frac{RTc_k}{c_t \mathcal{D}_{jk}} \left(\frac{D_{T,k}}{c_k M_k} - \frac{D_{T,j}}{c_j M_j} \right), \tag{2.65}$$

where $D_{T,j}$ are the thermal diffusion coefficients. Note that the thermal diffusion coefficients may be expressed in terms of the Maxwell-Stefan diffusion coefficients as

$$D_{T,j} = \sum_{i=1}^{N} S_i^T \mathcal{D}_{ik}. \tag{2.66}$$

Finally, we express r_{qq} in terms of the thermal conductivity of the mixture λ_{mix} as $r_{qq} = 1/\lambda_{mix}T^2$. With the aid of the above identifications and by choosing component 1 as the independent component it is possible to rewrite the driving forces as

$$\begin{aligned}
X_q' &= \frac{1}{\lambda_{mix}T^2} \left[J_q' - \sum_{k=2}^{N} c_k q_k^* (v_k - v_1) \right] \\
X_i' &= -c_i q_i^* X_q' - \frac{Rc_i}{c_t} \sum_{k=1,k\neq 1}^{N} \frac{c_k}{\mathcal{D}_{k,i}} (v_k - v_i), \quad (i = 2, 3, \cdots N) \\
X_1' &= -\sum_{k=2}^{N} X_k'
\end{aligned} \tag{2.67}$$

The substitution of Eq. (2.67) into Eq. (2.60) leads finally to the sought expression for the entropy production rate of the films in terms of the fluxes and the transport coefficients. The methods used to compute thermal conductivity, Maxwell-Stefan diffusion coefficients and Soret coefficients are provided in Table D.3 in Appendix D.2.

In the calculation of the global entropy production rate, we shall again need the interface area, A, and the vapor and liquid film thicknesses, δ^π. Once they are available, the global forces in the films may be obtained by integrating the local forces over the corresponding film thickness δ^π, leading to

$$\begin{aligned}
X_q^\pi &= \int_0^{\delta^\pi} X_q'^\pi dx = \bar{X}'^\pi_q \delta^\pi = \frac{\delta^\pi}{\lambda_{mix}T^2} \left[J_q'^\pi - \sum_{k=1}^{N} c_k q_k^* (v_k - v_1) \right] \\
X_i^\pi &= \int_0^{\delta^\pi} X_i'^\pi dx = \bar{X}'^\pi_i \delta^\pi = -c_i q_i^* X_q^\pi - \frac{Rc_i \delta^\pi}{c_t} \sum_{k=1,k\neq 1}^{N} \frac{c_k}{\mathcal{D}_{k,i}} (v_k - v_i), \quad (i = 2, 3, \cdots N) \\
X_1^\pi &= -\sum_{k=2}^{N} X_k
\end{aligned} \tag{2.68}$$

Thus the global entropy production rate in the films is finally given by

$$\frac{dS_{irr}^{\pi,film}}{dt} = J_q^\pi \, A \, X_q^\pi + \sum_{i}^{4} v_i^\pi A \, X_i^\pi. \tag{2.69}$$

Now we turn to the contributions to the entropy production rate coming from the two bulks. From the entropy balance, and by considering unidirectional mass and heat transfer, these are given by

$$\begin{aligned}\frac{dS_{irr}^{L,bulk}}{dt} &= J_{q,n}^{\prime L} A\left(\frac{1}{T_n^L}-\frac{1}{T_{n-1}^L}\right)-\sum_{i=1}^{N} x_{i,n-1}\mathcal{L}_{n-1}\left(\frac{\mu_{i,n-1}^L(T_{n-1}^L)-\mu_{i,n-1}^L}{T_{n-1}^L}\right),\\ \frac{dS_{irr}^{V,bulk}}{dt} &= J_{q,n}^{\prime V} A\left(\frac{1}{T_{n+1}^V}-\frac{1}{T_n^V}\right)-\sum_{i=1}^{N} y_{i,n+1}\mathcal{V}_{n+1}\left(\frac{\mu_{i,n}^V(T_{n+1}^V)-\mu_{i,n+1}^V}{T_{n+1}^V}\right),\end{aligned} \tag{2.70}$$

where $x_{i,n-1}\mathcal{L}_{n-1}$ is the amount of mass of component i entering the nth tray from the stage above, $y_{i,n+1}\mathcal{V}_{n+1}$ is the amount of mass of component i entering the nth stage from the stage below, $\mu_{i,n}^L(T_{n-1}^L)$ is the chemical potential at the liquid composition at the nth stage and temperature of the $(n-1)$th. $\mu_{i,n}^V(T_{n+1}^V)$ is the chemical potential at the vapor composition of stage$n$ and the temperature of stage $n+1$. The calculation of the chemical potentials is obtained from the fugacities of the components in the liquid or vapor phases, respectively,

$$\begin{aligned}\frac{\mu_{i,n}^L(T_{n-1}^L)-\mu_{i,n-1}^L}{T_{n-1}^L} &= R\ln\left(\frac{f_{i,n}^L(x_n,T_{n-1}^L)}{f_{i,n-1}^L(x_{n-1},T_{n-1}^L)}\right)\\ \frac{\mu_{i,n1}^V(T_{n+1}^V)-\mu_{i,n+1}^V}{T_{n+1}^V} &= R\ln\left(\frac{f_{i,n}^V(y_n,T_{n+1}^V)}{f_{i,n+1}^V(y_{n+1},T_{n+1}^V)}\right),\end{aligned} \tag{2.71}$$

where f_i^{π} is the fugacity of component i evaluated at the corresponding nth stage liquid composition and temperature. Later on, both the fugacities and the chemical potentials of the mixture will be extracted from simulation results by using the Peng-Robinson property method (see Appendix D.2).

As an illustration of partial results required in our approach, in Fig. 2.3 we show the outcome of the calculation of the liquid thermal diffusion coefficients in each stage for the depropanizer column and for the batch column. We must point out that our numbers are consistent with values reported in the literature for liquid hydrocarbon mixtures [68–71].

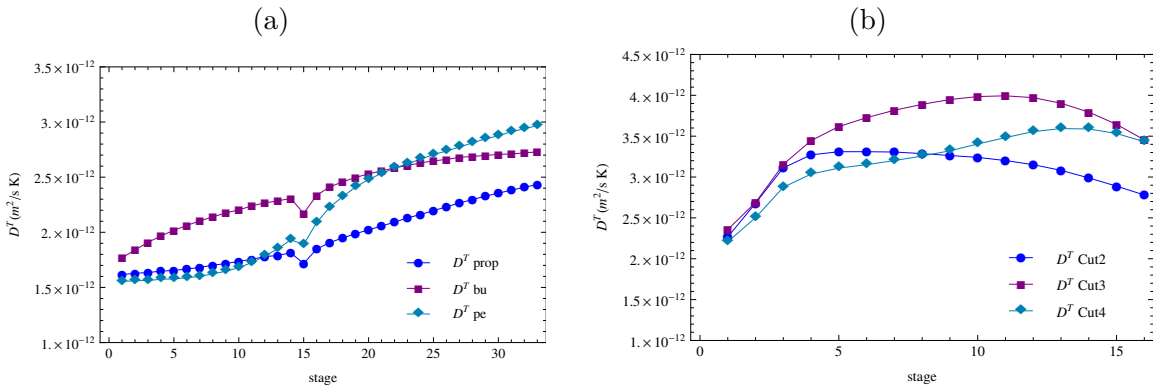

Figure 2.3: **Thermal diffusion coefficients in each stage**. (a) Hydrocarbon mixture of the depropanizer column. Here, D^T_{prop} is the thermal diffusion coefficient of propane, D^T_{but} refers to the thermal diffusion coefficient of butane and D^T_{pen} is the thermal diffusion coefficient of the pentane. (b) Mexican oil mixture. Here, D^T_{cut2} is the thermal diffusion coefficient of pseudo component 2, D^T_{cut3} refers to the thermal diffusion coefficient of pseudo component 3 and D^T_{cut4} is the thermal diffusion coefficient of pseudo component 4.

2.2.4 Exergy Analysis and Global Entropy Balance

We have already mentioned that the exergy analysis is a useful benchmark. The exergy loss on the nth stage, Ex_n^{loss}, (which represents the overall thermodynamic losses due to the waste heat and mass transfer and is directly proportional to the rate of entropy production in stage n due to irreversibilities) may be calculated from the exergy balance over the nth stage as

$$Ex_n^{loss} = \mathcal{V}_{n+1}Ex_{n+1}^V + \mathcal{L}_{n-1}Ex_{n-1}^L - \mathcal{V}_nEx_n^V - \mathcal{L}_nEx_n^L + Q_n\left(1 - \frac{T_0}{T_n}\right), \qquad (2.72)$$

where the reference temperature is $T_0 = 298.15\ K$. For one section in the distillation column, the exergy corresponding to each phase in the nth stage, Ex_n^π, is given by

$$Ex_n^\pi = \sum_{i=1}^{N} H_{i,n}^\pi - T_0 S_n^\pi, \qquad (2.73)$$

where $H_{i,n}^\pi$ and S_n^π are the values of the enthalpy and molar entropy of the mixture, respectively.

In a similar way, the entropy balance to quantify the global entropy production rate in the nth column stage may be expressed as

$$\frac{dS_{irr}^n}{dt} = \mathcal{V}_nS_n^V + \mathcal{L}_nS_n^L - \mathcal{V}_{n+1}S_{n+1}^V - \mathcal{L}_{n-1}S_{n-1}^L - F_n^V S_{Fn}^V - F_n^L S_{Fn}^L. \qquad (2.74)$$

where F_n is the feed molar flow (in mol/s) in the nth stage.

Chapter 3

Results and discussion

In the previous Chapter we have presented explicit expressions for the global entropy production rate as given by the film model, the integrated interface model, our approach, the exergy analysis and the global entropy balance analysis. In this section we will provide a comparison of the corresponding results. We start by comparing the global entropy production rates derived from the different models and approaches for our four cases of study. Such comparisons are shown in Figs. 3.1 and 3.2. Note that the agreement between all sets of data is fairly good.

In both Figs. the color code is as follows: orange for the results derived from the exergy analysis and green for the results calculated by us with either the film model or the integrated interface model. In Fig. 3.1, we use purple for the values obtained by Mendoza or by Kjelstrup and de Koeijer, respectively. On the other hand, in Fig. 3.2, blue is for the values computed from the entropy balance approach while green corresponds to the results derived with our approach.

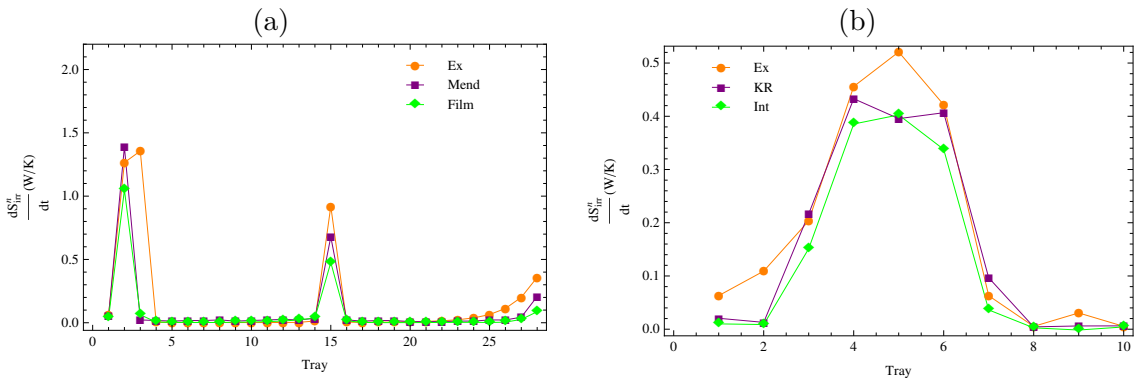

Figure 3.1: **Global entropy production rate of the extractive distillation columns for an ethanol-water mixture**. (a) Ext M column. Here, *Ex* is the exergy analysis, *Mend* correspond to the values obtained by Mendoza and *Film* are our results by using the film model. (b) Ext KR column. Here, *KR* correspond to the values obtained by Kjelstrup and de Koeijer and *Int* are our results by using the integrated interface model.

Considering the approximations that were used to estimate the total entropy production rate in Figs. 3.1 and 3.2, namely the values of the area of transfer and the

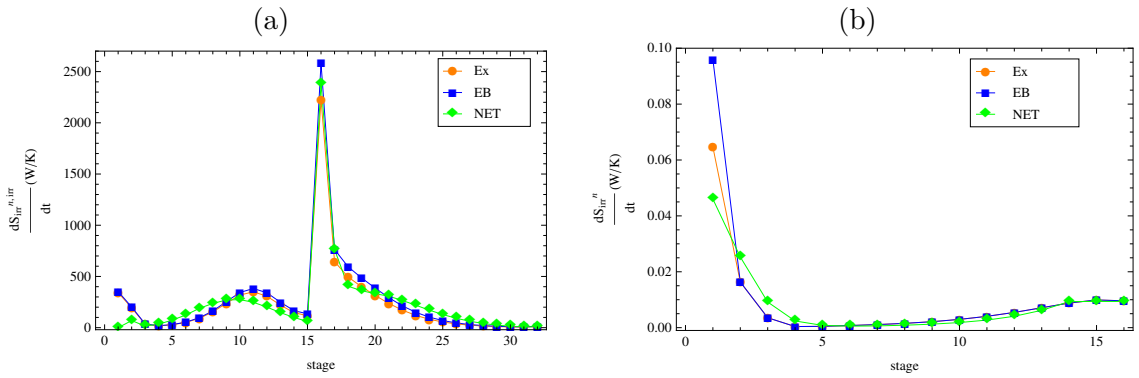

Figure 3.2: **Global entropy production rate of the hydrocarbon distillation columns.** Labels indicate the different theoretical approaches. *NET* corresponds to our nonequilibrium approach including the contribution of the two bulks; *Ex* refers to the exergy analysis and *EB* corresponds to the entropy balance analysis. (a) The depropanizer column. (b) The batch column with the Mexican oil mixture.

film thicknesses throughout the column, one can say that the exergy trends are reasonably reproduced by the theoretical lines resulting from the film model, the integrated interface model and the present approach.

The total entropy production rate in Figs. 3.1 and 3.2 displays a different behavior in each column due to the fact that both cases have different configurations, heat duty and main objective. For the Ext KR column (Fig. 3.1-b) and the depropanizer column (Fig. 3.2-a), in all the theoretical approaches the highest entropy production rate is located at the center of the column and the maximum value occurs at the feed stages. This is consistent with the fact that it is at the center of the column where the highest heat transfer rates and mass flow rates take place and so most of the separation happens there. In contrast, for the Ext M column (Fig. 3.1-a) and the batch column (Fig. 3.2-b), the entropy production rate takes on the highest values in two places in the column. For the Ext M, these values correspond also to the feed stages: stages 3 and 16, where the entrainer and the mixture ethanol-water are fed, respectively. On the other hand, for the batch column, the two maximum values are in the first three stages, where the vapor flow and the liquid flow in countercurrent present the greatest temperature difference in the column. The vapor mixture is at 320 K and the cold liquid reflux at 250 K. The second peak occurs at the last three stages (the bottom of the column) where the highest temperatures occur so that the mixture begins to evaporate. Furthermore, the behavior of the distillation columns studied in the present work agrees with the conclusions of de Koeijer *et. al.* [2], Kjelstrup *et. al.* [23], Liang *et. al.* [14] who claim that mass transfer is the main contribution to the global entropy production rate in a distillation column.

Note that the differences between the values of the entropy production rate of the stages with those of the *Ex* analysis are not only due to the fact that in the film model, the integrated interface model and the present approach one includes explicitly the transport coefficients, the heat and mass transfer couplings and the vapor and liquid thicknesses in the thermodynamic driving forces, but also to the fact that the *Ex* analysis takes into account all the sources of the irreversibilities including pressure drop

and phase mixing which have been neglected in the former [54].

Nevertheless, in Fig 3.2 our results using the present approach, apart from exhibiting similar trends to the ones of Liang *et al* [14], are closer to the values obtained with the exergy analysis and the entropy balance approach than the ones in Ref. [14], particularly for the depropanizer column. This feature reflects the fact that our present approach considers the contribution of both liquid and vapor bulks. In this system, the correlation coefficient between the results of the Ex analysis and those of the NET approach is $R^2 = 0.950$ while in the batch column this correlation was poorer, namely $R^2 = 0.907$.

In Fig. 3.3 we display the values of the vapor heat of transfer q^{*V} computed with Eq. (2.65). The heat of transfer q^* is the quantity that allows us to explicitly include and evaluate the effect of the thermal diffusion process in our hydrocarbon distillation column. We see that the values corresponding to the batch column using the Mexican oil, with large molecular weight, are four orders of magnitude greater than those of the light hydrocarbon mixture of the depropanizer column. Nevertheless, comparing such values of q^{*V} with those of the vapor enthalpy H^V, we consider that they are not unreasonable. The H^V values along the stages were on average $2 \times 10^5\, J/mol$. In the case of the liquid heat of transfer q^{*L}, although not shown, the trends and the results are similar in the sense that the Mexican oil leads to values one order of magnitude greater than those of the light hydrocarbon mixture.

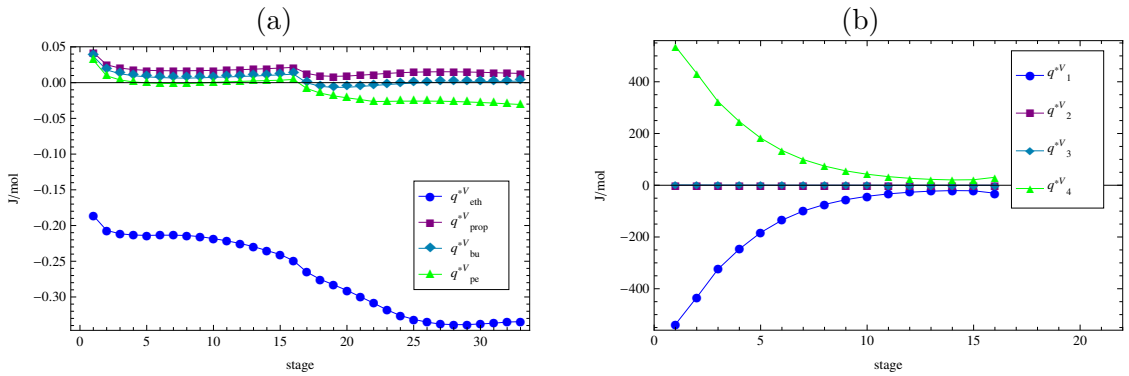

Figure 3.3: **Vapor heat of transfer.** (**a**) Vapor heat of transfer in the depropanizer column, where q^{*V}_{eth} is the ethane vapor heat of transfer, q^{*V}_{prop} is the propane vapor heat of transfer, q^{*V}_{bu} is the n-butane vapor heat of transfer and q^{*V}_{pe} is the n-pentane vapor heat of transfer. (**b**) Vapor heat of transfer in the batch column, where q^{*V}_1 is the pseudocomponent 1 vapor heat of transfer, q^{*V}_2 is the pseudocomponent 2 vapor heat of transfer, q^{*V}_3 is the pseudocomponent 3 vapor heat of transfer and q^{*V}_4 is the pseudocomponent 4 vapor heat of transfer.

The vapor heat of transfer of the fourth pseudocomponent, q^{*V}_4, which has the greatest molecular weight in the mixture, presents the largest values. They start at approximately, 513 J/mol and decrease to 32 J/mol. This is due to the fact that in the fractionating column, it is at the top where the heat and mass transfer take place while separating the compound of interest of the mixture. In contrast, for the depropanizer column, the values are more evenly distributed along the stages.

Another important question concerns the explicit inclusion of the coupling between heat and mass transfer in the thermodynamic driving forces, particularly for the vapor.

The contributions of q_i^{*V} in the thermal and mass driving forces are compared in Figs. 3.4 and 3.5. In this latter, only one of the independent forces (X_3) is displayed but the others show similar behavior. The results indicate that in the case of the depropanizer column, neglecting the thermal diffusion in this system will have a little effect on both the mass and the thermal driving forces. On the other hand, for the fractionating column this contribution makes an appreciable difference in these driving forces, specially in the three latest stages.

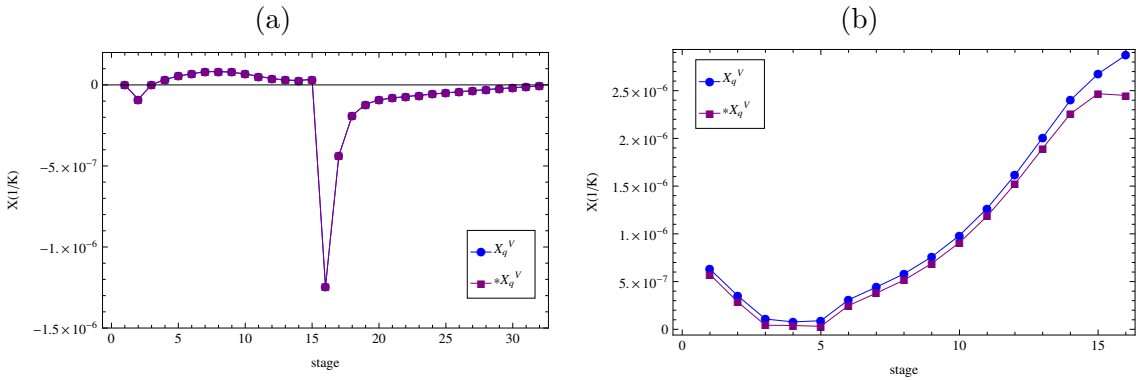

Figure 3.4: **Thermal driving forces.** (**a**) Vapor thermal driving force of the depropanizer column, where X_q^V includes the coupling between heat and mass transfer while $*X_q^V$ does not (**b**) Vapor thermal driving force of the batch column. The labels are the same of those of (a)

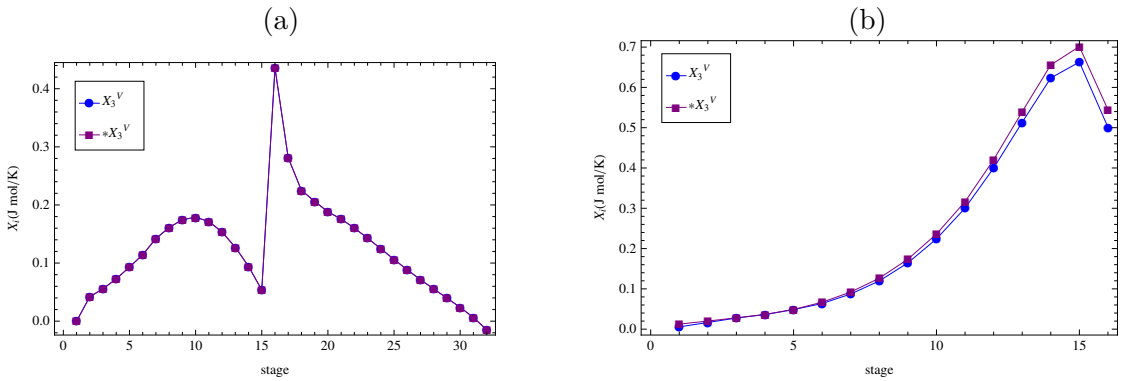

Figure 3.5: **Mass driving forces.** (a) Vapor thermal driving force of the depropanizer column, where X_3^V includes the coupling between heat and mass transfer and $*X_3^V$ does not (b) Vapor thermal driving force of the batch column. The labels are the same of those of (a).

As it is clearly seen in Fig. 3.3, the values of q^{*V} are higher in the fractionating column than the ones in the depropanizer column. This fact is also manifested in Figs. 3.4 and 3.5, where we evaluate the contribution of the inclusion of the coupling between heat and mass transfer in the thermodynamic driving forces. In the depropanizer column, neglecting thermal diffusion has a rather little effect on both driving forces and hence on the entropy production rate (see Fig. 3.6). Such behavior agrees with claims made by previous authors as Rosner [21], Taylor and Khrisna [3] and Bird et al. [22],

who suggest that there is a negligible influence of thermal diffusion in distillation. Also, DeLancey [72] concluded that the errors involved when neglecting thermal diffusion in the interfacial flux of a dilute three component hydrocarbon mixture do not appear to be significant when one considers the accuracy requirements of a design procedure. However, the generalization of such claims should be taken with care since other studies have indicated that thermal diffusion is sensitive to the details of intermolecular interaction, the structural behavior, such as the size and shape of the molecules [73–76] and this is reflected in the results for the fractionating column (*c.f.* Figs. 3.4, 3.5 and 3.6). In fact, depending upon the physical system, the Dufour and Soret effects may or may not be important [72]. In low-pressure gaseous mixtures and in ideal liquid mixtures, as the multicomponent hydrocarbon mixture in the depropanizer column, the thermal diffusion factor has been found to be small [70, 71, 73]. On the other hand, in non ideal mixtures or for heavier components, like the Mexican oil mixture in the fraccionating column, the thermal diffusion factor is larger than the one for ideal mixtures or the one for lighter components, respectively [68, 77]. Further, the thermal diffusion effect is appreciable in mass transfer situations with large molecular weight disparities and large temperature gradients, a situation that one encounters in the fractionating column but not in the depropanizer one.

Since in the proposed approach we have presented it is only possible to evaluate explicitly the effect of either including or not including the coupling between heat and mass transfer in the films, for the sake of completing the analysis and close this section we now present the results of their contributions to the global entropy production rates for both columns. These are displayed in Fig. 3.6.

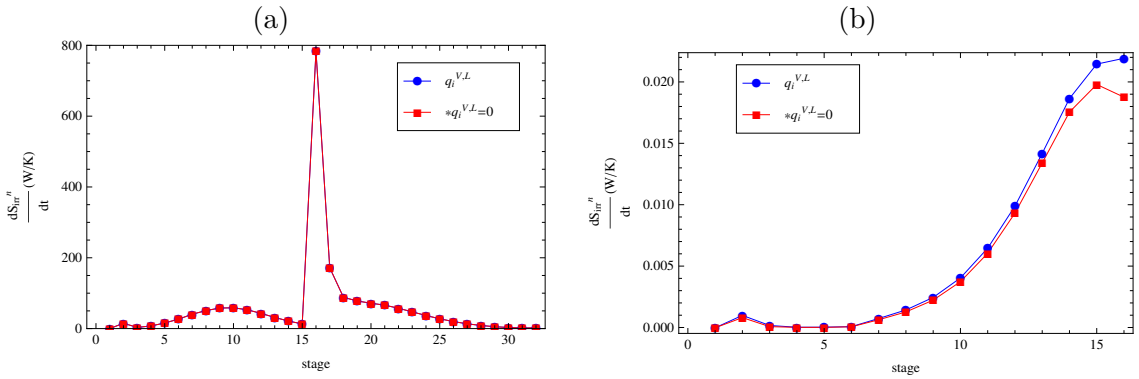

Figure 3.6: **Contribution of the liquid and vapor heats of transfer in the films to the global entropy production rates.** (a) Depropanizer column, in the cases where the thermal and mass driving forces include the coupling between heat and mass transfer and where they do not (b) batch column. The labels are the same of those of (a).

Note that as mentioned earlier, the main contribution to the global entropy production rates is due to mass transfer (compare with Fig. 3.2).

Chapter 4

Concluding Remarks

The aim of the thesis was to extend the application of NET to real processes. The use of the NET approach in the distillation of a truly multicomponent mixture is not only a big challenge but also is rather scarce. The closest attempt is the example of a depropanizer column from an oil refinery by Taylor and Krishna [3]. Here we have presented another example of the usefulness of such approach for the analysis of a multicomponent distillation process. Furthermore, the outcome of this thesis provides further support to the notion that the NET approach can be used satisfactorily to model this kind of complex processes.

In any nonequilibrium description of a system or process one should obtain force-flux relations and the expression for the entropy production. It is important to stress that one should be careful in the identification of fluxes and forces, as a wrong selection could destroy the reciprocal property of the phenomenological coefficients. Fortunately, the distillation process is a relatively well known process. This allows us to follow the suggestion generally admitted that the thermodynamic fluxes are the physical fluxes, mass and heat, while the forces are the conjugated terms, namely the gradients of temperature and chemical potentials [16].

Our work suggests that in order to properly describe the entropy production rate in a distillation column by using the NET approach, it is necessary to avoid the assumption of equilibrium at the vapor-liquid contact when treating the performance of the column. Additionally, the use of the rate-based model seems to be adequate and information of the transport coefficients, the transfer area and the vapor and liquid films thicknesses is required. A particularly rewarding outcome is that the agreement between the values obtained before by Mendoza [1], de Koeijer et. al. [2] and Taylor et. al [3], and our results is satisfactory.

The nonequilibrium models, the film model and the integrated interface model, differ by their choice of assumptions. In particular, the first one includes ways to deal with hydrodynamic effects, the transfer area and the film thicknesses are incorporated into the calculation indirectly and the interface is considered to be in equilibrium. On the other hand, in the interface integrated model one takes the Soret/Dufour effect and dissipation in the interface into account. Our approach is the result of the necessity to describe the hydrocarbon multicomponent mixture distillation somewhere in between an industrial use and in a more precise manner. Therefore we have decided to express

the thermodynamic driving forces in terms of resistances and fluxes and to include the coupling between heat and mass transfer for the description of the two chosen hydrocarbon multicomponent distillation processes. Furthermore, we have neglected the interface resistance whose importance was found to be not significant in the extractive column studied by Kelstrup and de Koeijer [23].

In general, the analysis and modeling of heat transfer in petrochemistry processes which involves multicomponent mixtures with wide range in molecular masses represents a big challenge. A popular way to treat hydrocarbon distillation problems is through the Ex analysis, but with it one can not distinguish the individual contributions to the total exergy loss. A point often overlooked in both the Ex analysis and in the equal thermodynamic distance analysis is the fact that there may be couplings among various transport phenomena such as the Soret effect or the Duffour effect which are not explicitly accounted for. On the contrary, the NET approach allows us to evaluate the contribution of all possible individual driving forces of the irreversible phenomena and thus account for such couplings in the global entropy production rate. In this respect, NET may profitably be used to complement the Ex analysis. In particular we have found that for the depropanizer column the inclusion of heat and mass transfer coupling has a negligible effect on the entropy production rate but for the fractionating column this is not so.

On the other hand, one of the key factors in describing a nonequilibrium system, such as a distillation column, is the correct evaluation of the phenomenological coefficients, a question not often considered in engineering. The hydrocarbon mixtures pose an additional difficulty due to the fact that almost all the correlations are empirical and hence it is necessary to test them in order to choose the adequate ones for the temperature and pressure ranges in the system. This is the strategy that we have followed in this thesis, where we have provided the explicit expressions to be used in our calculations.

It is clear that in our development, many simplifying assumptions of the distillation process in both columns, which are in fact less restrictive than the ones usually adopted for the modeling of hydrocarbon mixtures, have been made. Among them we have the choice of steady-state conditions, one dimensional flow of the vapor and liquid phases, that the vapor rising through the liquid within the tray is completely mixed and that there is no significant pressure gradient along the vapor and liquid flow directions. While of course such simplifications do impose some limitations on the actual numerical results, in our view they do not invalidate the main conclusions pertaining to the importance of explicitly accounting for the effect of the coupling of heat and mass transfer in distillation. Once we have gained this insight, a natural further step would be to remove some of these assumptions and hence get an even more realistic picture of what actually happens. This remains as an open problem that seems worth addressing in the not too distant future.

One final remark is in order. In this thesis we have relied on the Aspen Plus V8.4 software to compute the temperature, composition and flow profiles and extract other thermodynamic data. Also, the transport coefficients were computed with known correlations in the literature. It is conceivable that in some instances, all or some of these quantities could be directly measured. It is worth emphasizing that, were this the case, the NET approach would remain unaltered and still allow for the evaluation of the (real) effect of heat and mass transfer coupling on a particular distillation process.

Appendix A

Mexican oil mixture assay

The characteristics of the Mexican oil mixture are given through the crude assay provided by the Instituto Mexicano del Petróleo (IMP). This assay contains information on specification of the whole Mexican oil mixture as well as its products from atmospheric or vacuum distillation columns. Additionally, it contains gas chromatography analysis and API gravity.

A.1 Detailed hydrocarbon analysis

The detailed component analyses of the lighter ends and petroleum gases can be performed by gas chromatograpy. A chromatogram can be used to calculate the paraffins, isoparraffins, olefins and aromatic content of a sample. This cannot be said about heavier cuts. The results can be useful in yield calculations, since the correlations for the different processes contain parameters related to hydrocarbon family type.

The Mexican oil mixture presents for the first fraction 34 different components and for the second 112. We show in Table A.1 the representative components, those means with the greater concentration.

Table A.1: **Gas chromatography analysis.** The results correspond to the first and second fractions of the Mexican oil mixture. Here *% V* is the volume percent in the mixture.

First fraction		**Second fraction**	
Component	**% V**	**Component**	**% V**
n - pentane	17.70	toluene	5.76
2 - metilpentane	17.03	olefin C8	6.93
3 - metilpentane	11.07	n-heptane	6.08
n - hexane	28.42	meta-xilene	3.54

A.2 API gravity

The American Petroleum Institute (API) defined API gravity to quantify the quality of petroleum products and crude oils [31], namely

$$API\,gravity = \frac{141}{SG\,at 15.6C} \tag{A.1}$$

The API gravity can range from 8.5 for very heavy crudes to 44 for light crudes. The results for the Mexican oil mixture are shown in Table A.2.

Table A.2: **% Volumen vs API gravity in distillate.**

% V	**API gravity**
0	0
11	55.13
21	45.97
27	39.15
35	32.98
39	29.44
48	23.70
60	17.42

A.3 Properties of the pseudo components

Table A.3 shows the 8 pseudo components identified experimentally in the Mexican oil mixture with their corresponding properties.

Table A.3: **Properties of the Mexican oil pseudo components.** Here the satured, unsatured and aromatics are given in $\%V$ and the $Kfactor$ is dimensionless

Cuts	**NBP** (C)	**API** (m)	**K factor**	**Satured**	**Unsatured**	**Aromatics**
Naptha (l)	52.2	80.17	-	-	-	2.63
Naptha (m)	124.6	55.13	-	-	-	23.18
Naptha (h)	184.6	45.97	-	75.75	0.90	23.35
Distillate (l)	233.0	39.15	-	74.60	0.50	24.90
Distillate (h)	283.2	32.98	11.63	-	-	-
Gasoil (l)	324.8	29.44	11.63	-	-	-
Gasoil (h)	398.2	23.70	11.62	-	-	-
Residual	-	17.42	-	-	-	-

Table A.4: **Characteristics of the Mexican Oil mixture**. Here, (l) refers to light, (m) to medium, and (h) to heavy. Also, $\%V$ indicates the vaporized volume percent of the mixture.

Characteristic:			
Weight (g)	31,770		
Density at 288 K (ml/g)	0.9227		
Watson Factor	12		
Measurement	**gas analysis**		
Component	*% V*		
n-Pentane	0.0903		
n-Hexano	0.1477		
Fractions:			
Cut point	*g*	*T (K)*	*M* $(\frac{g}{mol})$
0. gas	161	-	-
1. Naphtha (l)	717	311 -344	92.53
2. Naphtha (m)	4,466	344 - 458	145.767
3. Naptha (h)	2,220	458 - 523	189.18
4. Distillate (l)	1,334	523 - 555	233.843
5. Distillate (h)	3,457	555 - 638	306.228
6. Gasoil (l)	2,663	638 - 723	394.163
7. Gasoil (h)	2,056	723 - 773	400.67
Residual	12,725	811	-
TBP curve:	**D2892-10**		
% V	*T (K)*	P (kPa)	
0	303.3	75.91	
4	347.6	75.85	
8	374.3	76.06	
12	393.3	76.26	
16	422.8	76.36	
20	452.6	76.40	
24	423.9	13.08	
28	452.2	13.05	
32	115.9	0.268	
36	411.6	0.268	
43	450.3	0.268	

Appendix B

Standard Test Method for Distillation of Crude Petroleum. ASTM D2892

This test method covers the procedure for the distillation of stabilized crude petroleum to a final cut temperature of 400 $°C$ Atmospheric Equivalent Temperature (AET). This method employs a fractionating column having an efficiency of 14 to 18 theoretical plates operated at a reflux ratio of 5:1. Also, the performance criteria for the necessary equipment is specified and a typical examples of the distillation column is presented in schematic form in Fig. B.1.

The ASTM D2892 test allows to collect the sample of cuts (pseudo components) at different boiling point ranges. These cuts can be treated as any defined component and be subjected to physical and chemical measurements. The TBP curve, is the basis for the characterization of crude oil and its pesudo components for the purpose of design and analysis.

This test provides an estimates of the yields of pseudo components of various boiling ranges and is therefore valuable in technical and commercial discussions. The complete test description can be consulted in [52].

B.1 Test method

A weighed sample of 1 to 30 L of stabilized crude petroleum is distilled to a maximum temperature of 400 $°C$ AET in a fractionating column having an efficiency at total reflux of at least 14, but no greater than 18, theoretical plates. The reflux ratio of 5:1 is maintained at all operating pressures, except that at the lowest operating pressure of 0.27 kPa (2 $mm\ Hg$), a reflux ratio of 2:1 is optional.

If the final cut point has not been reached, distillation can be continued at a lower pressure. Only one pressure level between 13.3 kPa (100 $mm\,Hg$) and 0.27 kPa is permitted. It is necessary to shut off the reflux valve and the heating system. This allows the contents to cool to such a temperature that the distillation can be commenced at 13.3 kPa without flooding. In the case of a pressure of 0.27 kPa, without boiling.

Where the maximum cut point is 400 $°C$ AET, the minimum pressure is recommended. Each of these operations may be taken as a separate distillation process. When the final cut point has been reached, the reflux valve and the heating system are turned off. This allows one to cool with the vacuum still applied.

Observations of temperature, pressure, volume, time are recorded at intervals and at the end of each cut or fraction. A summary of these data are presented in Appendix C. The mass and density of each cut or fraction are obtained. Distillation yields by mass are calculated from the mass of all fractions, including liquefied gas cut and the residue. The first and second distillate fractions, also called light ends, are submitted for analysis by gas chromatography. Finally, from these data the TBP curves (in % mass or % volume), versus AET are drawn.

B.2 Apparatus

The distillation flask shall be of a size that is at least 50 % larger than the volume of the charge. The heating of the flask shall be provided in such a way that full boilup can be maintained at a steady rate at all pressure levels.

An electric heating mantle covering the lower half of the flask and having one third of the heat in an element located in the bottom central area and the remaining two thirds in the rest of the hemisphere is recommended. Minimum wattage required to provide full boilup of crude petroleum is approximately 0.125 W/mL of charge. Twice this amount is recommended for quick heat-up.

The fractionating column must contain either particulate packing or real plates. We show in Table B.1 the data of the plates used in the IMP equipment where the ASTM D2892 is applied.

Table B.1: **Plates properties for the fractionating column.** Here, the height equivalent to one theoretical plate (HETP) is expressed as the percentage of one theoretical plate that is achieved on one real plate.

Properties	
Size (mm)	50
Boilup ($mL/h\,cm^2$)	640
Dynamic holdup (mL/theoretical plate)	12.4
HETP, (% of real plates)	65 %
Pressure drop (KPa/theoretical plate)	0.16

The column shall be enclosed in a heat insulating system, such as a glass-fabric mantle, capable of maintaining the temperature of the outer wall of the glass vacuum jacket equal to that of the internal vapor temperature.

The adjustable reflux divider shall be located about one column diameter above the top of the packing or topmost plate. It must be capable of dividing the condensate with an accuracy of better than 90 % .

The condenser shall have sufficient capacity to condense essentially all the C_4 and C_5 vapors from the crude at the specified rate, using a coolant temperature of $-20°C$.

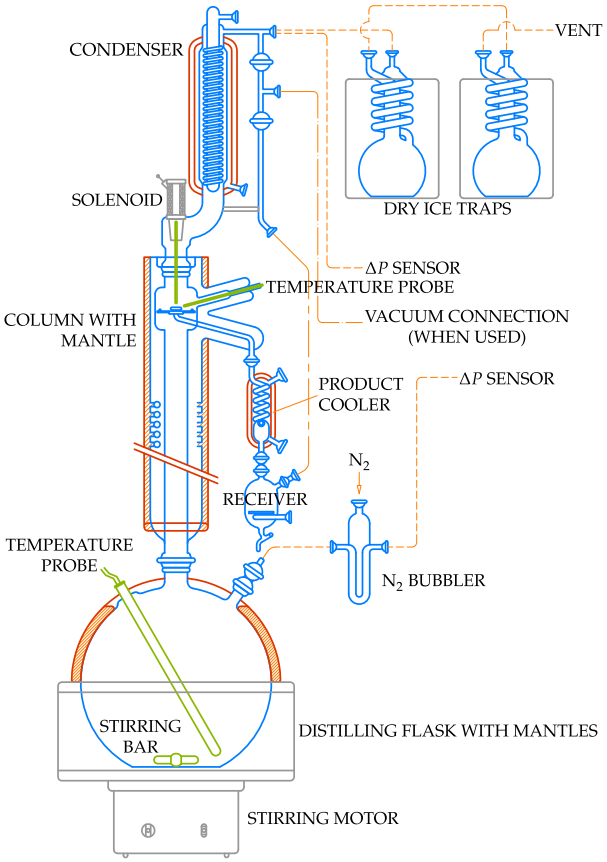

Figure B.1: **Batch column**. Typical distillation equipment with all components conforming to the requirements specified in ASTM D2892. ASTM distillation is carried out in a relatively simple apparatus consisting of a flask holding the sample connected to an inclined condenser, which condenses the rising vapors.

The receivers shall be of suitable size for the quantity of crude petroleum being distilled. The recommended capacity is from 100 to 500 mL. They shall be calibrated and graduated to permit reading to the nearest 1 %.

The vacuum system shall be capable of maintaining smooth pressure operation at all pressure levels. It shall have the capacity to draw down the pressure in the receiver(s) from atmospheric to 0.27 kPa in less than 30 s, so as to avoid disturbance of the system during emptying of receivers under vacuum.

The regulator shall maintain the pressure in the system essentially constant at all operating pressures. Automatic regulation can be achieved by a device that regulates the demand on the vacuum source.

The apparatus counts with a sensor for the vapor temperature and for the the liquid temperature. For the first one, the top of the sensor shall be located above the top of the packing or the topmost glass plate and in close proximity to the reflux divider but not in contact with the liquid reflux. Temperatures are recorded automatically and registered in duplicate.

Appendix C

TBP Distillation. Raw Results vs Time

A summary of the measurements of temperatures, flows, pressures and % volume are given in the present appendix. The mass of the sample charged was 31,770 g, with a denstity (at 15 $°C$) of 0.9227 g/mL and a *K factor* of 12. The Mexican oil mixture was analyzed by the IMP in August 2014.

Next we display the 3 operation stages. Table C.1 corresponds to the data obtained at atmospheric pressure, Table C.2 at 13.3 kPa and finally Table C.3 at 0.27 kPa. We omit the measurements registered at the shut down periods between each operation.

The atmospheric equivalent temperature, $T1$ *AET*, and the real temperature of the liquid, $T1$ *real*, in $°C$, were registered.

Also, the flux rate in mL/min and the pressure in $mm\,Hg$. These data allows us to drawn the TBP curves in % volume versus AET of the Mexican crude oil.

Table C.1: **Record of the experimental data at atmospheric pressure.**

Time (min)	T1 AET ($°C$)	% V	Rate mL/min	P $mm\,Hg$	T1 Real ($°C$)
141	38.51	0.00	0.00	569.41	30.00
195	65.95	2.63	14.42	569.89	56.86
205	70.94	3.02	14.97	570.11	61.76
232	86.75	4.26	15.55	570.34	77.26
286	105.96	6.94	14.81	569.30	96.02
340	115.53	9.26	13.64	569.97	105.44
394	125.57	11.32	11.60	572.16	115.42
412	130.36	11.99	12.44	571.04	120.05
448	140.60	13.31	11.82	571.50	130.12
502	153.23	15.06	9.83	572.35	142.58
520	157.92	15.64	10.95	572.61	147.20
556	165.95	16.77	9.92	572.82	155.10
610	177.03	18.28	9.27	574.09	166.07
664	187.67	19.63	8.21	573.94	176.51
701	194.86	20.51	7.70	573.05	183.53

Table C.2: **Record of the experimental data at 13.3 kPa.**

Time (min)	T1 AET ($°C$)	% V	Rate mL/min	P $mm\,Hg$	T1 Real ($°C$)
843	193.53	20.74	0.00	98.33	124.84
853	206.47	21.62	34.61	98.57	136.47
858	210.25	22.10	35.09	99.26	140.05
863	214.16	22.56	29.09	96.08	142.63
873	215.15	23.33	16.33	100.88	144.91
883	222.65	23.95	22.63	96.48	150.36
888	223.71	24.27	22.17	99.38	152.17
893	227.66	24.65	26.76	99.10	155.64
903	234.54	25.39	24.62	97.32	161.29
908	238.25	25.73	20.00	95.56	164.09
913	240.97	26.14	30.95	99.15	167.64
923	247.19	26.95	31.13	98.22	172.96
928	251.74	27.29	25.07	93.11	175.46
933	249.97	27.71	19.90	99.88	175.98
943	256.22	28.43	26.25	98.62	181.24
953	263.49	29.14	21.83	98.33	187.73

Table C.3: **Record of the experimental data at 0.27 kPa.**

Time (min)	T1 AET ($°C$)	% V	Rate mL/min	P $mm\,Hg$	T1 Real ($°C$)
1099	241.05	29.45	1.25	2.01	80.41
1121	254.23	29.79	5.75	2.01	90.52
1154	266.71	30.49	7.95	2.01	100.14
1198	281.59	31.51	9.75	2.01	111.70
1220	288.90	32.23	12.82	2.01	117.41
1264	297.93	33.65	10.25	2.01	124.47
1286	300.95	34.23	5.78	2.01	126.84
1308	306.08	34.80	10.46	2.01	130.88
1352	316.46	36.15	11.31	2.01	139.07
1374	321.63	36.85	12.49	2.01	143.13
1396	326.26	37.59	11.60	2.01	146.83
1440	333.93	38.86	5.48	2.00	152.83
1462	338.11	39.48	9.20	2.01	156.29
1484	344.50	40.19	11.31	2.01	161.40
1528	349.82	41.30	7.64	2.01	165.66
1572	361.73	42.53	10.51	2.01	175.25

Appendix D

Property Methods

A property method is a collection of models that Aspen Plus uses to compute thermodynamic and transport properties. The thermodynamic properties are the fugacity coefficient, the enthalpy and the entropy. On the other hand, the transport properties are the viscosity, the thermal conductivity, the diffusion coefficient and the surface tension. In particular, selecting an adequate property method is crucial for obtaining reliable simulation results of the particular distillation process and mixture.

D.1 The NRTL Property Method

The Non-Random Two Liquid (NRTL) property method can describe vapor and liquid equilibrium (VLE) properties of strongly nonideal solutions. Under this name the set of models shown in Table D.1 are embodied. The ethanol-water mixture used in the two extractive distillation columns, ExtM and ExtK respectively, is an example of a system that exhibits nonideality.

The NRTL property method requires binary parameters that are included in the Aspen Physical Property System (APPS) databanks. These parameters should be fitted in the temperature, pressure and composition range of operation. No component should be close to its critical temperature.

Table D.1: **NRTL Property Method.**

Thermodynamic properties	*Models*
Liquid mixture fugacity coefficient	NRTL
Gibbs energy	Extended Antoine Equation
	Henry's constant
	Belvi-O'Connell model
Enthalpy	General pure component ideal gas heat capacity
Entropy	General pure component heat of vaporization
Density	Rackett

The solubility of supercritical gases is modeled by using Henry's law. The property methods with a vapor phase model that can be used up to moderate pressures, have

the Poynting correction included in the liquid fugacity coefficient calculation. The heat of mixing is calculated by using the NRTL model. Next, we will briefly describe each model mentioned in Table D.1.

The thermodynamic model used for the vapor phase is the ideal gas since the operation of the column is at a relative low pressure. Under low pressure conditions, the intermolecular forces are so small that they can be neglected. In addition, since the empty space between the molecules is so large the volume of the molecules may be neglected in comparison with the gas volume. The universal form of the equation of state (EOS) is

$$PV = RT \tag{D.1}$$

where T is absolute temperature, P is the gas absolute pressure, V is the molar volume of an ideal gas and R is the universal gas constant in the proper units.

The submodel for calculating the vapor pressure of a liquid is the extended Antoine equation, namely

$$lnP_i^{*,L} = C_{1,i} + \frac{C_{2,i}}{T + C_{3,i}} + C_{4,i}T + C_{5,i}lnT + C_{6,i}T^{C_7} \tag{D.2}$$

where the parameters $C_{j,i}\,(j = 1, ..., 7)$ are the Antoine constants and are available from the APPS pure component databank. The asterisk is used to distinguish the pure component from the mixture.

The NRTL model calculates liquid activity coefficients γ_i. This coefficient is a parameter that indicates the degree of nonideality of the system. The model requires binary parameters that are included in the APPS databanks. The equation for the NRTL model is [78]

$$ln\gamma_i = \frac{\sum_j x_j\tau_{ji}G_{ji}}{\sum_k x_kG_{ki}} + \sum \frac{x_jG_{ij}}{\sum_k G_{kj}}\left[\tau_{ij} - \frac{\sum_m x_m\tau_{mj}G_{mj}}{\sum_k x_kG_{kj}}\right] \qquad T_{lower} \leq T \leq T_{upper} \tag{D.3}$$

where

$$G_{ij} = exp(-\alpha_{ij}\tau_{ij})$$

$$\tau_{ji} = \alpha_{ij} + b_{ij}/T + e_{ij}lnT + f_{ij}T$$

$$a_{ij} = c_{ij} + d_{ij}(T - 273.15K)$$

$$\tau_{ii} = 0$$

$$G_{ii} = 1,$$

where the parameters a_{ij}, b_{ij}, e_{ij} and f_{ij} are unsymmetrical and obtained from the databanks in the corresponding literature [49]. The recommended c_{ij} value for nonpolar substances is 0.30.

The Belvi-O'Connell model calculates the partial molar volume of a supercritical component i at infinite dilution in a pure solvent A, $V_{i,A}^{\infty}$. The general form of the model is [79]

$$V_{i,A}^{\infty} = fcn(V_i^{BO}, V_A^{BO}, V_A^{*L}) \tag{D.4}$$

where subindex i refers to the solute or dissolved gas component, A is the solvent component. Additionally, $V^{BO} = V_1 + TV_2$. The above correlation applies to both solute and solvent. For the liquid molar volume of mixtures, $V_i^{*.L}$, the Rackett mixture equation is used by default. The Rackett equation is given by [80]

$$V_i^{*,L} = \frac{RT_{ci}\left(Z_i^{*,RA\left[1+(1-T_r)^{\frac{2}{7}}\right]}\right)}{P_{ci}} \tag{D.5}$$

where P_{ci} is the critical pressure, $Tr = T/T_{ci}$ is the reduced temperature (always calculated by using absolute temperature units), T_{ci} is the critical temperature and $Z^{*,RA}$ is the Rackett parameter.

An important VLE relation is the relation for gas solubility in liquids. The Henry's constant model is used when Henry's law is applied to calculate K-values for dissolved gas components in a mixture. It can be formulated as

$$ln\left(\frac{H_i}{\gamma_i^{\infty}}\right) = \sum_A w_A ln\left(\frac{H_{i,A}}{\gamma_{i,A}^{\infty}}\right) \tag{D.6}$$

where

$$w_A = \frac{x_A(V_{cA})^{\frac{2}{3}}}{\sum_B x_B(V_{cB})^{\frac{2}{3}}}$$

$$lnH_{iA}(T, P_A^{*,L}) = a_{i,A} + b_{iA}/T + c_{iA}lnT + d_{iA}T + e_{iA}/T^2$$

The Henry's constants $a_{i,A}$, b_{iA}, c_{iA}, d_{iA}, and e_{iA} are specific to a solute-solvent pair. They can be obtained from regression or gas solubility data. The APPS has a large number of built-in Henry's constants of many solutes in solvents. These parameters were obtained by using data from the Dortmund Databank. Henry's law is a good approximation when the pressure is low (5 to 10 bar), the solute concentration in the solvent, x_A is low (not exceeding 0.03) and the temperature is well below the critical temperature of the solvent.

For a compound with known chemical structure, the ideal gas heat capacity polynomial is used, namely

$$C_p^{*ig} = C_{1i} + C_{2i}T + C_{3i}T^2 + C_{4i}T^3 + C_{5i}T^4 \tag{D.7}$$

where the parameters $C_{j,i}\,(j = 1, ..., 7)$ are constant for each compound available from the APPS pure component databank. Once C_p^{*ig} in known, the ideal gas enthalpy and entropy, H^{*ig} and S^{*ig}, may be determined.

The Watson equation is used to calculate heats of vaporization. It reads

$$\Delta_{vap}H_i^* = \Delta_{vap}H_i^*(T_1)\left(\frac{1 - T/T_{ci}}{1 - T_1/T_{ci}}\right)^{a+b} \tag{D.8}$$

where $H_i^* = \Delta_{vap}H_i^*(T_1)$ is the heat of vaporization at temperature T_1, a and b are constants whose default value is 0.38 and 0, respectively.

Once we have described the thermodynamic properties we can now address the transport properties. For the liquid mixture, the thermal conductivity coefficient is calculated by using Li's equation [78], namely

$$\lambda^L = \sum_i \sum_j \phi_i \phi_j \lambda_{ij} \tag{D.9}$$

where

$$\lambda_{ij} = 2\left[(\lambda_i^{*,L})^{-1} + (\lambda_j^{*,L})^{-1}\right]^{-1}$$

$$\phi_i = \frac{x_i V_i^{*,L}}{\sum_j x_i V_j^{*,L}}.$$

The pure component liquid thermal conductivity, $\lambda_j^{*,L}$ is calculated by the General pure component liquid thermal conductivity model which is comformed by several submodels (Sato-Riedel, NIST ThermoML polynomial and NIST PPDS8). It uses an internal defined parameter, TRNSWT/4, to determine which submodel will be applied [50]. The vapor mixture thermal conductivity at low pressure is calculated from the pure component values by using the Wassiljewa Mason Saxena equation [78]

$$\lambda^V(p=0) = \sum_i \frac{y_i \lambda_i^{*,V}(p=0)}{\sum_j y_i A_{ij}} \tag{D.10}$$

where

$\lambda_i^{*,V}$ is the pure component vapor thermal conductivity. Similarly to the vapor case, it is calculated using the General pure component liquid thermal conductivity model. Such model has also submodels (Stiel-Thodos, DIPPR, PPDS, IK-CAPE and NIST ThermoML polynomial) and uses the internal parameter (TRNSWT/4) to determine which submodel will be enforced [50].

$$\mathcal{A}_{ij} = \frac{\left[1+\left[\frac{\eta_i^{*,V}(p=0)}{\eta_j^{*,V}(p=0)}\right]^{\frac{1}{2}}\left(\frac{M_j}{M_i}\right)^{\frac{1}{4}}\right]^2}{\left[8(1+\frac{M_i}{M_j})\right]^{\frac{1}{2}}}$$

To compute the viscosity the software has incorporated submodels for the low pressure vapor (Chapman-Enskog-Brokaw, DIPPR, PPDS, IK-CAPE polynomial equation, NIST ThermoML polynomial) and also for the liquid (Andrade, DIPPR, PPDS, IK-CAPE polynomial equiation, NIST PPDS9 and NIST TDE equation). The software evaluates internally by using a defined parameter. Later, it selects which combination of submodels provides the best fit.

Liquid and vapor surface tension are computed analogously. Apen Plus chooses the best submodel of the set (Hakim-Steinberg-Stiel, DIPPR, PPDS, IK-CAPE polynomial equation, NIST TDE Watson equation and NIST TDE expansion) by using the corresponding defined parameter.

D.2 The Peng-Robinson Property Method

The ideal gas law is neither applicable to real gases nor to liquids where the volume of molecules cannot be ignored in comparison with the volume of gas. The Peng-Robinson property method (PENG-ROB) is designed to overcome these two issues of ideal gas law with mathematical convenience. It is the method recommended for refinery and petrochemical applications because it can treat nonpolar or mildly polar mixtures. For example, hydrocarbons and light mixtures. Therefore, the property method is applicable in the high temperature and high pressure regions, such as in hydrocarbon processing applications.

The PENG-ROB's set of models is given in Table D.2. It uses the standard Peng-Robinson cubic equation for all the thermodynamic properties except the liquid molar volume. This thermodynamic property considers two manners of handling hydrocarbon mixtures. In case of are dealing with pseudo components, PENG-ROB utilizes the API model. On the other hand, if are the real components, the model for computing the liquid molar volume is the Rackett approach (see Eq. D.5).

Table D.2: **Peng Robinson Property Method.**

Thermodynamic properties	*Models*
Vapor mixture, fugacity coefficient and density	Peng-Robinson
Enthalpy, entropy and Gibbs energy	General pure component ideal gas heat capacity Peng-Robinson
Liquid mixture and fugacity coefficient	Peng-Robinson

The Peng-Robinson property method uses the literature version of the alpha function and mixing rules [81]. The equation for this model is given by

$$P = \frac{RT}{V_m - b} - \frac{a}{V_m + b} + b(V_m - b) \tag{D.11}$$

where

$$b = \sum_i x_i b_i$$

$$a = \sum_i \sum_j x_i x_j (a_i a_j)^{0.5} (1 - c_{ij})$$

$$a_i = fcn(T, T_{ci}, P_{ci}, \omega_i)$$

$$c_{ij} = c_{ij}^{(1)} + c_{ij}^{(2)} T + c_{ij}^{(3)} / T$$

$$c_{ij} = c_{ji},$$

the binary parameter c_{ij} must be determined from regression of phase equilibrium data such as VLE data. The APPS also has built-in c_{ij} for large number of component pairs in its databank.

The molar volume for a mixture, using both the API approach and the Rackett model, V_m^L, is calculated from

$$V_m^L = x_p V_p^L + x_r V_r^L \tag{D.12}$$

where x_p is the mole fraction of the pseudo components and x_r is the mole fraction of real components. For pseudo components, the API approach is given by

$$V_p^L = fcn(T, T_b, API) \tag{D.13}$$

where fcn is a correlation based on API procedure 6A3.5 [82]. At high density the Ritter equation is used

$$V_p^L = \frac{1}{62.3636}\left[SG^2 - \frac{(1.2655SG - 0.5098 + 8.011 \times 10^{-5} T_b)(T - 519.67)}{T_b}\right]^{-1/2} \tag{D.14}$$

where SG is the specific gravity, T_b is the mean average boiling point, T is the temperature of the system.

To compute the gas heat capacity, enthalpy, entropy and Gibbs energy, the APPS has several submodels (Ideal gas heat capacity polynomial (see D.7), DIPR 107, Barin, PPDS, PML, IK-CAPE, NIST ThermoML and NIST Aly-Lee). It uses parameter THRSWT/7 to determine which submodel will be utilized.

For the vapor and liquid pure component thermal conductivity, the APPS has the following submodels, Stiel-Thodos, DIPPR, PPDS, IK-CAPE and NIST ThermoML polynomial. It uses the parameter TRNSWT/4 to determine which submodel will be used for the hydrocarbon mixture.

The software has incorporated submodels in order to compute the vapor viscosity (Chapman-Enskog-Brokaw, DIPPR, PPDS, IK-CAPE polynomial equation, NIST ThermoML polynomial).

The liquid mixture viscosity is computed analogously to the liquid molar volume. It considers two manners of handling hydrocarbon mixtures. In case of are dealing with pseudo components, PENG-ROB computed the liquid mixture viscosity by using the API equation, namely

$$\eta^L = fcn(T, x, T_{bi}, API, V_m^L) \tag{D.15}$$

where fcn is a correlation based on API procedures [82].

If one are dealing with the real components, the PENG-ROB property method has several submodels (Andrade, DIPPR101, PPDS, IK-CAPE polynomial equation and NIST TDE equation). Later, it evaluates internally by using a defined parameter and selects which submodel provides the best fit.

Finally, liquid mixture surface tension for hydrocarbons is calculated by using the API model.

$$\mathfrak{r}^L = fcn(T, x, T_{bi}, API, V_m^L) \tag{D.16}$$

where fcn is a correlation based on API procedures [82].

Once we have described the thermodynamic properties we can now address the transport properties. We have used the recommended procedures to handle crude oil systems and petrochemical applications described in Seader et. al. [29] and Riazi et. al. [32] in order to estimate the required transport and thermodynamic properties. The corresponding methods are summarized in Table D.3.

Table D.3: **Method used for the computation of the transport and thermodynamic properties.**

Property	Method	Source
Vapor thermal conductivity (λ^V_{mix})	General pure component vapor thermal conductivity mode	[48, 50]
Liquid thermal conductivity (λ^L_{mix})	Component liquid thermal conductivity model	[50]
Vapor mass transfer coefficient (k^V_{ij})	Onda's correlation	[63]
Liquid mass transfer coefficient (k^L_{ij})	Onda's correlation	[63]
Soret coefficient (S^T_i)	Nonequilibrium molecular dynamics approach	[83]
Vapor Maxwell-Stefan diffusion coefficient ($\mathcal{D}^V_{ij}$)	Film model	[84]
Liquid Maxwell-Stefan diffusion coefficient ($\mathcal{D}^L_{ij}$)	Film model	[84]
Liquid and vapor fugacity, (f^π_i)	Peng-Robinson Eq. of state	[81]

For the thermal conductivity of gases, the General pure component vapor thermal conductivity mode provides the basis of prediction, which is conformed by several submodels (Sato-Riedel, NIST ThermoML polynomial and NIST PPDS8). It uses an internal defined parameter, TRNSWT/4, to determine which submodel will be applied [48, 50].

The estimation of the liquid thermal conductivity is made by using the Component liquid thermal conductivity model, namely [50].

$$\lambda^L_i = \left[11.4 \times 10^5 (14.52 T_r - 5.14)^{\frac{2}{3}}\right] \frac{C_{pi}}{k}. \tag{D.17}$$

where, the subindex i refers to the corresponding component or pseudo component, C_{pi} is the constant pressure heat capacity (in $J/mol\,K$) of pseudo component i available from the APPS databank. Finally, k is a empirical coefficient and T_r is the reduce temperature given by

$$k = 1.11264 \frac{T_c^{\frac{1}{6}} M^{\frac{1}{2}}}{P_c^{\frac{2}{3}}}$$

Here and T_c is the critical temperature (in K), P_c is the critical pressure (in bar). For the mixture thermal conductivity of the liquid and vapor phases, the following mixture rules are recommended [32]

$$\begin{aligned} \lambda^V_{mix} &= \left[\sum_{i=1}^{4} \frac{y_i}{\lambda^V_i}\right]^{-\frac{1}{2}} \\ \lambda^L_{mix} &= \frac{1}{\sum_{i=1}^{4} \frac{x_i}{\lambda^L_i}} \end{aligned} \tag{D.18}$$

The $D^\pi_{T,i}$ may be obtained from the Soret S^T_i and Maxwell-Stefan diffusion coefficients $\mathcal{D}_{ij}$ as

$$D^\pi_{T,i} = \sum_{i=1}^{n} \Gamma_{ij} \mathcal{D}^\pi_{ij} S^T_i \tag{D.19}$$

where Γ_{ij} that represents the nonideality of the mixture is defined for a multicomponent liquid mixture as

$$\Gamma_{ij} = \delta_{ij} + x_i \frac{\partial ln \gamma_i}{\partial x_j}\bigg|_{T,P,\Sigma}, \tag{D.20}$$

where γ_i is the activity coefficient of component i and the symbol Σ is used to indicate that the differentiation of $ln\,\gamma_i$ with respect to the mole fraction x_j is to be carried out while keeping constant the liquid mole fractions of all the other species except the Nth. The mole fraction of species n must be eliminated using the fact that the x_i add to unity [3].

In Eq. D.19, we computed Γ_{ij} and $\mathcal{D}_{ij}^{\pi}$ by using the PENG-ROB property method, while S_i^T was obtained from literature. Expressions for the Soret coefficient in hydrocarbon mixtures [69] are available, but they involve the thermodiffusion factor and the activation energy of viscous flow of a complex physicochemical phenomenon, quantities which are not at hand. Therefore, we decided to use the results of measurements of the Soret coefficient s_T of crude oil samples (binary mixtures) held in reservoir initial conditions (a pressure of 350 bar and a temperature of $333\,K$) [85] which are of the same order of magnitude as the values reported in [69]. For an atmospheric condition the reported value is $s_T = 0.0212772\ 1/K$. Considering this value as a reasonable first approximation, we will set all of our Soret coefficients as $S_i^T = s_T$.

Appendix E

Transport coefficients for the case of study Ext KR extractive column

In order to estimate the resistivities on a tray for the appropiate composition and temperature by using the expression in Table 2.1, it is necessary first to compute the corresponding transport coefficients expressed in this Appendix.

The thermal conductivity was taken from Reid et. al [78], given by

$$\lambda_i = A_i^{\lambda} + B_i^{\lambda} T + C_i^{\lambda} T^2 + D_i^{\lambda} T^3 \tag{E.1}$$

The conductivity of a vapor mixture was the molar average one. For the thermal conductivity of a liquid mixture we follow the recommended quation by Yano et al. [86], namely:

$$\lambda = w_1 \lambda_1 + w_2 \lambda_2 - 0.45 w_1 w_2 |\lambda_1 - \lambda_2| \tag{E.2}$$

The heat capacities for the liquid and vapor, C_p^L and C_p^V respectively, were taken from Smith and Van Nesss [87] using the formulation from Kuiken [57]

$$\mathcal{D}_{1,2}^T = D_{1,2} \left(1 + \frac{\partial ln \gamma_1}{\partial ln x_1} \right) \tag{E.3}$$

A polynomial of the third degree in mole fraction and second degree in temperature was assessed to be sufficient to describe the experimental data for the diffusion coefficient. The model was created by starting with the suggested polynomial including all cross combinations. Then a linear regression was performed and the term with the highest p-value was taken out of the model. This was done until all p-values were below 10^7. The result was a polynomial with only 4 terms and a constant:

$$10^9 \mathcal{D}_{1,2}^L = 1.15 + \frac{T - 305}{50} (1.66 + 18.4 x_1 - 35.7 x_1^2 + 17.7 x_1^3 \tag{E.4}$$

The fuller relation was used for $D_{1,2}^V$, as proposed by the Taylor and Krishna [3]

$$\mathcal{D}_{1,2}^V = 1.01310^{-2} T^{1.75} \frac{\sqrt{\frac{M_1 + M_2}{M_1 M_2}}}{P \left(\sqrt[3]{V_1} + \sqrt[3]{V_2} \right)} \tag{E.5}$$

Kolonder et. al. [88] measured the Soret coefficient of a liquid ethanol-water mixture in the range from $283K$ to $313K$ and 0.05 to 0.6 ethanol mole fraction. The experimental results showed a shift in sign. A model for the s_T was presented, suitable for extrapolation:

$$10^3 s_T = \left(2.493 - \frac{T}{39.661}\right)\left[1 - 3.190\sqrt[3]{tanh\left(\frac{w - 0.2387}{0.1668}\right)^3}\right] \tag{E.6}$$

The temperature is given in K and w is the weighr fraction of ethanol. In the table E.1 the values of the constant used in Eqs.(E.1) – (E.5) are given.

Table E.1: Physical chemical properties

Component	**Ethanol**	**Water**	**Reference**
T^{boil} (K)	351.45	373.73	Sinnot et al. (1993) [89]
ρ^L (kg/m^3)	789	998	Sinnot et al. (1993) [89]
$\Delta_{vap}H(T^{boil})$, (J/mol)	38,770	40,683	Sinnot et al. (1993) [89]
$A^{C_p^V}$ (-)	3.518	3.470	Smith and Van Ness (1997) [87]
$B^{C_p^V}$ $(1/k)$	20.001×10^{-3}	1.450×10^{-3}	Smith and Van Ness (1997) [87]
$C^{C_p^V}$ $(1/K^2)$	6.002×10^{-6}	-	Smith and Van Ness (1997) [87]
$D^{C_p^V}$ (K^2)	-	0.121×10^5	Smith and Van Ness (1997) [87]
$A^{C_p^L}$ (-)	33.866	8.712	Smith and Van Ness (1997) [87]
$B^{C_p^L}$ $(1/k)$	-172.60×10^3	1.25×10^3	Smith and Van Ness (1997) [87]
$C^{C_p^V}$ $(1/K^2)$	349.1719×10^6	0.18×10^6	Smith and Van Ness (1997) [87]
A^{λ^V} (W/mK)	7.797×10^{-3}	7.341×10^{-3}	Reid et al (1987) [78]
B^{λ^V} (W/mK)	4.167×10^{-5}	-1.013×10^{-5}	Reid et al (1987) [78]
C^{λ^V} (W/mK)	1.214×10^{-8}	1.8017×10^{-7}	Reid et al (1987) [78]
D^{λ^V} (W/mK)	-5.184×10^{-11}	9.100×10^{-11}	Reid et al (1987) [78]
A^{λ^V} (W/mK)	2.629×10^{-1}	-3.838×10^{-1}	Reid et al (1987) [78]
B^{λ^V} (W/mK)	-3.847×10^{-4}	3.364×10^{-3}	Reid et al (1987) [78]
C^{λ^V} (W/mK)	2.211×10^7	3.667×10^{-6}	Reid et al (1987) [78]
V_i	90.96	113.79	Taylor and Khrishna (1993) [3]

Appendix F

Transport coefficient's results of the Mexican crude oil

The results obtained of the transport coefficients from the simulation with Aspen Plus are given in the present appendix. In Table F we have presented the corresponding to λ^{π}_{mix} are thermal conductivity, A_n is the interfacial area, h^{π} is the heat transfer coefficients and γ_{PCi} are the activity coefficient of the corresponding i pseudo component. Furthermore, we have displayed in Figs. F.1 and F.2 the low mass transfer coefficients, k^{π}_{ij}, and the Maxwell-Stefan diffusion coefficients, $\mathcal{D}^{\pi}_{ij}$.

Table F.1: **Transport properties of the Mexican oil mixture.**

λ^{L}_{mix} (W/m K)	λ^{V}_{mix} (W/m K)	A_n m^2	h^{L} m	h^{V} m	γ_{PC1}	γ_{PC2}	γ_{PC3}	γ_{PC4}
1.607	0	0	0	0	1.6824	0.04747	1.87E-03	6.29E-05
1.543	0.193	0.013727	500.069	55.977	2.9557	0.10390	0.00508	0.00022
1.464	0.196	0.014777	743.065	56.517	6.4501	0.31620	0.02105	0.00131
1.414	0.195	0.016196	785.423	58.323	10.2917	0.62588	0.05037	0.00390
1.398	0.195	0.016809	800.058	58.739	11.8781	0.77371	0.06607	0.00547
1.393	0.195	0.016993	807.166	58.772	12.3137	0.81620	0.07075	0.00596
1.392	0.196	0.016945	812.024	58.707	12.4549	0.83014	0.07231	0.00612
1.391	0.197	0.016803	816.027	58.619	12.5482	0.83941	0.07334	0.00623
1.390	0.199	0.016599	819.569	58.523	12.6588	0.85043	0.07458	0.00636
1.388	0.201	0.016328	822.788	58.420	12.8148	0.86606	0.07634	0.00655
1.385	0.204	0.015976	825.765	58.304	13.0446	0.88927	0.07897	0.00683
1.381	0.208	0.015529	828.583	58.165	13.3923	0.92482	0.08304	0.00727
1.376	0.213	0.014932	831.354	57.989	13.9340	0.98117	0.08958	0.00799
1.368	0.220	0.014249	834.248	57.753	14.8111	1.07489	0.10069	0.00924
1.356	0.229	0.013511	837.553	57.422	16.2962	1.24046	0.12102	0.01161
1.337	0.239	0.012799	1149.56	56.260	18.8998	1.55083	0.16123	0.01657
1.312	0.251	0.012216	1147.21	55.527	23.3271	2.13438	0.24322	0.02758
1.295	0.264	0	1150.50	55.087	61.7888	10	1.73996	0.31383

Due to the fact that the matrix of both the low mass transfer coefficients and the Maxwell-Stefan coefficients are symmetric ($k^{\pi}_{ij} = k^{\pi}_{ji}$ and $\mathcal{D}^{\pi}_{ij} = \mathcal{D}^{\pi}_{ji}$), we only display the six independent phenomenological coefficients.

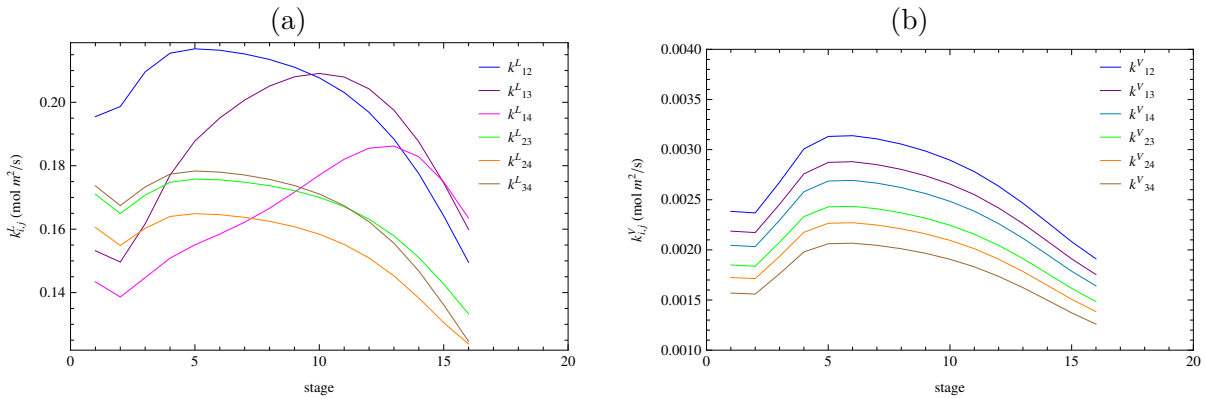

Figure F.1: **Low mass transfer coefficients in each stage**. (a) Liquid low mass transfer coefficients. Here, k^{L}_{ij} is the conjugate low mass transfer coefficient of the pseudo component i with the pseudo component j. (b) Vapor low mass transfer coefficients coefficients. The labels are the same of (a).

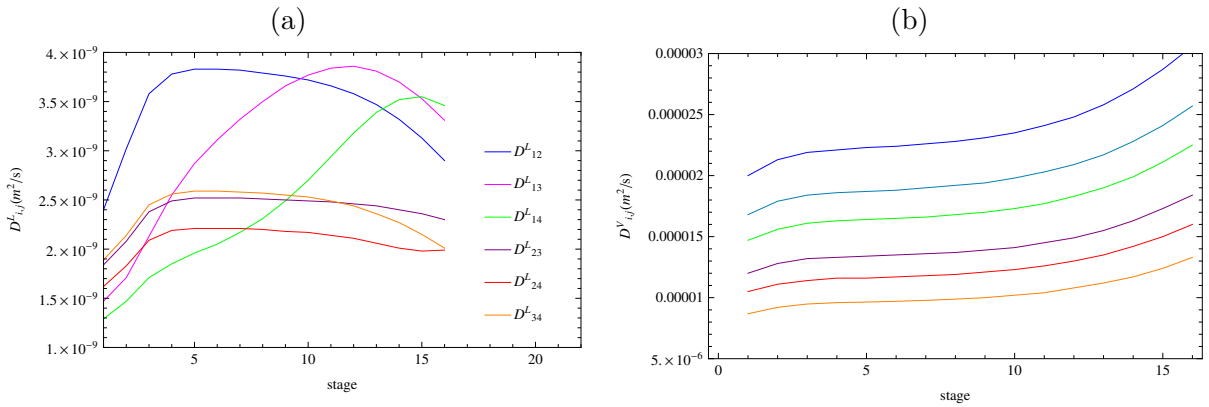

Figure F.2: **Maxwell Stefan diffusion coefficients in each stage**. (a) Liquid Maxwell Stefan diffusion coefficients. Here, D^{L}_{ij} is the conjugate low mass transfer coefficient of the pseudo component i with the pseudo component j. (b) Vapor Maxwell Stefan diffusion coefficients. The labels are the same of (a).

Appendix G

Manuscript: On entropy generation and the effect of heat and mass transfer coupling in a distillation process

Q1 P. Burgos-Madrigal*, D. F. Mendoza and M. López de Haro

On Entropy Generation and the Effect of Heat and Mass Transfer Coupling in a Distillation Process

https://doi.org/10.1515/jnet-2017-0039
Received August 08, 2017; revised October 18, 2017; accepted October 27, 2017

Abstract: The entropy production rates as obtained from the exergy analysis, entropy balance and the nonequilibrium thermodynamics approach are compared for two distillation columns. The first case is a depropanizer column involving a mixture of ethane, propane, n-butane and n-pentane. The other is a weighed sample of Mexican crude oil distilled with a pilot scale fractionating column. The composition, temperature and flow profiles, for a given duty and operating conditions in each column, are obtained with the Aspen Plus V8.4 software by using the RateFrac model with a rate-based nonequilibrium column. For the depropanizer column the highest entropy production rate is found in the central trays where most of the mass transfer occurs, while in the second column the highest values correspond to the first three stages (where the vapor mixture is in contact with the cold liquid reflux), and to the last three stages (where the highest temperatures take place). The importance of the explicit inclusion of thermal diffusion in these processes is evaluated. In the depropanizer column, the effect of the coupling between heat and mass transfer is found to be negligible, while for the fractionating column it becomes appreciable.

Keywords: exergy, distillation column, multicomponent mixture, hydrocarbon mixture, irreversible thermodynamics, thermal diffusion

1 Introduction

One of the most fundamental processes in the petroleum refining and petrochemical industries is the distillation of crude oil. This process involves a high energy consumption and has an inherently low thermodynamic efficiency. In this regard, energy optimization in such distillation processes is an important issue [1–3], and so the reduction of energy consumption in distillation has been the subject of intensive research [4–7]. One may address these problems through four kinds of thermodynamic methods applied to the analysis of energy consumptions: using only energy balances, considering second law efficiency, by studying the exergy behavior and through nonequilibrium thermodynamics [8–10], the two latter combining both the first and second laws. Nonequilibrium thermodynamics, *NET*, aims to provide a description of transport processes in systems that are out of equilibrium. In this approach, the second law of thermodynamics is reformulated in terms of the local entropy production in the system. In turn, this latter quantity involves the so-called thermodynamic driving forces and their conjugate fluxes [11–19].

To our knowledge, the use of the *NET* approach in the distillation of a truly multicomponent mixture is rather scarce. Notable exceptions in binary distillation are the works of Liang, Zhou, Wu, Geng and Zhang

***Corresponding author: P. Burgos-Madrigal,** Institute of Renewable Energy, National Autonomous University of Mexico (U.N.A.M), Priv. Xochicalco S/N, Temixco, Morelos 62580, Mexico, E-mail: pabum@ier.unam.mx, paulina.burgos.m@gmail.com
D. F. Mendoza, Mechanical Engineering Department, Faculty of Engineering, Autonomous University of the Caribbean, Barranquilla, Colombia, E-mail: diego.mendoza24@uac.edu.co
M. López de Haro, Institute of Renewable Energy, National Autonomous University of Mexico (U.N.A.M), Priv. Xochicalco S/N, Temixco, Morelos 62580, Mexico, E-mail: malopez@unam.mx

[20], Tsirlin and Grigorevsky [21] and Wesselingh [22]. Here we will consider two further examples, one theoretical (a depropanizer distillation column) and one of a real (laboratory scale) fractionating distillation column, in which the application of this approach may provide valuable information and pave the way to the *NET* analysis application to industrial scale oil mixtures. The scarcity of work related to the *NET* approach mentioned before is due to the fact that modeling a multicomponent distillation system, where simultaneous heat and mass transfer occurs, is a challenging task. The difficulty is not only related to the interaction effects among the different components in the mixture but also because one has to decide whether to account explicitly for the direct coupling of heat and mass transfer or to ignore this coupling. It is common to neglect such coupling in distillation since the Soret and the Dufour effects are considered to have little significance in unit operations [23, 24]. Nevertheless, several works [25–27] claim that the coupling between heat and mass transfer is needed to correctly describe the distillation process. In a relatively recent paper, van der Ham and Bock and Kjelstrup [28] have presented a model for coupled transfer of mass and thermal energy in the vapor-liquid region of a nitrogen–oxygen mixture. This study served as a basis to incorporate mass-heat transfer coupling to model a nonequilibrium distillation stage [29].

In this article, we will address the importance of including the coupling between heat and mass transfer in the thermodynamic driving forces for the description of the two chosen multicomponent distillation columns. Furthermore, the two different mixtures used in the respective distillation columns allow us to assess the effect of the difference in size of the molecules on the coupling between heat and mass transfer. In the depropanizer column, the molecules of all constituents of the mixture are similar in size and structure. On the other hand, for the Mexican oil, the components molecules may be very disparate in size.

To evaluate the importance of thermal diffusion, we have done with the aid of the Aspen Plus V8.4 software to compute the temperature, composition and flow profiles. Also, we will use a set of transport equations for heat and mass transfer in our hydrocarbon mixture that includes the necessary empirical correlations for the phenomenological transport coefficients. Finally, in order to assess the *NET* results, we compare the entropy production rate obtained for both cases with the exergy analysis, *Ex* and the global entropy balance, *EB*, both useful benchmarks.

The article is organized as follows. In the next section we describe our two cases of study, namely the depropanizer column and the laboratory scale fractionating column and we present the expressions for the global independent driving forces as well as fluxes, and the entropy production rate involved in the distillation process as required by *NET*. Section 3 contains the evaluation of the global heat and mass transfer rates, the global thermal and mass transfer driving forces, the assessment of the relative values of the partial contributions to these forces and a comparison of the results for the entropy production rate derived from the different formulations (*Ex*, *EB* and *NET*). The article is closed in the final section with some discussion and concluding remarks.

2 Entropy production rate on a tray

This section is devoted to a brief description of our two cases of study and the determination of both the local entropy production rate and the global entropy production rate in the trays of the columns. This will allow a comparison with the estimates for the same quantities derived from the *Ex* analysis and the global *EB*.

The distillation process may be analyzed in three different scales. The first one embodies the whole column. The analysis in this scale allowed us to obtain the operational profiles in Subsection 2.2. The intermediate scale is the one associated to a stage as illustrated in Figure 4a. Finally, the smallest scale is the region around the liquid–vapor interface, depicted in Figure 4b. We begin by providing the characteristics and operation details of both distillation columns.

2.1 Distillation columns

We first consider a prototype example in distillation, namely the depropanizer column described by Taylor and Krishna [23]. In this column, the main objective is to isolate propane from a mixture containing butane

and other components. The column consists of 35 theoretical stages (trays) and has been designed to separate 1000 mol/s of a four component mixture containing ethane, propane, n-butane and n-pentane. The operation takes place at a pressure of 1500 kPa, the fluid enters the column with a temperature of 298 K and a 2.5 reflux ratio. For simplicity we will neglect heat and pressure losses in the column.

The second system consists of a (laboratory scale) fractionating distillation column used in the Instituto Mexicano del Petroleo (IMP) to study and characterize a weighed sample of Mexican crude oil. This column employs 18 trays and the distillate may be collected at a constant rate. The method used to characterize this oil and its derivatives (petroleum fractions or cuts) obtained in the distillation process is the Test Method for Distillation of Crude Petroleum D2892-10 [30]. The test method involves operating at three different pressures, namely an atmospheric pressure (101.3 kPa) for the low boiling fractions and two other pressures (13.33 kPa and 2.66 kPa) for the high boiling fractions. Each of these three operations may be taken as a separate distillation process. Here, for the sake of having access to all the necessary data, we will restrict to the distillation taking place at 13.33 kPa, a reflux ratio of 2:1 and a maximum temperature of 453 K. A key point in this case of study, not feasible in the theoretical case of the depropanizer column, is that we will be able to combine real operation data of the column with the Aspen simulation to obtain the corresponding composition, temperature and flow profiles.

The Mexican oil mixture whose distillation we analyze consists of eight pseudocomponents, also referred to as petroleum fractions or cuts. In this article we only worked with the four cuts that volatilize in the operation up to a pressure of 13.33 kPa, corresponding to 28 % of the mixture. Also, we present the data from a true boiling point distillation test (TBP) that allows us to group hydrocarbons with close boiling points. All the information about the mixture was provided by the Instituto Mexicano del Petróleo after they performed the characterization of the mixture. The laboratory distillation process was carried out in April 2014. The detailed information of the two columns is presented in Tables 1 and 2.

Table 1: Operating and stream characteristics used in the simulation with the Aspen Plus V8.4 software for the depropanizer and fractionating columns. For both cases of study we took the RateFrac model with a rate-based nonequilibrium column and the Peng–Robinson property method.

	Depropanizer	**column**		**Fractionating column**
Streams:	*Feed 1*	*Top*	*Bottom*	
Stage	16	1	35	18
Pressure (kPa)	1500	1500	1500	13.33
Vapor fraction	0	1	0	0
Temperature (K)	298.15	308.15	378.15	303.15
Flow (l/min)	-	-	-	4×10^{-4}
Charge (g)	-	-	-	31,770
Flow (mol/s)				
Ethane	100	100	1.5×10^{-3}	-
Propane	300	296.7	3.329	-
n-Butane	500	3.328	496.7	-
n-Pentane	100	9.2×10^{-3}	100	-
Total flow	1000	400	600	-
Sections:	1	2		
First stage	2	16		2
Last stage	15	34		17
Column internals	Sieve tray	Sieve tray		Sieve tray
Column diameter(m)	4.820	6.170		0.80
Number of flow passes	5	5		4
Tray spacing (m)	0.5	0.5		0.09
Hole pinch (m)	0.01807	0.01685		0.0127

Table 2: Characteristics of the Mexican Oil mixture. Here, (*l*) refers to light, (*m*) to medium, and (*h*) to heavy. Also, %*V* indicates the vaporized volume percent of the mixture.

Characteristic:			
Weight (g)	31,770		
Density at 288 K	0.9227		
Watson Factor	12		
Fractions:			
Cut point	g	*T* (K)	*M* (g/mol)
0. gas	161	-	-
1. Naphtha (l)	717	311 - 344	92.53
2. Naphtha (m)	4,466	344 - 458	145.767
3. Naphtha (h)	2,220	458 - 523	189.18
4. Distillate (l)	1,334	523 - 555	233.843
5. Distillate (h)	3,457	555 - 638	306.228
6. Gas oil (l)	2,663	638 - 723	394.163
7. Gas oil (h)	2,056	723 - 773	400.67
Residual	12,725	811	-
TBP curve:	**D2892-10**		
% V	*T* (K)	P (kPa)	
0	303.3	75.91	
4	347.6	75.85	
8	374.3	76.06	
12	393.3	76.26	
16	422.8	76.36	
20	452.6	76.40	
24	423.9	13.08	
28	452.2	13.05	
32	115.9	0.268	
36	411.6	0.268	
43	450.3	0.268	

In our study for both columns, the further following assumptions will also be made: steady-state conditions, one-dimensional flow of the vapor and liquid phases that the vapor rising through the liquid within the tray is completely mixed and that there is no significant pressure gradient along the vapor and liquid flow directions. Moreover, for both cases of study, the operation RateFrac model was used since it allows us to simulate the distillation with the rate-based model. We have used the recommended procedures to handle crude oil systems and petrochemical applications described in Refs. [31] and [32] in order to estimate the required transport and thermodynamic properties. The property method utilized is the Peng–Robinson method, which is recommended due to its capacity for treating hydrocarbons and light mixtures. The corresponding methods are summarized in Table 3. The explicit expressions for these quantities will be omitted but are available upon request to any of the authors.

Once we have briefly described our systems we can now address the operational profiles. $\int$

2.2 Composition, temperature and flow profiles of our two cases of study

In this subsection we provide the composition, temperature and flow profiles obtained from the simulation with the rate-based model for our two cases of study, namely the depropanizer column and the laboratory fractionating column. In this model, two films are distinguishable on a distillation stage, as pictured in Figure 4, one on either side of the interface, through which the components diffuse. One also considers a heat flux through the films.

We will now briefly describe the standard balance equations of the rate-based model. We will use the superindex "π" to refer to liquid and vapor bulk or film. The mass balance for a component *j* in the liquid and

Table 3: Method used for the computation of the transport and thermodynamic properties.

Property	Method	Source
Vapor thermal conductivity (λ^V_{mix})	General pure component vapor thermal conductivity model	[33]
Liquid thermal conductivity (λ^L_{mix})	Component liquid thermal conductivity model	[33]
Vapor mass transfer coefficient (k^V_{ij})	Onda's correlation	[34]
Liquid mass transfer coefficient (k^L_{ij})	Onda's correlation	[34]
Soret coefficient (S^T_i)	Nonequilibrium molecular dynamics approach	[35]
Vapor Maxwell–Stefan diffusion coefficient ($\mathcal{D}^V_{ij}$)	Film model	[36]
Liquid Maxwell–Stefan diffusion coefficient ($\mathcal{D}^L_{ij}$)	Film model	[36]
Liquid and vapor fugacity, (f^π_i)	Peng–Robinson Eq. of state	[37]

vapor, $M^\pi_{j,n}$, phases for an nth column tray can be written as

$$\begin{aligned} M^L_{j,n} &: x_{j,F_n}F^L_n + x_{j,n-1}\mathcal{L}_{n-1} - x_{j,n}L_n - \mathcal{N}^L_{j,n} = 0 \\ M^V_{j,n} &: y_{j,F_n}F^V_n + y_{j,n+1}\mathcal{V}_{n+1} - y_{j,n}V_n - \mathcal{N}^V_{j,n} = 0 \end{aligned} \tag{1}$$

The last term in eq. (1) represents the net gain or loss of component j in the phase due to vapor–liquid mass transfer. It is calculated as the integral of the local mass transfer rates J_j over the stage interface area A_n.

$$\mathcal{N}^\pi_{j,n} = \int_0^{A_n} J^\pi_{j,n}\,dA \tag{2}$$

The flux is positive when directed from the vapor to the liquid phase. As mentioned above, in a steady-state operation there is no accumulation of mass in any part of the system, which means that mass transfer flows are equal on each side of the vapor–liquid transfer region

$$\mathcal{N}^V_{j,n} - \mathcal{N}^L_{j,n} = 0 \tag{3}$$

The total mass balances for the liquid and vapor phases, M^L_n and M^V_n are, respectively,

$$\begin{aligned} M^L_n &: F^L_n + L_{n-1} - L_n - \mathcal{N}_{T,n} = 0 \\ M^V_n &: F^V_n + V_{n+1} - V_n - \mathcal{N}_{T,n} = 0 \end{aligned} \tag{4}$$

The last term in eq. (4) is the total mass flow of the components in the mixture, $\mathcal{N}_{T,n} = \sum_{j=1}^{n}\mathcal{N}_{j,n}$.
The energy balance for the vapor and liquid phases, E^V_n and E^V_n, reads, respectively,

$$\begin{aligned} E^L_n &: Q^L_n + F^L_n H^L_{F_n} + L_{n-1}H^L_{n-1} - L_n H^L_n - \mathcal{E}^L_n = 0 \\ E^V_n &: Q^V_n + F^V_n H^V_{F_n} + V_{n+1}H^V_{n+1} - V_n H^V_n - \mathcal{E}^V_n = 0 \end{aligned} \tag{5}$$

where Q^V_n and Q^L_n represent the external heat transfer for the vapor and liquid phases, if it is the case, and H^π is the enthalpy of the stream. The terms $\mathcal{E}^L_n$ and $\mathcal{E}^V_n$ in eq. (5) are the net energy flows across the liquid and vapor phases, respectively

$$\mathcal{E}^\pi_n = \int_0^A J'^\pi_{e,n}\,dA \tag{6}$$

where J_e is the flux of energy in the respective phase

$$J_e'^{\pi} = J_q'^{\pi} + \sum_{k=1}^{N} J_i'^{\pi} \bar{H}_i^{\pi} \tag{7}$$

The first term on the right-hand side, J_q', is the measurable heat flux, the second term is the energy transported by component k associated with the partial molar enthalpy, $\bar{H}_k$.

The energy balance around the vapor–liquid transfer region, E_n^I, in the steady state, shows that the net energy change in the two phases is zero, namely

$$E_n^I = \mathcal{E}_n^L - \mathcal{E}_n^V = 0 \tag{8}$$

In Figure 1 we show the liquid and vapor temperature profiles. For the depropanizer column [case (a)], the liquid and vapor temperature profiles are almost coincident. In contrast, in the fractionating column more quantitative differences are apparent.

The liquid and vapor flows profiles appear in Figure 2. In the depropanizer column it is clear that from the early stages up to stage 16, the feed stage, the vapor flow is the predominant flow. After the feed stage, the flow behavior is reversed and the liquid flow becomes the predominant one. On the contrary, for the fractionating column in all stages but the first one, where the reflux is carried out, the vapor flow predominates over the liquid flow.

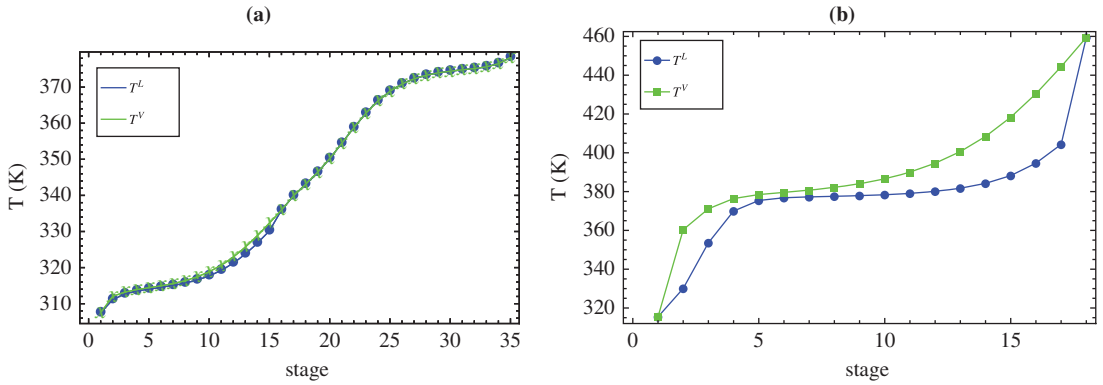

Figure 1: Liquid and vapor temperature profiles. (**a**) Depropanizer column. T^L is the liquid temperature and T^V is the vapor temperature. (**b**) Laboratory fractionating column. The labels are the same as those of (a).

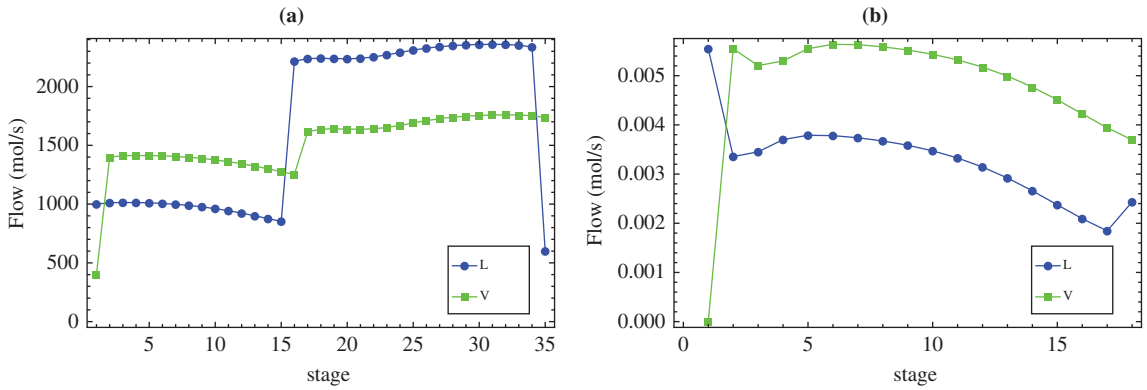

Figure 2: Flow profiles vs. stage number. (a) Depropanizer column. (b) Laboratory fractionating column.

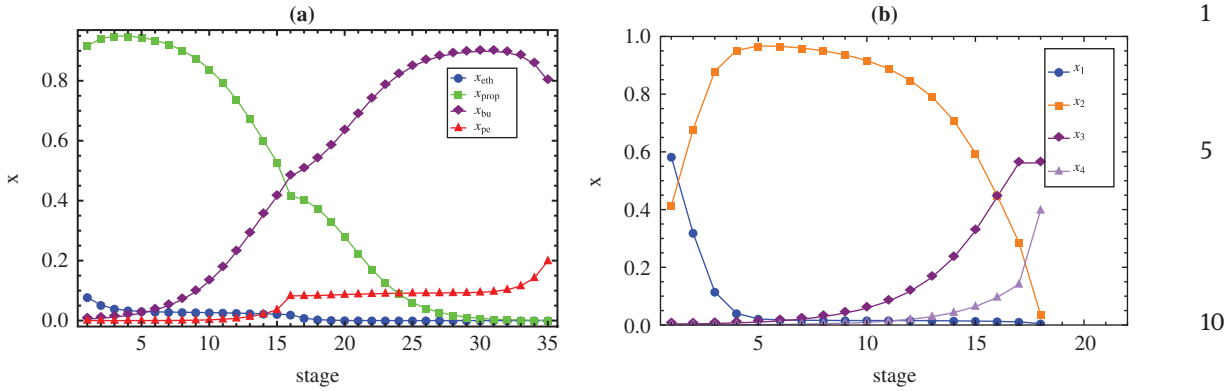

Figure 3: Liquid composition profiles vs. stage number. (a) Depropanizer column, where x_{eth} is the ethane mole fraction, x_{prop} is the propane mole fraction, x_{bu} is the n-butane mole fraction and x_{pen} is the n-pentane mole fraction. (b) Laboratory fractionating column, where x_1 is the pseudocomponent 1 mole fraction, x_2 is the pseudocomponent 2 mole fraction, x_3 is the pseudocomponent 3 mole fraction and x_4 is the pseudocomponent 4 mole fraction.

Now we turn to the liquid composition profiles shown in Figure 3. Both composition profiles vary strongly along the respective column. In the case of the depropanizer column, ethane (x_{eth}) and propane (x_{prop}) are concentrated at the top, while, butane (x_{bu}) and pentane (x_{pen}) are at the bottom. The two minor components, ethane and pentane, vary very little in composition in most parts of the two sections. In the fractionating column, the pseudocomponent 1 (x_1), which is the more volatile one, decreases its composition as it moves down the column, while pseudocomponent 2 (x_2) increases its composition up to the 6th tray and then declines. The pseudocomponents 3 (x_3) and 4 (x_4) are present in low concentration and the latter increases its composition relatively rapidly beyond stage 14.

2.3 Nonequilibrium description

We now turn to the *NET* analysis. The separation of the i^{th}-component occurs when the liquid and vapor phases are in contact and exchange heat and mass, as depicted in Figure 4. This includes such contact within the tray, bubbles and droplets. In our case, we will distinguish three regions, namely, the liquid bulk, the vapor bulk and the vapor–liquid region which includes the vapor film, the liquid film and the interface.

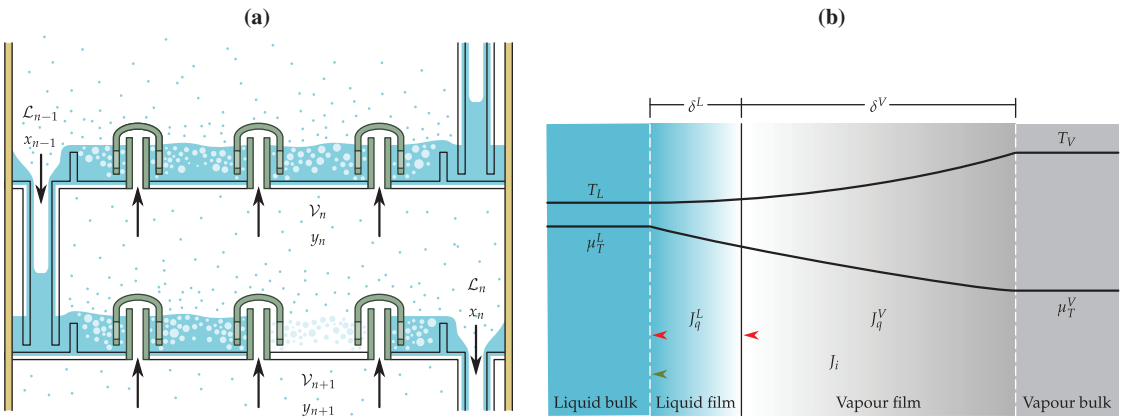

Figure 4: The system. (a) This is a representative scheme of a tray (stage) in the distillation columns studied with a high concentration of vapor. (b) We show a representation of a nonequilibrium stage. Notice that for both cases studied the vapor film is thicker than the liquid film.

Therefore, our thermodynamic system in both cases consists of the sum of these two bulks, the two films and the interface, as shown in the figure.

The model used to calculate the rates of heat and mass transfer is the classical film model developed by Taylor and Krishna [23]. The mass transfer rates across the liquid–vapor interface vary as a bubble rises on one tray, but due to the fact that the operation of the column reaches a stationary state, we will consider the average mass and heat transfer rates for each tray. The mass transfer rates are constant through the films, while the heat transfer rate has a discontinuity due to the enthalpy differences between liquid and vapor. We also take into account the sign convention that the positive direction of transport is from vapor to liquid. The transfer rates through the interface regions are functions of transfer coefficients and of the differences in temperature or composition between the bulk phases. This means that the rates of mass transfer can be calculated with the bulk compositions and temperatures equal to those of the streams leaving the stage.

The entropy production rate in a stage is the sum of the contributions of the liquid and vapor bulks and the liquid and vapor films, namely

$$\frac{dS_{irr}^{n}}{dt} = \sum_{\pi=L}^{\pi=V} \left(\frac{dS_{irr}^{\pi,bulk}}{dt} + \frac{dS_{irr}^{\pi,film}}{dt} \right), \tag{9}$$

The entropy production rate at the interface is zero. According to our previous assumptions, contributions to the entropy production from turbulence or pressure drop will be neglected.

The global entropy production rate in the films is obtained by integrating the local entropy production rate σ^{π} over the film thickness δ^{π} (to be specified below), namely

$$\frac{dS_{irr}^{\pi,film}}{dt} = \int_{0}^{\delta^{\pi}} \sigma^{\pi} A \, dx \tag{10}$$

where A is the interface area. Then our first task is to determine σ^{π}.

Note that in nonequilibrium thermodynamics, the second law is reformulated in terms of the local entropy production, σ. This quantity may be computed as the sum of the products of the so-called conjugate fluxes, J_{α}, and thermodynamic driving forces, X_{α}, in the system [11–19]. In the case of a multicomponent mixture it reads

$$\sigma = J_q' \cdot \nabla \frac{1}{T} - \sum_{i=1}^{N} \frac{J_i}{T} \cdot \nabla \mu_{i,T} = J_q' \cdot X_q' + \sum_{i=1}^{N} v_i \cdot X_i' \tag{11}$$

where N is the number of components, J_q' is the measurable heat flux, J_i is the molar mass flux of component i, μ_i is the chemical potential of component i and $\nabla \mu_{i,T}$ is the gradient of the chemical potential of component i at constant temperature and the velocity of component i with respect to the interface is defined as $v_i = J_i/c_i$ where c_i is the molar density of component i. Further, $X_q' \equiv -\frac{1}{T^2} \nabla T$ and $X_i' \equiv -\frac{c_i}{T} \nabla \mu_{i,T}$ are the local forces conjugate to the corresponding heat and mass fluxes. Note that, to treat all the forces on an equal ground, in eq. (11) we have included all the component driving forces, not only the independent ones. In fact, the component forces are related by the Gibbs–Duhem equation [13], namely

$$\sum_{i=1}^{N} X_i' = 0 \tag{12}$$

so that only $N - 1$ of these forces are independent. According to linear irreversible thermodynamics, X_q' and X_i' may be expressed in terms of the fluxes and the resistivities r_{qq}, r_{qi}, r_{ki} and r_{iq} as follows

$$X'_q = r_{qq}J'_q + \sum_{k=1}^{N} r_{qk}v_k$$
$$X'_i = r_{iq}J'_q + \sum_{k=1}^{N} r_{ik}v_k, \qquad (i = 1, 2, 3, \cdots N) \tag{13}$$

These resistivities obey the Onsager reciprocity relations, that is $r_{qi} = r_{iq}$ and $r_{ik} = r_{ki}$ and so from eq. (12) it follows that $\sum_{i=1}^{N} r_{ki} = \sum_{i=1}^{N} r_{ik} = 0$ and $\sum_{i=1}^{N} r_{qi} = \sum_{i=1}^{N} r_{iq} = 0$. It is convenient to rewrite eq. (13) in the form

$$X'_q = r_{qq}\left[J'_q - \sum_{k=1}^{N} c_k q^*_k v_k\right]$$
$$X'_i = -c_i q^*_i X'_q + \sum_{k=1,k\neq 1}^{N} R_{ki}(v_k - v_i), \qquad (i = 1, 2, 3, \cdots N) \tag{14}$$

where $q^*_i = -1/c_i\,(r_{qi}/r_{qq})$ is the heat of transfer and $R_{ik} = r_{ik} - (r_{iq}r_{qk}/r_{qq})$. In view of the symmetry relationships between the resistivities, one has that $R_{ik} = R_{ki}$, that $\sum_{i=1}^{N} c_i q^*_i = 0$ and that $\sum_{i=1}^{N} R_{ki} = \sum_{i=1}^{N} R_{ik} = 0$. We now follow Krishna and Wesselingh [38] and Kjelstrup and Bedeaux [17] in order to relate the resistivities R_{ik} and the heats of transfer q^*_i to the Maxwell–Stefan diffusion coefficients and the thermal diffusion coefficients. The result is

$$R_{ik} = -\frac{Rc_i c_k}{c_t \mathcal{D}_{ik}} \qquad (i \neq k), \tag{15}$$

where $R = 8.314$ J/K mol is the gas constant. Here $c_t = \sum_{i=1}^{N} c_i$ is the total molar density and $\mathcal{D}_{j,i}$ are the Maxwell–Stefan diffusion coefficients. The diagonal elements R_{ii} are obtained from the relationship $\sum_{i=1}^{N} R_{ik} = 0$. Further, the heat of transfer is given by

$$q^*_j = \sum_{k=1}^{N} \frac{RTc_k}{c_t \mathcal{D}_{jk}} \left(\frac{D_{T,k}}{c_k M_k} - \frac{D_{T,j}}{c_j M_j}\right), \tag{16}$$

where $D_{T,j}$ are the thermal diffusion coefficients and M_j is the molecular weight of component j. Note that the thermal diffusion coefficients may be expressed in terms of the Maxwell–Stefan diffusion coefficients as

$$D_{T,j} = \sum_{i=1}^{N} S^T_i \mathcal{D}_{ik} \tag{17}$$

where S^T_i is the Soret coefficient. Finally, we express r_{qq} in terms of the thermal conductivity of the mixture λ_{mix} as $r_{qq} = 1/\lambda_{mix}T^2$. With the aid of the above identifications and by choosing component 1 as the independent component it is possible to rewrite the driving forces as

$$X'_q = \frac{1}{\lambda_{mix}T^2}\left[J'_q - \sum_{k=2}^{N} c_k q^*_k (v_k - v_1)\right]$$
$$X'_i = -c_i q^*_i X'_q - \frac{Rc_i}{c_t} \sum_{k=1,k\neq 1}^{N} \frac{c_k}{\mathcal{D}_{k,i}} (v_k - v_i), \qquad (i = 2, 3, \cdots N)$$
$$X'_1 = -\sum_{k=2}^{N} X'_k \tag{18}$$

The substitution of eq. (18) into eq. (11) leads finally to the sought expression for the entropy production rate of the films in terms of the fluxes and the transport coefficients. The methods used to compute thermal conductivity, Maxwell–Stefan diffusion coefficients and Soret coefficients, are provided in Table 3.

In the calculation of the global entropy production rate, we shall need the interface area, A, and the vapor and liquid film thicknesses, $\delta^{V,L}$. The film thicknesses may be computed using the relationship between the mass transfer coefficients k_{ij}^{π} and the Maxwell–Stefan diffusion coefficients $\mathcal{D}_{ij}^{\pi}$ [39], given by

$$\mathcal{D}_{ij}^{\pi} = \delta^{\pi} k_{ij}^{\pi}. \tag{19}$$

The reason for this election is based on the fact that the heat and mass transfer thicknesses in the vapor phase tend to be similar and also because the mass transfer coefficient comes from experimental data [39]. The interface area A and the mass transfer coefficients k_{ij}^{π} are obtained by using empirical correlations that apply to the particular type of physical stage being considered. We will be extracted from the Aspen simulation results which are derived by using the correlation proposed in Ref. [34]. Note that eq. (19) leads to a range of values for the film thicknesses. We selected the ones that lead to entropy production rates closer to the results of the *EB* approach which we took as our benchmark. Once they are available, the global forces in the films may be obtained by integrating the local forces over the corresponding film thickness δ^{π}, leading to

$$\begin{aligned}
X_q^{\pi} &= \int_0^{\delta^{\pi}} X_q'^{\pi} dx = \bar{X}_q'^{\pi} \delta^{\pi} = \frac{\delta^{\pi}}{\lambda_{mix} T^2} \left[J_q'^{\pi} - \sum_{k=1}^{N} c_k q_k^* (v_k - v_1) \right] \\
X_i^{\pi} &= \int_0^{\delta^{\pi}} X_i'^{\pi} dx = \bar{X}_i'^{\pi} \delta^{\pi} = -c_i q_i^* X_q^{\pi} - \frac{R c_i \delta^{\pi}}{c_t} \sum_{k=1,k\neq 1}^{N} \frac{c_k}{\mathcal{D}_{k,i}} (v_k - v_i), \quad (i = 2, 3, \cdots N) \\
X_1^{\pi} &= -\sum_{k=2}^{N} X_k
\end{aligned} \tag{20}$$

Thus the global entropy production rate in the films is finally given by

$$\frac{dS_{irr}^{\pi,film}}{dt} = J_q^{\pi} A X_q^{\pi} + \sum_{i}^{4} v_i^{\pi} A X_i^{\pi}. \tag{21}$$

Now we turn to the contributions to the entropy production rate coming from the two bulks. From the entropy balance, and by considering unidirectional mass and heat transfer, these are given by

$$\begin{aligned}
\frac{dS_{irr}^{L,bulk}}{dt} &= J_{q,n}'^{L} A \left(\frac{1}{T_n^L} - \frac{1}{T_{n-1}^L} \right) - \sum_{i=1}^{N} x_{i,n-1} \mathcal{L}_{n-1} \left(\frac{\mu_{i,n-1}^L (T_{n-1}^L) - \mu_{i,n-1}^L}{T_{n-1}^L} \right), \\
\frac{dS_{irr}^{V,bulk}}{dt} &= J_{q,n}'^{V} A \left(\frac{1}{T_{n+1}^V} - \frac{1}{T_n^V} \right) - \sum_{i=1}^{N} y_{i,n+1} \mathcal{V}_{n+1} \left(\frac{\mu_{i,n}^V (T_{n+1}^V) - \mu_{i,n+1}^V}{T_{n+1}^V} \right),
\end{aligned} \tag{22}$$

where $J_{q,n}^{'L,V}$ is the heat transfer rate in the nth tray, $x_{i,n-1}\mathcal{L}_{n-1}$ is the amount of mass of component i entering the nth tray from the tray above, $y_{i,n+1}\mathcal{V}_{n+1}$ is the amount of mass of component i entering the nth tray from the tray below, $\mu_{i,n}^L(T_{n-1}^L)$ is the chemical potential at the liquid composition at the nth tray and temperature of the $(n-1)$th. $\mu_{i,n}^V(T_{n+1}^V)$ is the chemical potential at the vapor composition of tray n and the temperature of tray $n+1$. The calculation of the chemical potentials is obtained from the fugacities of the components in the liquid or vapor phases, respectively,

$$\frac{\mu^L_{i,n}(T^L_{n-1}) - \mu^L_{i,n-1}}{T^L_{n-1}} = R \ln\left(\frac{f^L_{i,n}(x_n, T^L_{n-1})}{f^L_{i,n-1}(x_{n-1}, T^L_{n-1})}\right)$$
$$\frac{\mu^V_{i,n1}(T^V_{n+1}) - \mu^V_{i,n+1}}{T^V_{n+1}} = R \ln\left(\frac{f^V_{i,n}(y_n, T^V_{n+1})}{f^V_{i,n+1}(y_{n+1}, T^V_{n+1})}\right) \quad (23)$$

where $f_i^{V,L}$ is the fugacity of component i evaluated at the corresponding nth tray liquid composition and temperature. Once more, both the fugacities and the chemical potentials of the mixture will be extracted from the simulation results by using the Peng–Robinson equation of state [37].

Once the temperature, concentration and flows profiles are known, all the transfer rates may be determined with the rated-based model by the Aspen simulation and one may then compute $dS^{L,V\ bulk}_{irr}/dt$ as given by eq. (22). Finally, after substitution of this result and the one given by eq. (21) into eq. (9), one arrives at the final expression for the global entropy production rate in each tray as given by the *NET* approach.

2.4 Exergy analysis and global entropy balance

In order to asses the *NET* results, the exergy analysis is a useful benchmark. The exergy loss and entropy production rate in distillation are related to each other by the Gouy–Stodola theorem [13], namely

$$\frac{dS^n_{irr}}{dt} = \frac{Ex^{loss}_n}{T_0} \quad (24)$$

where the reference temperature is $T_0 = 298.15$ K and Ex^{loss}_n is the exergy loss on the nth tray. This latter may be calculated from the exergy balance over the nth tray as

$$Ex^{loss}_n = \mathcal{V}_{n+1}Ex^V_{n+1} + \mathcal{L}_{n-1}Ex^L_{n-1} - \mathcal{V}_nEx^V_n - \mathcal{L}_nEx^L_n + Q_n\left(1 - \frac{T_0}{T_n}\right), \quad (25)$$

where Q_n is the duty (in J/s), $\mathcal{L}_n$ is the liquid flow and $\mathcal{V}_n$ the vapor flow in mol/s. The exergy of one section $Ex^{V,L}_n$ is given by

$$Ex^{\pi}_n = \sum_{i=1}^{N} H^{\pi}_{i,n} - T_0 S^{\pi}_n, \quad (26)$$

where the values of the enthalpy $H^{\pi}_{i,n}$ and molar entropy of the mixture S^{π}_n are again obtained from the results of the simulation.

In a similar way, the entropy balance to quantify the global entropy production rate in the n-th column tray is expressed as

$$\frac{dS^n_{irr}}{dt} = \mathcal{V}_nS^V_n + \mathcal{L}_nS^L_n - \mathcal{V}_{n+1}S^V_{n+1} - \mathcal{L}_{n-1}S^L_{n-1} - F^V_nS^V_{Fn} - F^L_nS^L_{Fn} \quad (27)$$

where F_n is the feed molar flow (in mol/s) in the nth tray.

3 Results

In the previous section we have presented explicit expressions for the global entropy production rate as given by the *NET*, the *Ex* analysis and the global *EB* analysis. In this section we will provide a comparison of the corresponding results. We start with the comparison of the global entropy production rates given by the different approaches. This is presented in Figure 5.

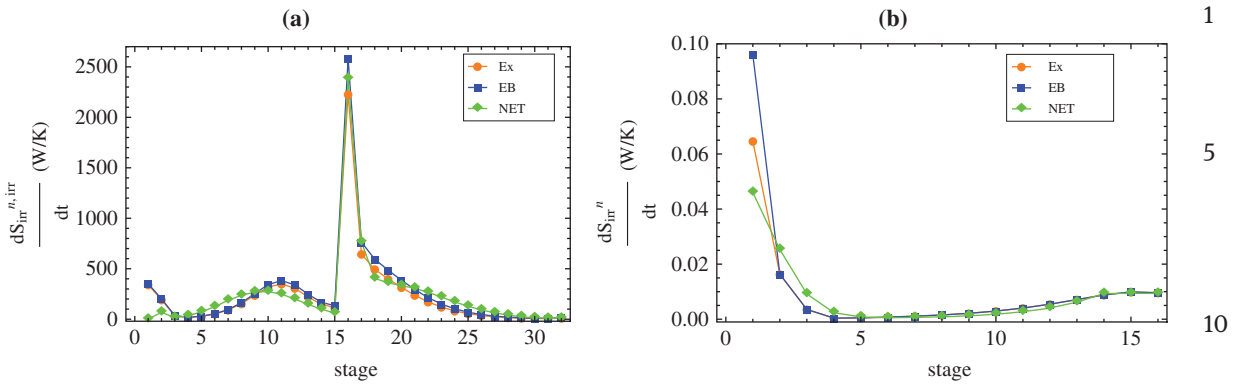

Figure 5: Global entropy production rate. Labels indicate the different theoretical approaches. *NET* corresponds to our nonequilibrium approach including the contribution of the two bulks; Ex is the the exergy analysis and EB corresponds to the entropy balance analysis.(a) Global entropy production rate in the depropanizer column. (b) Global entropy production rate in the fractionating column.

The total entropy production rate in Figure 5 displays a different behavior in each column due to the fact that both cases have different configurations, heat duty and main objective. For the depropanizer column, in all the three theoretical approaches the highest entropy production rate is located at the center of the column and the maximum value occurs at the feed stage. This is consistent with the fact that it is at the center of the column where the highest heat transfer rates and mass flow rates take place and so most of the separation happens there. In contrast, for the fractionating column, the entropy production rate takes on the highest values in two places in the column: in the first three stages, where the vapor flow and the liquid flow in countercurrent present the greatest temperature difference in the column. The vapor mixture is at 320 K and the cold liquid reflux at 250 K. The second place is in the last three stages (the bottom of the column) where the highest temperatures occur so that the mixture begins to evaporate.

The differences between the values of the entropy production rate of the trays as obtained with the *NET* approach and with the *Ex* analysis are likely due to the fact that in the former one includes explicitly the transport coefficients, the heat and mass transfer couplings and the vapor and liquid thicknesses in the thermodynamic driving forces, while in the latter one does not.

Nevertheless, our results using the *NET* approach, apart from exhibiting similar trends to the ones of Liang et al. [20], are closer to the values obtained with the exergy analysis and entropy balance approach than the ones in Ref. [20], particularly for the depropanizer column. In this system, the correlation coefficient between the results of the *Ex* analysis and those of the *NET* approach is $R^2 = 0.950$. In the fractionating column this correlation was poorer, namely $R^2 = 0.907$.

In Figure 6 we display the values of the vapor heat of transfer q^{*V} computed with eq. (16). We see that the values corresponding to the fractionating column using the Mexican oil, with large molecular weight, are four orders of magnitude greater than those of the light hydrocarbon mixture of the depropanizer column. In the case of the liquid heat of transfer q^{*L}, although not shown, the trends and the results are similar in the sense that the Mexican oil leads to values one order of magnitude greater than those of the light hydrocarbon mixture.

The vapor heat of transfer of the fourth pseudocomponent, q_4^{*V}, which has the greatest molecular weight in the mixture, presents the largest values. They start at approximately, 513 J/mol and decrease to 32 J/mol. This is due to the fact that in the fractionating column, it is at the top where the heat and mass transfer take place while separating the compound of interest of the mixture. In contrast, for the depropanizer column, the values are more evenly distributed along the trays.

A more important question concerns the explicit inclusion of the coupling between heat and mass transfer in the thermodynamic driving forces, particularly for the vapor. The contributions of q_i^{*V} in the thermal and mass driving forces are compared in Figures 7 and 8. In this latter, only one of the independent forces

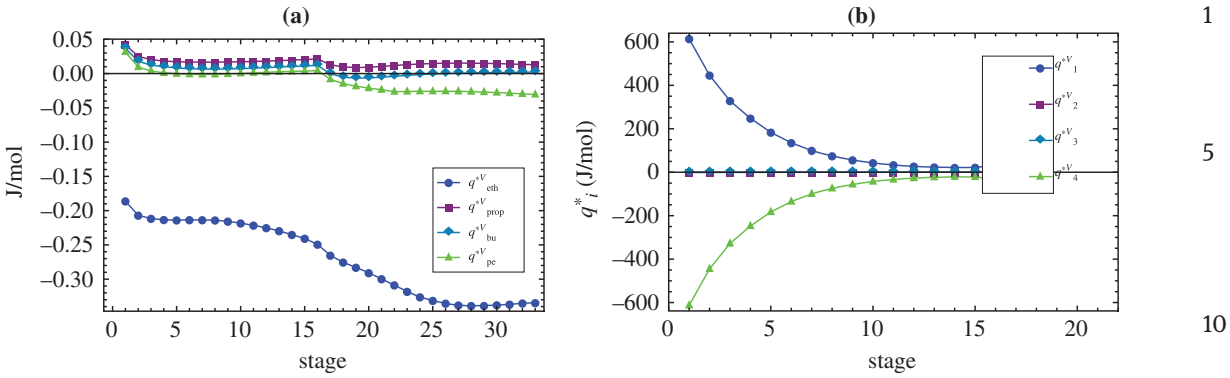

Figure 6: Vapor heat of transfer. (a) Vapor heat of transfer in the depropanizer column, where q^{*V}_{eth} is the ethane vapor heat of transfer, q^{*V}_{prop} is the propane vapor heat of transfer,q^{*V}_{bu} is the n-butane vapor heat of transfer and q^{*V}_{pe} is the n-pentane vapor heat of transfer. (b) Vapor heat of transfer in the fractionating column, where q^{*V}_{1} is the pseudocomponent 1 vapor heat of transfer, q^{*V}_{2} is the pseudocomponent 2 vapor heat of transfer,q^{*V}_{3} is the pseudocomponent 3 vapor heat of transfer and q^{*V}_{4} is the pseudocomponent 4 vapor heat of transfer.

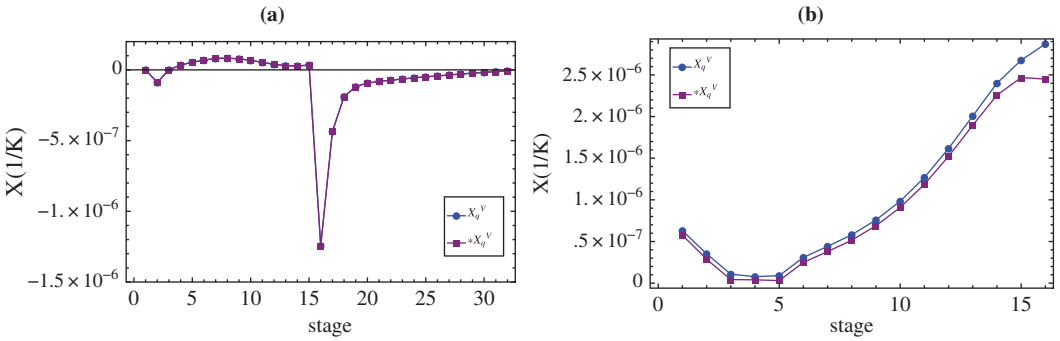

Figure 7: Thermal driving forces. (a) Vapor thermal driving force of the depropanizer column, where X^{V}_{q} includes the coupling between heat and mass transfer while $*X^{V}_{q}$ does not (b) Vapor thermal driving force of the fractionating column. The labels are the same of those of (a)

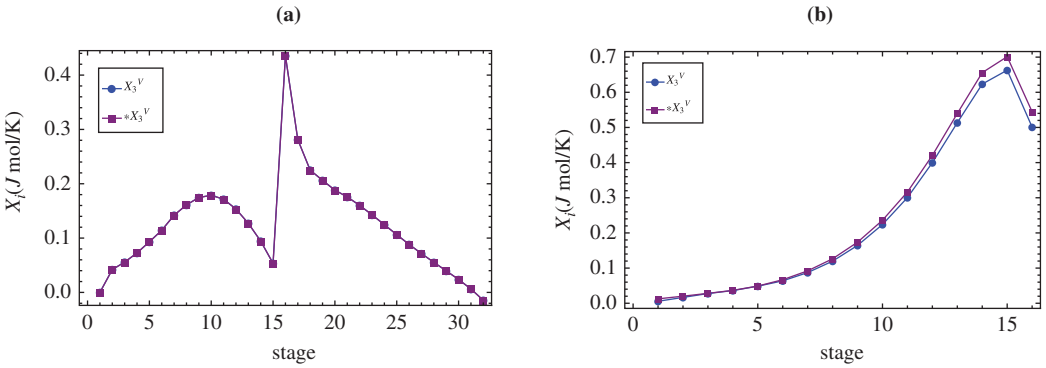

Figure 8: Mass driving forces. (a) Vapor thermal driving force of the depropanizer column, where X^{V}_{3} includes the coupling between heat and mass transfer and $*X^{V}_{3}$ does not (b) Vapor thermal driving force of the fractionating column. The labels are the same of those of (a).

(X_3) is displayed but the others show similar behavior. The results indicate that in the case of the depropanizer column, neglecting the thermal diffusion in this system will have a little effect on both the mass and the thermal driving forces. On the other hand, for the fractionating column this contribution makes an appreciable difference in these driving forces, specially in the three latest trays.

Since in the *NET* approach we have presented it is only possible to evaluate explicitly the effect of either including or not including the coupling between heat and mass transfer in the films, for the sake of completing the analysis and close this section we now present the results of their contributions to the global entropy production rates for both columns. These are displayed in Figure 9.

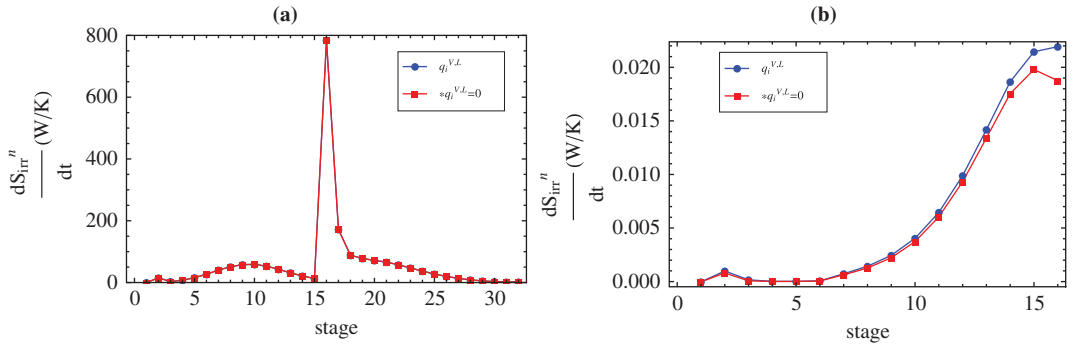

Figure 9: Contribution of the liquid and vapor films to the global entropy production rates. (a) Depropanizer column, in the cases where the thermal and mass driving forces include the coupling between heat and mass transfer and where they do not (b) Fractionating column. The labels are the same of those of (a).

4 Discussion and concluding remarks

The results of the previous sections deserve further consideration. The heat of transfer q^* is the quantity that allows us to explicitly include and evaluate the effect of the thermal diffusion process in our cases of study. As it is clearly seen in Figure 6, the values of q^{*V} are higher in the fractionating column than the ones in the depropanizer column. This fact is also manifested in Figures 7 and 8, where we evaluate the contribution of the inclusion of the coupling between heat and mass transfer in the thermodynamic driving forces. In the depropanizer column, neglecting thermal diffusion has a rather little effect on both driving forces and hence on the entropy production rate (see Figure 9). Such behavior agrees with claims made by previous authors as Rosner [40], Taylor and Khrisna [23] and Bird et al.[24], who suggest that there is a negligible influence of thermal diffusion in distillation. Also, DeLancey [41] concluded that the errors involved when neglecting thermal diffusion in the interfacial flux of a dilute three component hydrocarbon mixture do not appear to be significant when one considers the accuracy requirements of a design procedure. However, the generalization of such claims should be taken with care since other studies have indicated that thermal diffusion is sensitive to the details of intermolecular interaction, the structural behavior, such as the size and shape of the molecules [42–45] and this is reflected in the results for the fractionating column (*c.f.* Figures 7, 8 and 9). In fact, depending upon the physical system, the Dufour and Soret effects may or may not be important [41]. In low-pressure gaseous mixtures and in ideal liquid mixtures, as the multicomponent hydrocarbon mixture in the depropanizer column, the thermal diffusion factor has been found to be small [42, 46, 47]. On the other hand, in nonideal mixtures or for heavier components, like the Mexican oil mixture in the fractionating column, the thermal diffusion factor is larger than the one for ideal mixtures or the one for lighter components, respectively [48, 49]. Further, the thermal diffusion effect is appreciable in mass transfer situations with large molecular weight disparities and large temperature gradients, a situation that one encounters in the fractionating column but not in the depropanizer one.

In general, the analysis and modeling of heat transfer in petrochemistry processes which involve multicomponent mixtures with wide range in molecular masses represents a big challenge [50]. A popular way to treat hydrocarbon distillation problems is through the *Ex* analysis, but with it one cannot distinguish the individual contributions to the total exergy loss. A similar remark applies to other approaches, such as the equal thermodynamic distance approach that has been used for a diabatic column [51]. A point often overlooked in both the *Ex* analysis and in the equal thermodynamic distance analysis is the fact that there may

be couplings among various transport phenomena such as the Soret effect or the Duffour effect which are not explicitly accounted for. On the contrary, the *NET* approach allows us to evaluate the contribution of all possible individual driving forces of the irreversible phenomena and thus account for such couplings in the global entropy production rate. In this respect, *NET* may profitably be used to complement the *Ex* analysis.

Here we have presented one example of the usefulness of such approach for the analysis of a distillation process in both a theoretical case and in a real multicomponent mixture. This example has allowed us, among other things, to conclude that it may not be appropriate to neglect heat and mass transfer couplings in the analysis of some distillation processes. Furthermore, the outcome of this paper provides further support to the notion that the *NET* approach can be used satisfactorily to model this kind of complex processes. It is clear that in our development, many simplifying assumptions of the distillation process in both columns, which are in fact less restrictive than the ones usually adopted for the modeling of hydrocarbon mixtures, have been made. Among them we have the choice of steady-state conditions, one-dimensional flow of the vapor and liquid phases, that the vapor rising through the liquid within the tray is completely mixed and that there is no significant pressure gradient along the vapor and liquid flow directions. While of course such simplifications do impose some limitations on the actual numerical results, in our view they do not invalidate the main conclusions pertaining to the importance of explicitly accounting for the effect of the coupling of heat and mass transfer in distillation. Once we have gained this insight, a natural further step would be to remove some of these assumptions and hence get an even more realistic picture of what actually happens. We hope to address this step in the not too distant future.

One final remark is in order. In this article we have relied on the Aspen Plus V8.4 software to compute the temperature, composition and flow profiles and extract other thermodynamic data. Also, the transport coefficients were computed with known correlations in the literature. It is conceivable that in some instances, all or some of these quantities could be directly measured. Were this the case, the *NET* approach would remain unaltered and still allow for the evaluation of the (real) effect of heat and mass transfer coupling on a particular distillation process.

Acknowledgment: The authors gratefully acknowledge the assistance of Instituto Mexicano del Petróleo which provided the information on the oil mixture and access to their fractionating distillation column. P. Burgos Madrigal wants to thank Maria Beatriz de la Mora for useful discussions about distillation columns and Victor Duarte Alaniz from the Department of Physical Chemistry of the Institute of Chemistry (UNAM) for the artwork presented in this article.

This research did not receive any specific grant from funding agencies in the public, commercial, or not-for-profit sectors.

Nomenclature

A	interfacial area, m^2
c_t	total molar density, mol/m^3
c_i	molar density of component i, mol/m^3
dS^n_{irr}/dt	entropy production rate, J/s K
$\mathcal{D}_{ij}$	Maxwell–Stefan diffusion coefficient, m^2/s
F_n	Feed molar flow, mol/s
k_{ij}	mass transfer coefficients, mol m^2/s
H	enthalpy, J/mol
J	transfer rate, mol/s or J/s
J'	flux, mol/s m^2 or J/s m^2
$\mathcal{L}$	liquid flow mol/s

M	molecular weight, kg/mol
$\mathcal{N}_i$	mass transfer rate of i, mol/s
q_i^*	heat of transfer, J/mol
R	ideal gas constant, J/mol K
S_n	molar entropy of n- stage, J/ mol K
S_i^T	Soret coefficient of component i, 1/K
T	temperature, K
$\mathcal{V}$	vapor flow mol/s
v_i	velocity of component i, m/s
x	liquid molar fraction, dimensionless
X	global force conjugate rate, J/mol K or 1/K
X''	local force , J/mol K m or 1/K m
y	vapor molar fraction, dimensionless.

Greek letters

δ	film thickness, m
λ	thermal conductivity, W/m K
μ	chemical potential, J/mol
σ	local entropy production rate, W/K m^3

Subscripts and superscripts

i	component
L	liquid
q	heat
n	stage number
T	total
V	vapor
π	liquid or vapor

References

[1] Alhajji M, Demirel Y. Energy and environmental sustainability assessment of a crude oil refinery by thermodynamic analysis. Int J Energy Res. 2015;39:1925–1941.

[2] Wugen G, Kan W, Yuqing H, Bingjian Z, Qinglin C, Chi-Wai H. Energy optimization for a multistage crude oil distillation process. Chem Eng Technol. 2015;38:1243–1253.

[3] Waheed MA, Oni AO. Performance improvement of a crude oil distillation unit. Appl Therm Eng. 2015;75:315–324.

[4] de Koeijer GM, Kjelstrup S, Salamon P, Siragusa G, Schaller M, Hoffmann KH. Comparison of entropy production rate minimization methods for binary diabatic distillation. Ind Eng Chem Res. 2002;41:5826–5834.

[5] de Koeijer GM, Rosjorde A, Kjelstrup S. Distribution of heat exchange in optimum diabatic distillation columns. Energy. 2004;29:2425–2440.

[6] Demirel Y. Sustainable Operations for Distillation Columns. Chem Eng Process Tech. 2013;1:1005:2–15.

[7] Benyounes H, Shen W, Gerbaud V. Entropy flow and energy efficiency analysis of extractive distillation with a heavy entrainer. Ind Eng Chem Res. 2014;53:4778–4791.

[8] Pinto FS, Zemp R, Jobson M, Smith R. Thermodynamic optimisation of distillation columns. Chem Eng Sci. 2011;66:2920–2934.

[9] Demirel Y. Thermodynamic analysis of separation systems. Sep Sci Technol. 2004;39:3897–3942.

[10] Rosen MA. Using exergy to correlate energy research investments and efficiencies: Concept and case studies. Entropy. 2013;15:262–286.

[11] de Groot SR, Mazur P. Non-equilibrium thermodynamics. London: Dover, 1984.
[12] Haase R. Thermodynamics of irreversible processes. London: Dover, 1990.
[13] Kuiken GDC. Thermodynamics of irreversible processes. Applications to diffusion and rheology. Wiley tutorial series in theoretical chemistry, 1st ed. New York, USA: John Wiley & Sons, Inc., 1994.
[14] Demirel Y, Sandler SI. Linear-nonequilibrium thermodynamics theory for coupled heat and mass transport. Int J Heat Mass Transfer. 2001;44:2439–2451.
[15] Criado-Sancho M, Casas-Vázquez J. Termodinámica Química y de procesos irreversibles. Madrid, España: Pearson, 2004.
[16] öttinger HC. Beyond equilibrium thermodynamics. John Wiley & Sons, Inc., 2005.
[17] Kjelstrup S, Bedeaux D. Non-equilibrium thermodynamics of heterogeneous systems, volume 16 of advances in statistical mechanics. New Jersey, USA: World Scientific, 2008.
[18] Lebon G, Jou D, Casa-Vázquez J. Understanding Non-equilibrium thermodynamics. foundations, applications, frontiers. Springer, 2008.
[19] Demirel Y. Nonequilibrium thermodynamics, 3rd ed. Elsevier, 2014.
[20] Liang YC, Zhou Z, Wu YT, Geng J, Zhang ZB. A nonequilibrium model for distillation processes. AIChe J. 2006;52:4229–4239.
[21] Tsirlin AM, Grigorevsky IN. Thermodynamical estimation of the limit potentialities of irreversible binary distillation. J Non-equilib Thermodyn. 2010;35:213–233.
[22] Wesselingh JA. Non-equilibrium modelling of distillation. Trans IChemE. 1997;75:529–538.
[23] Taylor R, Krishna R. Multicomponent mass transfer. New York, USA: John Wiley & Sons, Inc., 1993.
[24] Bird RB, Stewart WE, Lightfoot EN. Transport phenomena. New York, USA: John Wiley and Sons, 2002.
[25] Kjelstrup S, de Koeijer GM. Transport equations for distillation of ethanol and water from the entropy production rate. Chem Eng Sci. 2003;58:1147–1161.
[26] Bedeaux D., Kjelstrup S. Irreversible thermodynamics—a tool to describe phase transitions far from global equilibrium. Chem Eng Sci. 2004;59:109–118.
[27] Kjelstrup S, de Koeijer GM. Application of irreversible thermodynamics to distillation. Int J Thermodyn. 2005;7:1–8.
[28] van der Ham LV, Bock R, Kjelstrup S. Modelling the coupled transfer of mass and thermal energy in the vapour–liquid region of a nitrogen–oxygen mixture. Chem Eng Sci. 2010;65:2236–2248.
[29] Mendoza DF, Kjelstrup S. Modeling a non-equilibrium distillation stage using irreversible thermodynamics. Chem Eng Sci. 2011;66:2713–2722.
[30] Designation: D2982-10. Standard test method for distillation of crude petroleum (15-theoretical plate column)1. ASTM international, Barr Harbor Drive, PO Box C700, West Conshohocken, PA 19428-2959, United States., 2010.
[31] Riazi MR. Characterization and properties of petroleum fractions. ASTM manuals series: Philadelphia, USA: MNL50, 1st ed. American Society for Testing and Materials, 2005.
[32] Seader JD, Siirola JJ, Barnicki SD. Perry's chemical engineers' handbook, chapter 13, 7th ed., 56–81. New York, USA: McGraw Hill, 1992.
[33] Reid RC, Prausnitz JM, Poling BE. The properties of gases and liquids. New York, USA: McGraw-Hill, 1987.
[34] Onda K, Takeuchi H, Okumoto Y. Mass transfer coefficient between gas and liquid phases in packed columns. J Chem Eng. 1968;1:56–62.
[35] Artola PA, Rousseau B. Thermal diffusion in simple liquid mixtures: what have we learnt from molecular dynamics simulations? Mol Phys. 2013;111(22-23):3394–3403.
[36] Krishnamurthy R. A generalized film model for mass transfer in non-ideal fluid mixtures. Chem Eng Sci. 1977;32:659–667.
[37] Peng DY, Robinson DB. A new two-constant equation-of-state. Ind Eng Chem Fundam. 1976;15:59–64.
[38] Krishna R, Wesselingh JA. The Maxwell - Stefan approach to mass transfer. Chem Eng Sci. 1997;52:861–911.
[39] Wesselingh JA, Krishna R. Mass transfer in multicomponent mixtures. The Netherlands: Delft: University Press, 2006.
[40] Rosner DE. Thermal/ Soret / diffusion effects on interfacial mass transport rates. PCH/Phy Chem Hydrodyn. 1980;1:159–185.
[41] DeLancey GB. The effect of thermal diffusion in multicomponent gas absorption. Chem Eng Sci. 1972;27:555–556.
[42] Kincaid JM, Cohen EG, López de Haro M. The Enskog theory for multicomponent mixtures. IV. Thermal diffusion. J Chem Phys. 1986;86:963–974.
[43] Shukla K, Firoozabadi A. A new model of thermal diffusion coefficients in binary hydrocarbon mixtures. Ind Eng Chem Res. 1998;37:3331–3342.
[44] Firoozabadi A, Ghorayeb K, Shukla K. Theoretical model of thermal diffusion factors in multicomponent mixtures. AIChE J. 2000;46.
[45] Eslamian M, Ziad Saghir M. Thermodiffusion in binary and ternary nonpolar hydrocarbon + alcohol mixtures. J Non-equilib Thermodyn. 2012;37:329–351.
[46] Seshasai S, Ziad Saghir M. Thermodiffusion in ternary hydrocarbon mixtures. Part 1: n-dodecane/isobutylbenzene/tetralin. J Non-equilib Thermodyn. 2011;36:243–258.
[47] Seshasai S, Ziad Saghir M. Thermodiffusion in ternary hydrocarbon mixtures. Part 2: n-dodecane/isobutylbenzene/tetralin. J Non-equilib Thermodyn. 2012;37:99–113.
[48] Yan Y, Blanco P, Ziad Saghir M, Mounir Bou-Ali M. An improved theoretical model for thermal diffusion coefficient in liquid hydrocarbon mixtures: Comparison between experimental and numerical results. J Chem Phys. 2008;129:194507.

[49] de Mezquia DA, Wang Z, Lapeira E, Klein M, Wiegand S, Mounir M. Thermodiffusion, molecular diffusion and Soret coefficient of binary and ternary mixtures of n-hexane, dodecane and toluene. Eur Phys J E. 2014;37:2–10.
[50] Morteza E., Ziad Saghir M, Mounir Bou-Ali M. Investigation of the Soret effect in binary, ternary and quaternary hydrocarbon mixtures: New expressions for thermodiffusion factors in quaternary mixtures. Int J Therm Sci. 2010;49:2128–2137.
[51] Schaller M, Hoffmann KH, Siragusa G, Salamon P, Andresen B. Numerically optimized performance of diabatic distillation columns. Comp Chem Eng. 2001;25:1537.

Bibliography

[1] D. F. Mendoza, Análisis y minimización de la entropía generada en un proceso de destilación extractiva para la deshidratación de etanol, Ph.D. thesis, Universidad Nacional de Colombia (2011).

[2] G. de Koeijer, R. Rivero, Entropy production and exergy loss in experimental distillation columns, Chem. Eng. Sci. 58 (8) (2003) 1587–1597.

[3] R. Taylor, R. Krishna, Multicomponent mass transfer, John Wiley & Sons, Inc., New York, United States, 1993.

[4] B. Hafskjold, T. Ikeshoji, Non equilibrium molecular dynamics simulation of coupled heat- and mass transport across a liquid/vapor interface, Molecular Simulation 16 (1996) 136–150.

[5] G. M. de Koeijer, S. Kjelstrup, P. Salamon, G. Siragusa, M. Schaller, K. H. Hoffmann, Comparison of Entropy Production Rate Minimization Methods for Binary Diabatic Distillation, Ind. Eng. Chem. Res. 41 (23) (2002) 5826–5834.

[6] G. de Koeijer, Distribution of heat exchange in optimum diabatic distillation columns, Energy 29 (12-15) (2004) 2425–2440.

[7] Y. Demirel, Sustainable Operations for Distillation Collumns, Chem. Eng. Process Tech. (2013) 2–15.

[8] H. Benyounes, W. Shen, V. Gerbaud, Entropy Flow and Energy Efficiency Analysis of Extractive Distillation with a Heavy Entrainer, Ind. Eng. Chem. Res. 53 (12) (2014) 4778–4791.

[9] Y. Demirel, Thermodynamic Analysis of Separation Systems, Sep. Sci. Technol. 39 (16) (2004) 3897–3942.

[10] F. S. Pinto, R. Zemp, M. Jobson, R. Smith, Thermodynamic optimisation of distillation columns, Chem. Eng. Sci. 66 (13) (2011) 2920–2934.

[11] M. Rosen, Using Exergy to Correlate Energy Research Investments and Efficiencies: Concept and Case Studies, Entropy 15 (1) (2013) 262–286.

[12] F. B. Petlyuk, Distillation Theory and its Application to Optimal Design of Separation Units, Cambridge Series in Chemical Engineering, Cambridge University Press, New York, United States, 2011.

[13] R. M. Velasco, L. S. García-Colín, F. J. Uribe, Entropy Production: Its Role in Non-Equilibrium Thermodynamics, Entropy 13 (2011) 82–116.

[14] Y.-C. Liang, Z. Zhou, Y.-T. Wu, J. Geng, Z.-B. Zhang, A Nonequilibrium Model for Distillation Processes, AIChe Journal 52 (2006) 4229–4239.

[15] D. F. Mendoza, C. A. M. Riascos, Entropy Production Analysis in Extractive Distillation Using Non-Equilibrium, 10th International Symposium on Process Systems Engineering - PSE2009 (2009) 1–7.

[16] Y. Demirel, S. I. Sandler, Linear-nonequilibrium thermodynamics theory for coupled heat and mass transport, International Journal of Heat and Mass Transfer 44 (2001) 2439–2451.

[17] R. B. Currie, L. F. Phillips, Non-equilibrium thermodynamics of the gas-liquid interface: Measurement of the Onsager heat of transport for ammonia at the surface of water, J. Non-Equilib. Thermodyn 34 (2009) 265–275.

[18] L. XiaoHua, J. YuanHui, L. HongLai, Non-equilibrium thermodynamics analysis and its application in interfacial mass transfer, Sci China Chem 54 (10) (2011) 1659–166.

[19] S. Kjelstrup, A. Rosjorde, E. Johannessen, Chapter 1. Non-equilibrium thermodynamics for industry, in T.M. Letcher (ed.) *Chemical thermodynamics for industry*, RSC, London, G.B., 2004, pp. 1–11.

[20] J. A. Wesselingh, Non-equilibrium modelling of distillation, Trans IChemE 75 (1997) 529–538.

[21] D. E. Rosner, Thermal (Soret) diffusion effects on interfacial mass transport rates, PCH (1980) 159–185.

[22] R. Bird, W. Stewart, E. N. Lightfoot, Transport phenomena, John Wiley & Sons, Inc., N.Y., 2002.

[23] S. Kjelstrup, G. de Koeijer, Transport equations for distillation of ethanol and water from the entropy production rate, Chem. Eng. Sci. 58 (7) (2003) 1147–1161.

[24] D. Bedeaux, S. Kjelstrup, Irreversible thermodynamics—a tool to describe phase transitions far from global equilibrium, Chemical Engineering Science 59 (1) (2004) 109–118.

[25] S. Kjelstrup, Application of Irreversible Thermodynamics to Distillation, Int. J. of Thermodynamics (2005) 1–8.

[26] S. Kjelstrup, D. Bedeaux, Non-Equilibrium Thermodybamics of Heterogeneous Systems, Vol. 16 of Advances in Statistical Mechanics, World Scientific, New Jersey, United States, 2008.

[27] L. V. van der Ham, R. Bock, S. Kjelstrup, Modelling the coupled transfer of mass and thermal energy in the vapour–liquid region of a nitrogen–oxygen mixture, Chemical Engineering Science 65 (6) (2010) 2236–2248.

[28] D. F. Mendoza, S. Kjelstrup, Modeling a non-equilibrium distillation stage using irreversible thermodynamics, Chemical Engineering Science 66 (12) (2011) 2713–2722.

[29] J. D. Seader, J. J. Siirola, S. D. Barnicki, Perry's Chemical Engineers' Handbook, 7th Edition, Mc Graw Hill, New York, United States, 1992, Ch. 13, pp. 56–81.

[30] C. D. Holland, Fundamentals of Multicomponent Distillation, McGraw-Hill, 1971.

[31] M. A. Fahim, T. A. Al-Sahhaf, A. S. Elkilani, Fundamentals of Petroleum Refining, Elselvier, U.K., 2010.

[32] M. R. Riazi, Characterization and Properties of Petroleum Fractions, 1st Edition, ASTM Manuals series: MNL50, American Socity for Testing and Materials, Philadelphia, United States., 2005.

[33] R. N. Watkins, Petroleum Refinery Distillation, 2nd Edition, Gulf, 1979.

[34] R. Taylor, H. A. Kooijman, J. S. Hung, A 2nd generation nonequilibrium model for computer-simulation ofmulticomponent separation processes, Comput. Chem. Eng. 18 (1994) 205–217.

[35] D. Mustapha, T. Sabria, O. Fatima, Distillation of a Complex Mixture. Part I: High Pressure Distillation Column Analysis: Modeling and Simulation, Entropy (2007) 1–15.

[36] A. C. Dimian, Integrated design and simulation of chemical processes, Vol. 13 of Computer-aided chemical engineering, Elselvier, Amsterdam, The Netherlands, 2003.

[37] Distillation design and control using Aspen simulation, 2nd Edition, John Wiley & Sons, Inc., New Jersey, U.S.A., 2014.

[38] M. Darabi, H. Mohammadiun, M. Mohammadiun, Advanced exergy analysis of distillation tower and simulation and optimization by HYSYS, International Journal of Scientific World (2015) 163–177.

[39] R. Rivero, C. Rendon, L. Monroy, The exergy of crude oil mixtures and petroleum fractions: Calculation and application, Int. J. Applied Thermodynamics 2 (3) (199) 115–123.

[40] R. Rivero, C. Rendon, L. Monroy, The Exergy of Crude Oil Mixtures and Petroleum Fractions: Calculation and Application, Int. J. Applied Thermodynamics 2 (2009) 115–123.

[41] M. Raja Kumar, B. Vijaya Kumar, U. Ramgopal, R. B. Vikas, Optimization of crude distillation system using aspen plus: Effect of binary feed selection on grass-root design, Chem. Eng. Res. Des. 88 (2010) 121–134.

[42] M. Arjmand, L. Moreno, L. Liu, Energy Saving in Crude Oil Atmospheric Distillation Columns by Modifying the Vapor Feed Inlet Tray, Chemical Engineering & Technology 34 (8) (2011) 1359–1367.

[43] M. Waheed, A. Oni, Performance improvement of a crude oil distillation unit, Appl. Therm. Eng. 75 (2015) 315–324.

[44] G. Wugen, W. Kan, H. Yuqing, Z. Bingjian, C. Qinglin, H. Chi-Wai, Energy optimization for a multistage crude oil distillation process, Chem. Eng. Technol. 38 (7).

[45] H. Al-Muslim, I. Dincer, Thermodynamic analysis of crude oil distillation systems, Int. J. Energy Res. 29 (2005) 637–655.

[46] M. Alhajji, Y. Demirel, Energy and environmental sustainability assessment of a crude oil refinery by thermodynamic analysis, Int. J. Energy Res. 39 (2015) 1925–1941.

[47] A. P. Hinderink, F. P. J. M. Kerkhof, A. Lie, J. De Swaan arons, H. van Der kooi, Exergy analysis with a flowsheeting simulator. pt. i: Theory; calculating exergies of material streams, Chem. Eng. Sci. 51 (1996) 4693–4700.

[48] Aspen Technology, Inc., Cambridge, USA, Getting Started Modeling Petroleum Processes (2004).

[49] Aspen Technology, Inc., Cambridge, USA, Aspen Plus User Guide (2000).

[50] Aspen Technology, Inc., California, USA, Units Operation Models. Reference Manual (1998).

[51] R. Rivero, L'analyse d'exergie: Application a la distillation diabatique et aux pompes a chaleur a absorption, Ph.D. thesis, Institut National Polytechnique de Lorraine (1993).

[52] ASTM International, Barr Harbor Drive, PO Box C700, West Conshohocken, PA 19428-2959, United States., Standard Test Method for Distillation of Crude Petroleum (15-Theoretical Plate Column) (2010).

[53] S. A. Ashrafizadeh, M. Amidpour, M. Abolmashadi, Exergy analysis of distillation column using concept of driving forces, J. Chem. Eng. Jpn 46 (7) (2013) 434–443.

[54] Y. Demirel, Nonequilibrium Thermodynamics, 3rd Edition, Elselvier, 2014.

[55] S. Kjestrup, D. Bedeaux, E. Johannessen, J. Gross, Non-equilibrium thermodynamics for engineers, The science and culture, World Scientific, 2010.

[56] G. Lebon, D. Jou, J. Casa-Vázquez, Understanding Non-equilibrium Thermodynamics. Foundations, Applications, Frontiers, Springer, 2008.

[57] G. Kuiken, Thermodynamics of Irreversible Processes. Aplications to difusion and theology, John Wiley & Sons, Inc.

[58] M. Criado-Sancho, J. Casas-Vázquez, Termodinámica Química y de procesos irreversibles, Pearson, Madrid, 2004.

[59] S. R. de Groot, P. Mazur, Non-Equilibirum Thermodynamics., •, Dover, London, 1984.

[60] R. Haase, Thermodynamics of Irreversible Processes, Dover, London, 1990.

[61] H. C. Öttinger, Beyond Equilibrium Thermodynamics, John Wiley & Sons, Inc., 2005.

[62] J. D. Seader, E. J. Henley, Separation process principles, John Wiley & Sons, Inc., New York, United States, 1998.

[63] K. Onda, H. Tekeuchi, Y. Okumoto, Mass Transfer Coefficient Between Gas and Liquid Phases in Packed Columns, J. Chem. Eng. 1 (1968) 56–62.

[64] T. H. Chilton, A. Colburn, Mass transfer (absorption) coefficients prediction from data on heat transfer and fluid friction, Ind. Eng. Chem. (26) (1934) 1183—-1187.

[65] J. Wesselingh, R. Krishna, Mass Transfer in Multicomponent mixtures, Delft: University Press, Netherlands, 2006.

[66] G. D. C. Kuiken, Thermodynamics of Irreversible Processes. Applications to Diffusion and Rheology, 1st Edition, Wiley Tutorial series in Theoretical Chemistry, John Wiley & Sons, Inc., New York, United States, 1994.

[67] R. Krishna, J. A. Wesselingh, The Maxwell - Stefan approach to mass transfer, Chem. Eng. Sci. 52 (6) (1997) 861–911.

[68] Y. Yan, M. Pablo Blanco asn Ziad Sahir, M. Mounir Bou-Ali, An improved theoretical model for thermal difffusion coefficient in liquid hydrocarbon mixtures: Comparison between experimental and numerical results, J. Chem. Phys. 129.

[69] M. Eslamian, M. Z. Saghir, M. M. Bou-Ali, Investigation of Soret effect in binary, ternary and quaternary hydrocarbon mixtures: New expressions for thermodiffussion factors in quaternary mixtures, Int. J. Therm. Sci. 49 (11) (2010) 2128–2137.

[70] S. Seshasai, M. Saghir Ziad, Thermodiffusion in ternary hydrocarbon mixtures. part 1: n-dodecaen/isobutylbenzene/tetralin, J. Non-Equilib. Thermodyn. 36 (2011) 243–258.

[71] S. Seshasai, M. Saghir Ziad, Thermodiffusion of ternary hydrocarbon mixtures. part 2: n-dodecaen/isobutylbenzene/tetralin, J. Non-Equilib. Thermodyn. 37 (2012) 99–113.

[72] G. DeLancey, The effect of thermal diffusion in multicomponent gas absortion, Chem. Eng. Sci. 27 (1972) 555–556.

[73] J. M. Kincaid, E. G. D. Cohen, M. López de Haro, The enskog theory for multicomponent mixtures. iv thermal diffusion, J. Chem. Phys. 86 (1986) 963–974.

[74] K. Shukla, A. Firoozabadi, A new model of thermal diffusion coefficients in binary hydrocarbon mixtures, Ind. Eng. Chem. Res. 37 (1998) 3331–3342.

[75] A. Firoozabadi, K. Ghorayeb, S. Keshawa, Theoretical model of thermal diffusion factors in multicomponent mixtures, AIChE Journal 46.

[76] M. Eslamian, M. Ziad Saghir, Thermodiffusion in binary and ternary nonpolar hydrocarbon + alcohol mixtures, J. Non-Equilib. Thermodyn. 37 (2012) 329–351.

[77] D. A. de Mezquia, Z. Wang, E. Lapeira, M. Klein, S. Wiegand, M. Mounir, Thermodiffusion, molecular diffusion and Soret coefficient of binary and ternary mixtures of n-hexane, dodecane and toluene, Eur. Phys. J. E. 37 (2014) 2–10.

[78] R. C. Reid, J. M. Prausnitz, B. E. Poling, The properties of Gases and Liquids, 4th Edition, Chemical Engineering, McGraw-Hill, Inc., N.Y., USA, 1987.

[79] S. W. Brelvi, J. P. O'Connel, Corresponding states correlation for liquid compressibility and partial molal volumes of gases at infitine dilution in liquids, AIChe Journal 18 (6) (1972) 1239–1243.

[80] R. H. G., Equation of state for saturated liquids, J.Chem, Eng. Data 15 (4) (1970) 514–517.

[81] D. Y. Peng, D. B. Robinson, A New Two - Constant Equation of state, Ind. Eng. Chem. Fundam. 15 (1976) 59–64.

[82] American Petroleum Institute, API Technical Data Book, Petroleum Refining, 6th Edition (1997).

[83] P. A. Artola, B. Rousseau, Thermal diffusion in simple liquid mixtures: what have we learnt from molecular dynamics simulations?, Mol. Phys. 111 (22-23) (2013) 3394–3403.

[84] R. Krishnamurthy, A generalized film model for mass transfer in non-ideal fluid mixtures, Chem. Eng. Sci. 32 (1977) 659–667.

[85] F. M. Georis, S. Van Vaerenbergh, Y. Decroly, J. C. Legros, Measurement of the Soret coefficient in crude oil, Society of Petroleum Engineers SPE 50573 (1998) 57–66.

[86] R. Yano, Y. Fukuda, T. Hashi, Thermal conductivity measurements of water-ethanol solutions by the laser-induced transient grating method, Chemical Physics 124 (315–319).

[87] J. Smith, H. Van Ness, Introduction to chemical engineering thermodynamics, 4th Edition, McGraw-Hill, inc., New York, U.S.A., 1987.

[88] P. Kolodner, H. Williams, C. Moe, Optical measurements of the soret coe cient of ethanol/water solutions, Journal of Chemical Physics 10 (88) (1988) 6512—-6524.

[89] R. Sinnot, J. Coulson, J. Richardson, An introduction to chemical engineering design, Vol. 6 of Chemical Engineering, Oxford: Pergamon Press, 1983.